Identification of Finite-Degree-of-Freedom Models for Ship Motions

Baha M. Suleiman

Dissertation submitted to the Faculty of the
Virginia Polytechnic Institute and State University
in partial fulfillment of the requirements for the degree of

Doctor of Philosophy
in
Engineering Mechanics

A. H. Nayfeh, Co-Chairman
M. R. Hajj, Co-Chairman
D. T. Mook
S. A. Ragab
S. Adjerid

December 11, 2000
Blacksburg, Virginia

Keywords: System Identification, Nonlinear, Ship Motion, Perturbation Techniques,
Higher-Order Spectra

Identification of Finite-Degree-of-Freedom Models for Ship Motions

Baha M. Suleiman

(ABSTRACT)

Accurate ship-motion prediction is important because it is directly related to the design, control, and economic operation of ships. Many methods are available for studying and predicting ship motions, including time-domain, strip-theory, and system-identification-based predictions. Time-domain and strip-theory predictions suffer from several physical and computational limitations. In this work, we use system-identification techniques to predict ship motions. We establish an identification methodology that can handle general finite-degree-of-freedom (FDOF) models of ship motions.

To establish this methodology, we derive the correct form of the equations of motion. This form contains all relevant linear and nonlinear terms. Moreover, it explicitly specifies the dependence of the linear and nonlinear parameters on the forward speed. The energy-formulation approach is utilized to obtain full nonlinear ship-motion equations. The advantages of using this formulation are that self-sustained motions are not allowed and the dependence of the parameters on the forward speed is derived explicitly.

The data required for the identification techniques are generated using the Large Amplitude Motions Program (LAMP) developed by the Science Applications International Corporation (SAIC). The ship studied in this work is a Series 60 ship, which is a military cargo ship. LAMP data for different sea states and forward speeds are used to identify and predict the ship motions.

For linear parametric identification, we use the Eigensystem Realization Algorithm (ERA) to determine the coefficients in the linearly coupled equations and the effects of the forward speed on these coefficients. For linear nonparametric identification, we present a new analysis technique, namely, the circular-hyperbolic decomposition (CHD), which avoids the leakage effects associated with the discrete Fourier transform (DFT). The CHD is then utilized to determine transfer functions and response amplitude operators (RAOs). For nonlinear parametric identification, we present a methodology that is a combination of perturbation techniques and higher-order spectral moments. We apply this methodology to identify the nonlinear parameters that cause parametric roll resonance. The level of accuracy of the models and the parameter estimates are determined by validations of the predicted ship motions with the LAMP data.

This work was supported by the Office of Naval Research under Grant No. N00014-96-1-1123.

Dedication

To my mother and father
my brothers and sisters
and my wife and daughter

Acknowledgments

I would like to thank my advisors Dr. Ali H. Nayfeh and and Dr. Muhammad R. Hajj for their invaluable guidance and advice throughout my Ph.D. studies. Their encouragement, thoughtfulness, and willingness to help are deeply appreciated. Their brilliance, resourcefulness, and patience are greatly admired.

I would like also to thank my committee members: Dr. Dean T. Mook, Dr. Saad A. Ragab, and Dr. Slimane Adjerid for their support and belief in me. It is an honor to have worked and learned from them.

I would like to thank all of the people and friends I have met at Virginia Tech.

Thanks for Mrs. Sally Shrader and Mrs. Loretta Tickle for their help in the administrative matters.

I would like to thank the Office of Naval Research for their support of this research under Grant No. N00014-96-1-1123

Most importantly, I would like to thank my family without whose support and patience I would have never reached this point: my father, Mr. Mahmoud Suleiman, and my mother, Mrs. Aysheh Suleiman. I am forever grateful for their love, kindness, sensibility, and devotion.

Finally, thanks to All Mighty God for giving me the ability, mindset, and perseverance to be where I am now.

Contents

1 Introduction **1**

1.1 Background and Motivation 1

1.2 Research Objectives 3

2 Prediction of Ship Motions **5**

2.1 Prediction of Ship Motions Using Time-Domain Numerical Solutions 5

2.2 Prediction of Ship Motion Using Strip Theory 9

2.3 Prediction of Ship Motions Using System Identification Techniques 11

2.3.1 System Identification Concepts 12

2.3.2 Parametric Identification of Linear Systems 15

2.3.3 Nonparametric Identification of Linear Systems 19

2.3.4 Nonlinear System Identification 21

2.3.5 System Identification for Ship Motions Prediction 24

3 Nonlinear Equations of Ship Motion with Forward-Speed Effects **35**

3.1 Coordinate Systems and Transformation Equations 36

3.2 Energy Formulation 39
3.2.1 Index Notation 43
3.3 Nonlinear Equations of Ship Motion 46
3.4 Discussion 51

4 Linear Parametric Identification with Forward Speed Effects 53
4.1 Equations Governing Ship Motions 54
4.1.1 Effect of Forward Speed on Ship-Motion Parameters 59
4.2 The LAMP Code 62
4.3 Linear Parametric Identification 63
4.3.1 State-Space Formulation 63
4.3.2 Eigensystem Realization Algorithm 65
4.4 Identification of the Heave and Pitch Equations 68
4.5 Identification of the Sway, Roll, and Yaw Equations 70
4.6 Identification of 5 DOF Ship Motion 79

5 Linear Nonparametric Identification of Ship Motion 81
5.1 Signal Processing Background 82
5.1.1 Complex Exponential Algorithm 84
5.1.2 Circular-Hyperbolic Decomposition 88
5.2 Application to RAO Estimation 91

6 Nonlinear Parametric System Identification 99

6.1 Nonlinear Effects in Ship Motions 100
6.1.1 Nonlinear Effects in LAMP 101
6.1.2 Nonlinear LAMP Results 103
6.2 Methodology for Nonlinear System Identification 110
6.3 Higher-Order Spectra 110
6.4 Approximate Solutions to Equations of Ship Motions with Perturbation Techniques 112
6.4.1 Solvability Condition 112
6.4.2 Approximate Solutions for Parametric Resonance 115
6.4.3 Parametric Roll Resonance 124
6.4.4 Nonlinear Identification Procedure 126
6.5 Results of Nonlinear System Identification 129

7 Summary and Conclusions **136**

7.1 Summary and Conclusions of the Current Work 136
7.2 Recommendations for Future Work 139

Bibliography **155**

Vita **156**

List of Figures

3.1 Coordinate systems 37

4.1 Fitting of the calculated damping coefficients using three different methods . 72

4.2 Prediction of ship motion for sea state 3 and $U = 0.4$ 73

4.3 Prediction of ship motion for sea state 7 and $U = 0.25$ 74

4.4 Polynomial fits of the calculated damping coefficients 75

4.5 Prediction of ship motion for sea state 3 and $U = 0.4$ 77

4.6 Prediction of ship motion for sea state 4 and $U = 0.25$ 78

4.7 Prediction of ship motion for different forward speeds and sea states 80

5.1 The heave motion of a Series 60 ship 94

5.2 The pitch motion of a Series 60 ship 95

5.3 Amplitude of the heave motion 95

5.4 Phase of the heave motion 96

5.5 Amplitude of the pitch motion 96

5.6 Phase of the pitch motion 97

5.7 The RAO for the heave motion 97

5.8 The RAO for the pitch motion 98

6.1 The heave and pitch motions for sea state 3 and $U = 0.2$ 104

6.2 The sway, roll, and yaw motions for sea state 3 and $U = 0.2$ 105

6.3 The heave and pitch motions for sea state 7 and $U = 0.2$ 106

6.4 The sway, roll, and yaw motions for sea state 7 and $U = 0.2$ 106

6.5 Amplitude-response curves of the heave and pitch motions 108

6.6 Frequency-response curves of the heave and pitch motions 109

6.7 Time-domain data for nonlinear parametric roll resonance. 131

6.8 Frequency-domain data for nonlinear parametric roll resonance. 132

6.9 Variation of the roll amplitude with the bi-spectral quantities. 133

6.10 Prediction of the roll motion for the case of heave-roll parametric resonance. 133

6.11 Prediction of the roll motion for the case of pitch-roll parametric resonance. . 134

6.12 Prediction of the roll amplitudes for the case of heave-roll parametric resonance. 134

6.13 Prediction of the roll amplitudes for the case of pitch-roll parametric resonance. 135

List of Tables

4.1 Accuracy of the predicted data as compared with the LAMP data 71

4.2 Accuracy of the predicted data as compared with the LAMP data 76

Chapter 1

Introduction

1.1 Background and Motivation

Ship-motion prediction is important because it is directly related to the safe and economic operation of ships. One important concern is the problem of capsizing in extreme weather conditions. Other concerns include the safe landing of aircraft, efficient transfer of payloads between marine vehicles, improved performance of tracking devices, and improved missile launching capability. Ship-motion prediction is also important in the design stage of ships. Design engineers can save time and resources by being able to anticipate the ship's performance in early stages. Conventionally, the stability of ships is assessed using static considerations only. This proved to be insufficient (Burton and deKat, 1998 [1]), especially for large motions where dynamic considerations should be taken into account. Any capable dynamic stability analysis requires physics-based mathematical models and time-domain multi-dimensional predictive methods.

Many methods are available for studying and predicting ship motions. These include time-domain, strip-theory, and system-identification-based predictions. Time-domain codes (Zhu at al, 1995 [2]; LAMP, 1998 [3]; Wellicome et al, 1995 [4]) solve the governing potential-flow

equation around the ship with the corresponding free-surface and body boundary conditions. Although the potential-flow equation (Laplace's equation) is linear, nonlinearities are introduced through Bernoulli's equation and through the nonlinear free-surface and body boundary conditions. Time-domain potential-flow solutions are usually very expensive and inadequate for real-time predictions. Furthermore, the issues of nonlinearities at the free-surface and body boundary conditions pose severe challenges.

Strip-theory predictions (Korvin-Korvosky and Jacobs, 1957 [5]; Salvesen at al, 1970 [6]; Ogilvie and Tuck, 1969 [7]) are based on 2D evaluations of the ship parameters, whereby the ship is divided into several 2D transverse sections (strips) along the ship's longitudinal axis. These sections are assumed not to interact with each other. The 2D parameters are usually evaluated using potential-flow theories. The three-dimensional (3D) parameters are found by integrating the forces acting on the individual strips. The strip theory has many limitations, including its intrinsic linearization approach, the 2D approach, and the treatment of the free-surface conditions; many attempts have been done to overcome some of these limitations as will be discussed later.

System identification techniques are widely used to study and predict ship motions. These techniques include nonparametric approaches where the motions are identified without using models (governing equations) and parametric approaches that aim to uncover a set of parameters of an adopted model. System identification techniques require data usually obtained from numerical codes or from model-scale or full-scale testing of the ship. The testing is usually done in towing tanks (Spouge and Ireland (1986) [8]; Spouge and Collins (1986) [9]) and, occasionally, in real seas (Abkowitz, 1980 [10]). The numerical codes are usually potential-flow codes. The data gathered from these tests or codes are then processed to extract information related to the physics of the ship motions. In the case of parametric identification, this information is given in terms of parameters that appear in the governing equations of motion (models). In situations where the interest is in the amplitude and statistics of the ship motion, the prediction is usually based on nonparametric quantities, such as transfer functions and response amplitude operators (RAOs).

Small-amplitude motions can be modeled as linearly uncoupled or coupled modes. On the other hand, for large-amplitude motions, one needs to examine the nonlinear coupling among ship modes. Nonlinearities cause resonances that can amplify certain motions significantly. Besides being important by itself, identification of the linear coefficients is a prerequisite for the identification of the nonlinear coefficients. Besides the linear and nonlinear coefficients, other physics come into play and must be considered. For instance, the linearly coupled equations governing ship motions contain coefficients that depend on its forward speed. Accurate parametric models for ship motion must account for all parameters and physics of ship motions.

Based on the above discussion and on the literature review, it is obvious that there is a need for a methodology to establish a 6DOF model for ship-motion prediction. Time-domain numerical codes that solve potential-flow equations are usually expensive to run. Also, they cannot be used for applications that require fast calculations, unless simplifications are imposed on the physical problem. Strip-theory codes are much cheaper to run, but they also involve many simplifications. Some time will pass before reliable strip-theory codes can be established, which can handle nonlinearities and large-amplitude motions. Another concern in using strip-theory methods is the effect of the froward speed. The correct dependence of the parameters on the forward speed is not clear since different strip-theory methods give different forms of this dependence. On the other hand, system-identification techniques are very helpful in characterizing, predicting, and controlling ship motions. Based on the above review, most of the identification work has focused on one- or two-degree-of-freedom models.

1.2 Research Objectives

In this work, we attempt to establish an identification methodology that can handle general finite-degree-of-freedom (FDOF) models of ship motions. The first step in achieving this objective is to derive the correct form of the equations of motion. This form should

contain all relevant linear and nonlinear terms. Moreover, it should explicitly specify the dependence of the linear and nonlinear parameters on the forward speed. In this work, the energy-formulation approach is utilized to obtain full nonlinear ship-motion equations. The advantages of using the energy formulation are that self-sustained motions are not allowed (Nayfeh et al, 1974 [11]) and the dependence of the parameters on the forward speed is derived explicitly (Marshall et al, 1982 [12]). An efficient index notation is used to derive the full nonlinear equations up to third order. The method can be easily extended to obtain nonlinear equations of higher order. Numerical data generated with the LAMP code are used to identify the parameters of the models. The ship studied in this work is a Series 60 ship, which is a military cargo ship. We use state-of-the-art analysis and identification techniques to determine the coefficients in the linearly coupled equations and the effects of the forward speed on these coefficients. We also present a new analysis technique, namely, the circular-hyperbolic decomposition (CHD), which avoids the leakage effects associated with the discrete Fourier transform (DFT). We use this technique to determine quantities such as transfer functions and response amplitude operators (RAOs). We also present a methodology for the identification of the nonlinear coefficients in the coupled equations.

Chapter 2

Prediction of Ship Motions

In this chapter, a summary of the use of time-domain potential-flow solvers and strip-theory methods in ship-motion prediction is presented. This summary is followed by two sections on system identification. The first one discusses system-identification concepts in general terms and the second one reviews the application of identification techniques for the prediction of ship motions.

2.1 Prediction of Ship Motions Using Time-Domain Numerical Solutions

The fluid flow around ships is usually considered to be potential; that is, inviscid and irrotational. This assumption is reasonable since the effects of viscous damping on ship motions are small. One exception is the roll motion, where viscous damping has a significant effect and must be considered for accurate predictions. The potential flow is governed by Laplace's equation, which is linear. Two kinds of boundary conditions are involved in the problem of ship motions in seas. The first is the body boundary condition, which represents the fact that the fluid cannot penetrate the solid surface and must slide along the surface. The

second is the free-surface boundary condition, which represents the fact that the air and water pressures on both sides of the interface must be equal and that water particles cannot penetrate the free surface. Nonlinearity is involved in applying both boundary conditions. The main difficulty in treating these boundary conditions is that the shape of the free surface is not known in advance and that the wetted part of ship changes with time. For an accurate solution, the shape of the free surface should be calculated as part of the solution and the updated wetted surface should be taken into account.

Once the potential-flow equation is solved, Bernoulli's equation is applied to find the pressure distribution over the ship's hull. The pressure is then integrated to yield the total hydrodynamic forces and moments exerted on the ship. Because Bernoulli's equation is nonlinear, the hydrodynamic forces and moments are also nonlinear. Adding the hydrodynamic, hydrostatic, and propulsion forces and moments yields the total forces and moments acting on the ship's body. These total forces and moments cause the ship motions and determine the position and orientation of the ship. The hydrostatic forces and moments result from the hydrostatic pressures caused by a displacement of the water volume (buoyancy). The hydrodynamic forces and moments can be divided into different components, which include radiation, forward speed, wave, and diffraction forces and moments.

1. **Radiation forces and moments** are due to the oscillatory motion of the ship. They include both the added mass and damping effects. The added mass is associated with the acceleration of the fluid adjacent to the ship's body. The damping forces and moments result from the generation of surface waves due to the ship motion. The added-mass forces and moments are proportional to the ship accelerations, while the damping forces and moments are proportional to the ship velocities.

2. **Forward speed forces and moments** are exerted on the ship due to its motion in the forward direction. These forces and moments cause the ship to sink and trim.

3. **Wave forces and moments (Froude-Kriloff)** are the result of the existence of the wave potential, assuming no interaction between the waves and the body.

4. **Wave diffraction forces and moments** result from the diffraction potential due to the interaction between the body and the waves.

The hydrostatic and Froude-Kriloff forces should be calculated with the ship at its exact position, taking into account the real wetted surface. This requirement introduces nonlinearities. Also, when solving for the potential, the nonlinear boundary conditions should be applied at the exact wetted and free surfaces. A brief review about advances in applying the nonlinear free-surface conditions can be found in O'Dea and Wladen (1985) [13].

Solving the full nonlinear problem with exact boundary conditions is extremely difficult, if not impossible. Many simplifications are usually made for engineering applications. One simplification is to linearize the body boundary condition at the mean wetted surface. Another simplification is to linearize the free-surface condition at the mean free surface. Also, the hydrostatic and Froude-Kriloff forces can be calculated considering the mean wetted surface of the ship, which renders them linear. Numerical codes that solve the potential flow around the ship differ in the degree of the assumed simplifications and in the implementations used for solving the flow. One implementation for solving the potential-flow problem is to use the panel method. A simplified description of this method is to divide the ship into a number of panels and then locate a potential source in each panel. Each panel source has a potential that affects the other panels and the flow around the ship. The problem is transformed into finding the source strengths that will satisfy all boundary conditions and do not generate a net mass. Instead of using sources, one can formulate the problem using Green functions. Another option is to use Rankine sources or a combination of Rankine sources and Green functions. Also, one can panelize part of the free surface. Finite-element methods (FEM) have also been used in solving potential-flow problems.

Wellicome et al (1995) [4] introduced a method based on slender-body theory to calculate the sway force and yaw moment on a slender ship under a drifted forward motion. Vortex shedding from the bilge corner was also taken into account. The hull sections were represented by source elements and discrete vortices. The calculations were performed for three

different ships. Reasonable agreement was obtained for the sway force. The agreement for the yaw moment was not as good. Ohyama and Tsuchida (1994) [14] developed a numerical method for the analysis of ship motions in a harbor. The method is a combination of a three-dimensional boundary-element model and a two-dimensional finite-element method. The added mass and damping coefficients calculated using this method were compared with coefficients obtained using a conventional model and the results showed a favorable agreement. Zhu and Katory (1995) [2] introduced a time-domain mathematical model for solving the problem of a 3-D body moving in sea with constant forward speed. This model allows the body boundary conditions to be exactly fulfilled. The diffraction-radiation problem was also considered. No restrictions were placed on the wave direction and the motions could be large. Comparisons with other theoretical and experimental results showed excellent agreement. Van Oortmerssen at al. (1986) [15] described a model for the prediction of motions of and loads on ships in irregular waves, wind, and current. This model was validated by comparison with experimental data; good agreement was obtained. Wu and Taylor (1990) [16] presented a mathematical formulation of the linearized potential theory for a slowly translating body undergoing oscillations in deep water. The derivation is based on a perturbation series in terms of the forward speed. The results showed good agreement with finite-element solutions. Wong and Calisal (1996) [17] presented numerical algorithms for the calculation of the hydrodynamic forces acting on slender bodies using parabolized slender-body theory. The parabolized formulation transforms the three-dimensional potential problem into a series of two-dimensional wave-maker problems. Nonlinear free-surface conditions are used in the calculations. The computation marches from the bow to the stern along the ship length.

In this work, a potential-flow code called "Large Amplitude Motions Program" developed by the Science Applications International Corporation (SAIC) is used to generate simulated data of a ship motion (LAMP, 1998 [3]; Lin et al [133]). LAMP can predict time-domain linear and nonlinear motions of and loads on floating bodies with and without forward speed in various sea states. In LAMP, the submerged body surface at each time step is divided into a number of panels over which linearized transient free-surface sources are distributed.

Linearized free-surface conditions are also used. Both body-linear and body-nonlinear conditions are implemented. For nonlinear calculations, the position and orientation of the body are updated at each time step and the underwater body surface is repanelized. Several types of formulations are used. The first formulation utilizes transient Green functions. The second formulation utilizes a mixed source formulation in which both Rankine sources and transient Green functions are used. The third formulation is based on impulse response functions (IRF). Viscous effects on the roll motion are introduced with empirical equations.

2.2 Prediction of Ship Motion Using Strip Theory

Strip theory is the most used approach for determining the parameters of the ship-motion equations. This reality stems from its simplicity and efficiency of calculations. However, strip theory suffers from many disadvantages, which include the 2D approach, linear assumptions, and simplifications of the boundary conditions. In strip theory, the 3D-ship-motion coefficients are expressed in terms of integrals of 2D sectional coefficients. These coefficients are then calculated with the assumption that the 2D sections do not interact with each other, which is physically not true. There are several ways to calculate the 2D coefficients (Salvesen et al, 1970 [6]). These include the Lewis-forms method, the Tsai-Porter close-fit mapping method, and the Frank close-fit source distribution method. In all three methods, the linear water-wave theory is applied, and the viscous effects are neglected. In these methods, a velocity potential is determined for a cylinder oscillating in an otherwise undisturbed free surface in the sway, heave, and roll motions. Bernoulli's equation is then applied to the velocity potential to calculate the pressure distribution on the cylinder. Integration of the pressure yields the added mass and damping forces. The three methods differ in the way the boundary condition (cylinder-wall condition) is applied.

The use of strip theory to determine ship motions started with Korvin-Korvosky (1955) [19] and Korvin-Korvosky and Jacobs (1957) [5]. Formulas for the added mass and damping

coefficients were theoretically derived. However, the coefficients do not satisfy the symmetry conditions obtained by Timman and Newman (1962) [20]. Since then, many attempts to improve this theory have been made. Among these attempts are the rational strip theory of Ogilvie and Tuck (1969) [7] and the new strip theory of Salvesen et al (1970) [6]. The results of both attempts satisfy the symmetry conditions. The formulation of Salvesen et al (1970) [6] includes the heave, roll, pitch, sway, and yaw equations. One main difference between the different strip theories is the dependence of the coefficients on the forward speed and the treatment of the boundary conditions. In general, all of the strip-theory calculations give satisfactory results for slender-body ships with small amplitude motions, where the nonlinear and three-dimensional effects are insignificant.

Many attempts have been made to overcome some of the shortcomings of strip theory. Wang (1976) [21] combined the strip-theory approximation and the dynamic theory to derive the hydrodynamic coefficients of ship motions. The dynamic theory treats the fluid and the body together as one dynamical system. The classical dynamic theory treats the fluid as an unbounded medium, while Wang's formulation takes into account the existence of the free surface. The results of this approach were very similar to those derived by Salvesen et al (1970) [6]. As a matter of fact, the two methods become identical when the interaction between the body and the free surface is neglected. Troesch (1981) [22, 23] used the slender-body theory to derive formulas for the sway, roll, and yaw motion coefficients. The results were compared with experimental data; where the theory was found to compare well with the experimental results. Liu et al (1996) [24] tried to extend the strip theory and apply it to large-amplitude motions. An attempt was done to include some nonlinear effects by taking into account the instantaneous variations of the wetted hull surface during motion and its effects on the ship hydrodynamic characteristics. The method is a quasi-steady approach, which does not take into account the memory effects. Crossland et al (1993) [25] conducted a series of experiments to measure the heave and pitch decay-time histories of a model ship. The aim of these experiments was to explain the overprediction of the sectional damping obtained using a strip-theory program. The overprediction of the damping resulted in poor

predictions of free-decay motions. This issue has not been resolved completely and it has been concluded that strip theory should be used only in low-amplitude motions when making seakeeping predictions. Tao and Incecik (1998) [26] presented a time-domain prediction method based on strip theory. The method accounts for the nonlinear restoring and damping forces. The added mass and damping coefficients are calculated at the instantaneous submerged section. The calculations were validated by a series of experiments.

A program called "FREDYN", based on a time-domain extended strip-theory approach, has been developed to simulate extreme motion behaviors (Burton and deKat, 1998 [1]). FREDYN has been developed by a consortium called "Cooperative Research Navies" (CRNav). The group consists of members from the Australian, Canadian, Netherlands, United Kingdom, and United States Navies, in addition to the U.S. Coast Guard, the Maritime Research Institute Netherlands (MARIN), and other research establishments. As mentioned before, many research works are devoted to improving strip-theory predictions, including the applicability to situations where the 3D and nonlinear effects are significant. A brief review of the progress in this area can be found in Tao and Incecik [26].

2.3 Prediction of Ship Motions Using System Identification Techniques

System identification models the physics of ship motions and allows for improved prediction and control. Many techniques can be used for system identification. These techniques can be classified into several categories. In this section, a brief review of system-identification concepts is given. Then, applications of these concepts and techniques to ship-motion prediction is presented.

2.3.1 System Identification Concepts

System identification involves characterization of the dynamic behavior of a system based on its input-output data. In practice, sufficient a priori information about the system might not be available. Therefore, one needs to conduct experiments on the system to observe its behavior and collect the necessary input-output data. A traditional definition of system identification is given by Zadeh (1962) [27] as "Identification is the determination, on the basis of input and output, of a system within a specified class of systems, to which the system under test is equivalent". Thus, the identification process involves three categories: a class of models, a class of input signals, and an error criterion. Reviews of system-identification techniques are given in several books (Eykhoff, 1974 [28]; Juang, 1985 [29]; Bendat, 1990 [30]; Unbehauen and Rao, 1987 [31]; Goodwin and Robert, 1977 [32]; Norton, 1986 [33]) and survey papers (Astrom and Eykhoff, 1971 [34]; Billings, 1980 [35]; Mehra, 1979 [36]; Niederliski and Hajdasinski, 1979 [37]; Strejc, 1979 [38]; Young, 1979 [39]; Unbehauen, 1998 [40]).

Model Structures

Model structures are characterized in many different ways, parametric versus nonparametric, linear versus nonlinear, continuous versus discrete, deterministic versus stochastic, time-domain versus frequency-domain, etc. Since many of the identification techniques can be formulated for both discrete and continuous systems, differentiation between these two categories will only be made as needed.

Nonparametric Identification

Nonparametric system identification is used when no or little information is available about the actual form of the system dynamics. This type of identification does not require the specification of a system order explicitly. Rather, it gives quantities that allow for replica-

tion of the system output. This type of representation includes impulse-response functions for continuous systems, pulse-response functions for discrete systems, transfer functions, response-amplitude operators, and Volterra series.

Parametric Identification

Parametric system identification is used when enough knowledge about the system dynamical behavior is known. A model that describes this behavior is constructed with unknown coefficients to be determined. This type of identification, for linear and nonlinear systems, has different representations including input-output, state-space, and modal representations. A parametric model can be described as "linear in the parameters" if the generalized error (discussed below) is linear in the parameters. This concept is related to the relation between the dependent variables and the parameters. This is to be distinguished from the concept of dynamic linearity, which is related to the relation between the dependent and independent time variables (Astrom and Eykhoff, 1971 [34]).

It is also worth noting that there is no well-defined cut for distinction between the parametric and nonparametric representations. Many times, it is possible to convert parametric identification results into a nonparametric form and vice versa. For instance, response functions can be analyzed to obtain information about the natural frequencies and damping ratios, which are parameters that can be found directly by other parametric techniques.

Input Signals

Different identification techniques require different input signals, such as impulse functions, step functions, sinusoidal functions, random inputs, white noise, free response, etc. In general, it is desirable to have techniques that can work with different types of inputs. Restrictions on the type of input are at times required to obtain consistent estimates. Some identification techniques require input signals that are independent of the process distur-

bances. A very important restriction is the condition of "persistent excitation", which is required for consistency in least-squares and maximum-likelihood estimates (Astrom and Eykhoff, 1971 [34]; Goodwin and Robert, 1977 [32]).

Error Criterion

Any system-identification technique requires the minimization of a scalar function. This function is sometime called the objective function or the loss function. It is mostly expressed as a functional of an error that needs to be minimized in a least-squares sense. In this sense, the identification becomes an optimization problem. This function represents the difference between the real system behavior and the model behavior. Different choices of the error representation have been given (Astrom and Eykhoff, 1971 [34]). These choices include the output error, the input error, and the generalized error (which includes the effects of the two previous errors, with a special case called the equation error). The form of the error determines the type of the noise filter implemented in the technique, and thus it also determines the type of noise that can be handled by the identification technique (e.g., white noise, autocorrelated noise, etc.). Based on the error criterion, different identification techniques can be distinguished, including the least-squares (LS) method, the generalized least-squares (GLS) method, and the maximum likelihood (ML) method.

Implementations of Identification Techniques

The numerical implementations for the solution of the estimation problem can be of different types: direct, recursive, iterative, and real-time implementations.

- In the **direct implementation**, no recursion or iteration is utilized and matrix inversion is required.
- In the **recursive implementation**, the estimation problem is formulated in such a way that the parameter estimates at a certain time step are equal to the parameter

estimates at the previous time step plus a correction that depends on the error in the estimates at the previous step. This is suitable for on-line estimations, where one does not need to use the whole time record to find the new parameters at each time step. Only the last available input-output pair along with the error at the previous time step are utilized.

- The **iterative implementation** is similar to the recursive implementation except that the time step is replaced by the iteration number.
- **Real-time identification** is required when the parameters are time varying. Techniques, such as the recursive least-squares and Kalman filter, can be utilized for this purpose.

Quality of Estimation

There is no universal way to assess the quality of the estimation. The estimation can be accurate in one way and very inaccurate in another way (Astrom and Eykhoff, 1971 [34]). Usually the accuracy is associated with the goal of the identification. For example, if the goal of the identification is the prediction, then the accuracy can be defined based on the deviation between the model and real outputs. The quality can also be assessed based on a statistical description, such as the bias of the estimate.

2.3.2 Parametric Identification of Linear Systems

This section reviews parametric system-identification techniques for three different representations, namely, the input-output, state-space, and modal representations. Other forms of representations exist, such as the canonical forms for both state-space and input-output representations. Canonical forms seek to represent the problem in a simple way and with a small number of parameters. They can be obtained by performing transformations on the system metrics (Niederliski and Hajdasinski, 1979 [37]).

Input-Output Representations

The most important model in this representation is the ARMA (auto regressive moving average) model (Pandit and Wu, 1993 [41]) and its variant the ARMAX (X is for eXogeneous) model. Different identification methods are designed for this model, with variations that depend on the form of the implemented noise filter. The least-squares (LS) method and its extensions are used in connection with the ARMA model. The LS method estimates the parameters for the ARMA model, which minimize the output error. It provides unbiased estimates of the parameters if the error is described by white noise. If the noise is autocorrelated (colored), the estimation will be biased. In this case, the LS method can be extended to handle other kinds of noise by introducing additional filtering for the autocorrelated (colored) error to reduce it to white noise. The parameter vector in the LS method does not include "error parameter". The extended methods include those parameters with various complexity. Among these methods are the maximum likelihood (ML), the instrumental variable (IV), and the repeated least-squares (RLS). These extended methods require more than one step for the solution of the parameters.

State-Space Representations

State-space models are sets of equations of a particular form that enjoy certain advantages, including the availability of efficient computational techniques for solving them. A state can be defined as a set of quantities that are independent of each other and independent of present and future inputs, and for which the present state is sufficient for predicting the present and future outputs given the present and future inputs. A state-space formulation of ship-motion equations is given in Section 4.3.1.

- **Kalman Filter**

  The Kalman filter (KF) is widely used in state estimation problems. It provides an optimal estimate of the system states provided that the system and noise dynamics are

completely known. The noise should be Gaussian, zero mean, and white, with known covariance (Juang, 1994 [29]). The initial state should be a Gaussian distribution and the initial state covariance should be known. The performance of the Kalman filter deteriorates if these conditions are not met. Although the KF is a state estimation technique, it is often used as a parameter estimation technique. This is accomplished by creating an augmented state filter, which contains both the system states and the estimated parameters where the parameters are considered as constant states. When the KF is applied, the parameters converge when their values become constant with time. So, in principle, there is no large difference between the state estimation and parameter estimation techniques (Eykhoff, 1974 [28]). Actually, it can be shown that the KF and recursive LS methods are equivalent (Astrom and Eykhoff, 1971 [34]).

- **Lainiotis Filter**

  Another filter that proved to be effective is the Lainiotis filter (LF) (Lainiotis and Kaisikas, 1989 [42]). It has an advantage over the KF when the system model is partially unknown or time varying. For systems that are completely known, the matched Kalman filter provides the best state estimate. Otherwise, the Lainiotis filter outperforms the KF (mismatched Kalman filter) (Lainiotis et al, 1992 [43]).

- **Eigensystem Realization Algorithm (ERA)**

  The ERA is a least-squares fit of the Markov parameters (pulse-response function) of a system. It is applicable to multi-degree-of-freedom (MDOF) discrete systems. It utilizes the singular value decomposition (SVD) to find a minimum realization of a system (Juang and Pappa, 1985 [44]). The idea of minimum realization identification started with Ho and Kalman (1965) [45], where it was formulated for noise-free data. Modifications of the minimum realization technique were introduced to handle noisy data. Among these modifications is the utilization of the SVD. The ERA can be used to find the system matrices, which provide information about the number of modes, the natural frequencies, the damping ratios, the modes shapes, and the initial

modal amplitudes (Juang and Pappa, 1985 [44]). The ERA in general gives biased estimates. Juang (1994) [29] presented a new implementation for the ERA utilizing data correlation to remove the effect of bias. A description of the ERA is given in Section 4.3.2.

Modal Representations

The modal representation is a summation over the different modes participating in the signal. Each term in the summation involves modal parameters, which include the eigenvalues (frequencies and decay rates) and eigenvectors (mode shapes). Some techniques estimate all of the modal parameters and other techniques estimate a partial set of these parameters.

- **Ibrahim Time Domain (ITD) Method**

  Ibrahim and Mikulcik (1977) [46] introduced a method for the direct identification of the modal parameters (number of modes, natural frequencies, damping ratios, and mode shapes) from free-decay data. This method is basically a least-squares fit of the free-decay response and is applicable for MDOF discrete systems. The method cannot provide information about the masses or the initial modal amplitudes because it utilizes free-decay data. However, modifications can be formulated to provide that information. The ITD can accommodate oversized mathematical models over a wide range of frequency separations, damping ratios, mode-response levels, and signal to noise ratios (Ibrahim and Pappa, 1981 [47]; Pappa and Ibrahim, 1981 [48]).

- **Prony's Method**

  If a signal is one-dimensional (1D), then it can be analyzed using Prony's method (Prony, 1795 [49]). This method is a transformation procedure, which provides an exact map between the data and the results. It is a least-squares algorithm that can be used to uncover the frequency, phase, and damping information of the signal in the absence of noise. Mode shapes cannot be determined using Prony's method.

- **Complex Exponential Algorithm**

  The complex exponential algorithm (CEA) (Spitznogle and Quazi, 1970 [50]; Brown et al, 1979 [51]) is a generalization of Prony's method. It is an estimation procedure that uncovers the frequencies, phases, and damping information of a signal in the presence of Gaussian noise. If the noise is not white, then the estimate is biased.

- **Circular-Hyperbolic Decomposition**

  The circular-hyperbolic decomposition (CHD) is a special case of the CEA (Fahey et al, 2000 [52]; Suleiman et al, 2000 [53]). If the signal does not decay or grow with time (e.g., steady-state solutions), then the CEA can be constrained to yield a symmetry relationship that reduces the minimum number of samples required for the estimation. The CHD provides information about the frequencies and the associated phases and amplitudes of a signal with no leakage effects.

Surveys of the linear frequency- and time- domain modal estimation techniques are found in (Fahey and Pratt, 1998 [54]; Fahey and Pratt, 1998 [55]).

2.3.3 Nonparametric Identification of Linear Systems

As mentioned earlier, nonparametric techniques do not require extensive knowledge about the form of the system dynamics. This section briefly introduces some of these techniques.

- **Response Functions**

  Among the oldest nonparametric tools in modal system identification are the frequency-response functions (FRF) and the impulse-(pulse-) response functions (I(P)RF). The FRF is the Laplace (z-) transform of the (I(P)RF). Many traditional test procedures are available for their identification, including shock tests, sine-dwell tests, sine-sweep tests, and tests that involve random inputs. The measured time-domain input and output signals (e.g., due to a random input) can be transformed into the frequency

(z-) domain and analyzed to obtain the FRF or PRF. The transformation to the frequency domain is usually performed using the discrete Fourier transform (DFT). The inverse discrete Fourier transform (IDFT) is used to transform the results back into the time domain, if needed. In ship motions, interest is usually in the RAO, which is the amplitude of the transfer function. The RAO is frequently determined using the DFT, which suffers from leakage effects. In our work, CHD is applied to find ship RAOs to avoid the leakage problem, as explained is Section 5.

- **Bayes' Estimation**

  According to this method, an estimate is the probability distribution conditional on the past history (Strejc, 1979 [38]). So, one estimates the future value of the output based on the past values for the input and output and the current value of the input, without knowing the system parameters. The Bayes' concept calculates the probability distribution of the future output conditional on the current input and the past output.

- **Observer/Kalman Filter Identification (OKID)**

  The OKID technique is a method that can be used to obtain the pulse-response functions (Markov parameters) in the time domain (Juang, 1994 [29]), without the need to transform the results into the frequency domain. It uncovers the Markov parameters in a multi-step solution. First, the observer Markov parameters are calculated. Then, the system parameters are calculated. This method utilizes LS fits and is closely related to the Kalman filter technique.

- **Random Decrement**

  The random decrement technique is a tool that can be used to extract the free-decay response of a system from its random forced response (Caughey and Stumpf, 1961 [56]). The method utilizes output measurements only. Strictly speaking, the result of the random decrement represents the autocorrelation function (Vandiver et al, 1982 [57]). If the input is a random white noise, then the result of the random decrement also represents the free-decay response of the system. As long as the response is

band limited and the input is broadband, the result of the random decrement can be interpreted as the free-decay response, even if the input is not white noise. It should be noted that this method has been extended to nonlinear systems (Ibrahim, 1977 [58]; Haddara, 1992 [59]).

2.3.4 Nonlinear System Identification

Nonlinear systems are modeled in state-space and input-output representations. Some nonlinear identification techniques include the following:

- **Least-squares methods** which were described in connection with linear parametric identification. The same concepts apply to the nonlinear case.
- **Gradient techniques** whereby the loss function is minimized using its gradient with respect to the parameters.
- **Stochastic approximations** which provide means for choosing the correction term (gain) in a recursive identification.
- **Quasilinearization techniques** whereby the problem is linearized at each time step using the Jacobian of the nonlinear vector.
- **Functional series methods** which include
  - the Volterra-series method, it is a generalization of the concept of the transfer function and the input-output convolution in the linear case. The use of this method involves the evaluation of the Volterra kernels.
  - Expansion of the nonlinearities in a series of orthogonal functions.
  - Expansion of the nonlinearities in power series.
- **Nonlinear filtering techniques**, such as the extended Kalman filter.

- **Perturbation-based techniques**.
- **Higher-order spectral moments**.
- **Combinations of perturbation techniques and higher-order spectra**.
- **Neural networks** which are used in adaptive control systems. System control is out of the scope of this proposal. Therefore, the method is mentioned here just in relation to nonlinear parametric identification.

Nonparametric Identification of Nonlinear Systems

Nonparametric identification seeks to determine the functional representation of the system to be identified. The Volterra series and the Wiener kernel are examples of this type of identification. These two methods are computationally expensive and sometimes have convergence problems. Another nonparametric technique is the expansion of the restoring forces in a series of Chebyshev polynomials and utilization of regression techniques to estimate the parameters in the series (Masri and Caughey, 1979 [60]). This technique was extended to MDOF systems and generalized for the use of arbitrary orthogonal sets of functions (Udwadia and Kuo, 1981 [61]). The nonlinear expansion can also be done in term of power series (Yang and Ibrahim, 1985 [62]). This type of identification suffers from some restrictions, such as the need for measurements of the displacement, velocity, and acceleration simultaneously. Haddara (1995) [63] combined the random decrement technique with neural networks for the identification of nonlinear systems.

Parametric Identification of Nonlinear Systems

Parametric identification seeks to determine a set of parameters in an assumed model. Least-squares methods are widely used in this type of identification, which usually involve matrix inversion. Filtering techniques are also used in nonlinear system identification. The applicability of the Kalman filter, discussed above in relation to linear parametric identification, has

been extended to estimating nonlinear parameters. The extended Kalman filter (EKF) is one example of this extension (Yun and Shinozuka, 1981 [64]). With this filter, the nonlinear system is linearized around a reference state and the linear filter is applied to the deviation from the linearized system.

Another example of the application of linear identification techniques to nonlinear systems can found in (Ibrahim, 1983 [65]; Horta and Hanks, 1983 [66]), where the Ibrahim time domain technique has been applied in a quasi-linear modal identification of nonlinear systems. Such an approach can be used to detect nonlinearities and their type by performing the identification at different levels of excitation and studying the changes in the parameters.

In general, the parametric techniques used in system identification involve a large number of unknown parameters, which need to be determined simultaneously. This creates a problem because matrix inversion is needed in one way or another. Also, many of the parameters are small and their effects on the response are also small. In many cases, the responses due to such parameters cannot be distinguished from the system noise. In such cases, the inverted matrix is usually ill-conditioned and the parameter estimates are inaccurate. Furthermore, many of the parametric estimation techniques require two or three variables to be measured simultaneously (e.g., displacement, velocity, and acceleration), which is inconvenient.

An unconventional approach is to use modern methods of nonlinear dynamics to find approximate analytical solutions to a nonlinear system and conduct numerical or experimental tests to gather response data. The parameters of the analytical solution are then determined by performing a regressive analysis. This approach has the advantage that only few variables at a time are needed for the identification. The approximate solution can be found using perturbation techniques, such as the method of averaging (Krylov-Bogoliubov technique) and the method of multiple scales (Nayfeh, 1973 [67]; Nayfeh, 1981 [68]; Nayfeh and Mook, 1979 [69]). An example of the use of this approach can be found in Hanagud (1985) [70], where the method of multiple scale is used to identify a second-order system with cubic nonlinearly and is compared with other direct identification techniques. The results showed

that the perturbation-based approach outperformed the direct approach, especially for high noise-level cases and small nonlinearities.

A recent approach to the problem of parametric identification of nonlinear systems combines perturbation techniques with the exploitation of resonances associated with nonlinear dynamics (Nayfeh, 1985 [71]; El-Badawi, 2000 [72]; Fahey and Nayfeh, 1998 [73]; Feeny, 1986 [74]; Hajj et al, 1995 [75]; Nayfeh et al, 1997 [76]). These phenomena include subharmonic, superharmonic, combination, and ultraharmonic resonances, self-excited oscillations, jumps, saturation, bifurcation, and nonexistence of periodic responses to harmonic excitations (Nayfeh, 1985 [71]; Nayfeh and Mook, 1978 [77]; Oh et al, 1993 [78]; Nayfeh et al, 1973 [79]; Mook et al, 1974 [80]; Nayfeh, 1988 [81]; Nayfeh and Oh, 1995 [82]; Nayfeh, 1983 [83]; Nayfeh and Jebril, 1987 [84]). Using this approach, experiments can be designed with different types of resonances in order to identify a few parameters from each experiment. This allows for accurate predictions of the parameters since the response is large and only few parameters are identified in each experiment. Also, a parameter can be found using more than one experiment, which allows for a double checking of the estimated parameters. Using this approach, Hajj et al (1997,2000) [75, 85] proposed also using phase measurements with higher-order spectral moments (Hajj et al, 1993 [86]) to characterize damping and determine nonlinear parameters.

As a conclusion of this section, we note that an identification technique is characterized by a model structure, an input signal, and a criterion that quantifies the error and types of noise filtering. The choice of a particular method or another is dependent on the problem at hand and on the available experimental and numerical data. Most, if not all, of the methods discussed above have been applied to ship-motion identification.

2.3.5 System Identification for Ship Motions Prediction

A large body of research has been devoted to system identification for ship motions. The bulk of this research is focused on the roll motion, since it is the most important motion in relation

to ship safety and because roll damping is difficult to predict. Besides the roll motion, the heave and pitch motions and their coupling have been of great interest also. In general, most of the identification work is for a single-degree-of-freedom (SDOF) ship motion (e.g., roll) or two-degree-of-freedom (2DOF) ship motions (e.g., roll and pitch). Little work has been done to identify six-degree-of-freedom (6DOF) ship motions. Some of the identification techniques of ship motions were developed specifically for the roll motion and some of them, although formulated for a SDOF motion, can be extended to handle multi-degree-of-freedom (MDOF) motions. In the following, a review of the system-identification literature with respect to ship motions is presented. Differentiation among the different techniques is based on their applicability as real-time (on-line) or off-line techniques. Emphasis is given to the type of input and the data required for identification. Some of the techniques require random inputs (as a special case: white noise), while other techniques require free-decay data. Also, in some of the techniques, only the response data are needed (the excitation considered unmeasurable), while in other techniques both excitation and response data are needed.

Off-Line System Identification

Duthoit and Armand (1988) [87] proposed a "linearize-and-match" method for predicting the response statistics of nonlinear systems. The method consists of constructing an infinite series of linear systems. The excitation is assumed to be a zero-mean, stationary, and Gaussian random process with double-sided frequency spectrum. The method was applied to ship roll motion where the predictions compared well with simulated estimates. Gawthrop et al (1988) [88] described a method for estimating the parameters of a nonlinear SDOF model of ship roll motion. The estimation procedure utilizes a recursive linear LS algorithm and is based on the state-variable filter approach. The method applies to both free and forced excitation cases. The method allows for different kinds of excitations (e.g., sinusoidal, nonsinusoidal, modulated frequency and amplitude, etc.). The validity of the method was demonstrated by applying it to digitally simulated data and real data obtained from model

ships. Roberts (1985) [89] presented a method for the estimation of the linear and nonlinear roll damping parameters utilizing free-decay roll motion. The noise is assumed to be white. The method involves the use of a cubic spline interpolation of the peak amplitudes, followed by a parametric identification procedure. The method was applied to simulation and real free-decay data and accurate estimates were obtained. Roberts et al (1992,1994) [90, 91] developed a method for estimating the parameters of a SDOF nonlinear roll motion. The method utilizes the output alone, where the excitation force is assumed to be unmeasurable white noise. The method involves the use of Markov process theory and statistical linearization. It was applied to simulated data with both white and correlated noise input. Estimates of the nonlinear stiffness, damping parameters, and noise intensity levels were determined, and accurate results were obtained provided long-time records are available. For the case of a correlated excitation, the accuracy degraded, especially for high damping.

Smith and Werely (1999) [92] considered the identification of the nonlinear damping from SDOF transient data. Two methods were used: one is based on a Fourier series decomposition and the other is based on a Hilbert transform. Within some limits, both techniques produced accurate results for the nonlinear damping. Gawthrop (1984) [93] extended the state-variable method to transient unforced nonlinear systems corrupted with a constant offset and applied the method to simulated free-decay roll motion. Methods were developed by Mathisen and Price (1984) [94] for estimating linear and nonlinear roll-damping parameters from free-decay and forced tests. Two forms of forcing were considered: monofrequency motions and monofrequency excitations. The methods involve a Fourier series expansion and a constraint minimization technique. Two nonlinear damping models were considered: quadratic and cubic. The methods were tested using numerical and experimental data where reasonable accuracy was obtained. Kountzeris et al (1991) [95] presented an estimation technique based on the state-variable filter. The method was tested using experimental roll-motion data collected in a towing tank. The input force was estimated from wave-height measurements using transfer functions computed from diffraction theory. The method recursively estimates all of the parameters of the roll equation. Satisfactory conver-

gence characteristics were obtained and the final values were in good agreement with results obtained from alternate test methods.

Abkowitz (1980) [10] utilized the extended Kalman filter (EKF) to identify the hydrodynamic parameters of ships from simulated noisy data and real full-scale ship data. Linear and nonlinear parameters were identified. The identification included the study of the scaling and cancellation effects. The identification also provided a way for the direct measurement of ship resistance. Many maneuvering conditions were tested. The identification was applied to identify the surge, sway, and yaw motions. The input to the identification procedure consisted of the rudder deflection and the heading angle along with the above mentioned motions. The outputs were the hydrodynamic coefficients and the direction and magnitude of the current. The linear parameters were identified using mild maneuvers, and the nonlinear parameters were identified using moderate and violent maneuvers. The form of the equations used in the mathematical modeling was based on a Taylor series expansion, expressed in terms of linear and higher powers of the motion and control variables. The port-starboard symmetry was also taken into account. Very good agreement was obtained between the simulations based on the identified parameters and the full-scale trial data. It was shown that the smaller the number of the identified parameters is, the more accurate the parameters are.

Abkowitz and Liu (1988) [96] used system-identification techniques to estimate the resistance, powering, and maneuvering parameters of a ship from trials during a regular voyage, utilizing instruments normally used on board ships. Good accuracy was obtained. Comparisons with results from model tests revealed that scaling effects are significant. Liu (1993) [97] applied the EKF technique to estimate the ship resistance, utilizing simple sea trials during a ship's regular voyage. Good accuracy was obtained. Flower and Aljaff [98] obtained approximate analytical solutions of nonlinear differential equations, which represent a decaying roll motion using the Krylov-Bogoliubov averaging method. These solutions were fitted using experimental results taken from ship-model tests. The analytical solutions agreed well with the experimental data. Bass and Haddara [99] investigated the various forms of roll damping

of ships and introduced two techniques for the identification of the various roll parameters. These techniques were the "DEFIT" technique and the "energy method" (EM). The DEFIT is a parameter identification techniques based on fitting the experimental data to the solution of an assumed differential equation. The EM analysis is based on the equality of the rate of change of the total energy of a system to the rate of energy dissipated by damping. Simulated data was used to test both methods and good predictions were obtained. Haddara and Bennet (1989) [100] and Haddara and Cumming (1992) [101] used the EM to analyze roll-decay records of a set of experiments performed in towing tanks. Good prediction of the roll damping was obtained, which was dependent on the roll angle.

Haddara (1992) [59] and Haddara and Wu (1993) [102] extended the concept of random decrement, which is an averaging technique that has been used successfully to predict linear damping, to nonlinear systems. The extension involved the use of Markov process theory. Nonlinear roll damping was identified using this technique. The equations governing the random decrement were derived for a ship performing a rolling motion in random beam seas. The wave excitation was assumed to be an unmeasurable Gaussian white noise. Numerical simulations were used and accurate predictions of the equivalent nonlinear damping were obtained. On the other hand, predictions of the individual nonlinear parameters were not successful. Validation of the random decrement technique with experimental data (full scale and model tests) was also performed (Haddara et al, 1995 [103]). Good predictions of the natural frequencies were obtained. Predictions of the damping parameters were not consistently accurate due to the assumptions involved in the technique. Haddara (1995) [63] combined the random decrement technique with the neural networks technique to identify the parameters of the roll motion. The linear random decrement was utilized to estimate the natural frequency of the roll motion, while the neural networks technique was used to identify the linear damping and the nonlinear terms. The excitation level and the shape of the nonlinearities were not specified, although the excitation should be white noise. The method was applied to experimental data of a model ship. The results showed excellent agreement.

The above technique of Haddara (1995) [63] was also applied to identify the coupled linear heave and pitch equations (Haddara and Xu, 1999 [104]). They were modeled as a MDOF Markov process. The Markov process theory was then used to derive the random decrement equations. The input was assumed to be random white noise. The parameters in these equations were identified using neural networks. The method was validated using numerical and full-scale experimental results. As an input, both white noise spectra and JONSWAP spectra (which do not conform to the white noise assumption) were used for the simulation. For the JONSWAP spectra input, the method was found to be accurate for lightly damped motions. This is because the motion spectra are narrow banded compared to the input spectra. For heavily damped motions, the motions have broadband spectra, and the effect of the correlated input (nonwhite noise) becomes significant. Thus, the performance of the random decrement technique deteriorated and predictions became inaccurate. The neural networks were applied to study the sway and yaw motions (Haddara, 1996 [105]). The equations of the ship motion and the rudder deflection were derived using Taylor series expansions. The linear parameters were obtained using empirical data, while the nonlinear ones were obtained using neural networks. The method was tested using simulated data and the agreement was found to be very good. It should be stressed that several million iterations were needed to obtain this agreement.

Kountzeris (1988) [106] examined a SDOF roll motion. Simulated and real data were used to fit the roll equation. To identify the coefficients, the linear state-variable method, which can deal with both free and forced motions, was used. The results yielded accurate predictions, and bias effects due to noise were found to be negligible. Debonos (1993) [107] developed methods for estimating the linear and nonlinear damping and stiffness parameters of the roll motion and the stochastic excitation intensity. The validity of the methods were tested by applying them to simulated and model-test roll data. The developed techniques are the energy-envelope-based-identification method, the moment-equation-based identification method, and the spectral-analysis-based identification method. The stiffness parameters were found to be easily determined. The damping parameters were found to be much more

difficult to estimate. The results showed that it is not feasible to estimate both linear and nonlinear damping parameters in one step. The accuracy of the results were found to deteriorate with high damping, high nonlinearity, and narrow bandwidth of the excitation. Francescutto and Contento (1999) [108] presented theoretical, numerical, and experimental studies of the nonlinear phenomena associated with ship motion, namely, bifurcations and jump phenomena. Experimental model-scale roll data were analyzed using a technique based on the energy method (Haddara and Bennet, 1989 [100]). The identified parameters were used to obtain numerical simulations of the ship motion. Nonlinear phenomena were predicted using the numerical simulations based on the identified parameters.

Feeny (1986) [74] presented a system-identification scheme for a dynamic model of a ship at sea. The ship's equations of motion contained quadratic and cubic nonlinearities. The identification scheme was designed for the roll and pitch motions. The identification technique is based on the method of multiple scales and the exploitation of nonlinear resonances. The scheme utilizes the fact that the coefficients of each nonlinear term are manifested by only those resonances in which they play an important role. The scheme is not iterative and allows for a check of the estimated parameters several times. Nayfeh et al (1998) [109] discussed two mechanisms for roll instabilities and presented an approximate first-order closed-form solution based on the method of multiple scales. Fung (1998) [110] also utilized the techniques based on the method of multiple scales and the exploitation of parametric resonance. Heave, pitch, and roll equations were used in the study. The roll equation contained nonlinear terms that represent the parametric resonance due to the heave and pitch motions. The data used for the identification was numerically obtained using the LAMP code (LAMP, 1998 [3]). The nonlinear coupling parameters in the roll equation were accurately determined. Bikdash et al (1994) [111] studied the influence of different damping models on the nonlinear roll dynamics through a detailed Melnikov analysis. They introduced the concept of Melnikov equivalent damping and used phase-plane concepts to obtain simple expressions for the Melnikov damping coefficients. As an application, they considered the equivalence of the linear-plus-cubic and linear-plus-quadratic damping models, and they derived the condi-

tion under which the two models are equivalent. Simulations showed that, if this condition holds, then the two models not only have the same free-decay responses, but also have very similar forced steady-state and transient behaviors.

On-Line (or Real-Time) System Identification

The interest in real-time prediction started in the early sixties (Dalzell, 1965 [112]). The real-time prediction of ship motions is important for increasing the safety and operational capabilities of aircraft carriers. Cole (1968) [113] conducted analytical and experimental studies on the use of on-line analyses of random vibration. The results showed that on-line interpretation can be achieved by translation of the time history into a sum of autocorrelation functions. The results also showed that accurate on-line damping ratios, natural frequencies, mean-square values, and half-power points of the input can be obtained and that nonlinear systems can be detected. Kaplan (1968) [114] discussed various methods for short-term prediction of motion time history. The major result was the development of a means for calculating ship-motion time histories using a convolution integral representation. A kernel function derived from ship responses was applied to operate on input data in the form of current and past wave measurements at the ship bow. Model-ship motion predictions up to six seconds ahead were obtained. Yumori (1981) [115] studied the application and feasibility of real-time ship-motion prediction. He utilized a leading indicator method using an auto regressive moving average (ARMA) model to fit an input wave-sensor time history to the ship-response time history. Then, the obtained fit was used to predict the response from the most recent measurement. Experimental tests were conducted on a vehicle in sea states 4 to 5 at different speeds. Good predictions of the phase and amplitude of the heave motion were obtained for 2 to 4 seconds in advance, and good predictions of the phase were obtained for up to 8 seconds in advance.

The Kalman filter was utilized by Triantafyllou et al (1983) [116] to predict ship motions in real time. Estimation of the heave and pitch motions in one group and the roll, sway,

and yaw motions in another group were conducted for an application that involves VTOL aircraft. The Kalman filter was applied to numerically simulated data obtained using strip theory. Within certain limits, satisfactory approximations of ship motions were obtained. A multi-variate ARMA filter was utilized by Lin (1987) [117] to predict ship responses to random waves. The filter accounts for the directional response of the ship to ocean waves and the dynamic coupling of the ship motions. The filter was applied to the heave and pitch motions, and comparison with experimental tests showed that the ARMA filter accurately predicted the ship motion in real time (10 s ahead predictions were reported). Broome and Pittaras (1990) [118] studied short-time ship-motion prediction using an adaptive predictor. The predictor is based on the ARMA model. Adaptive predictors do not require prior information about the system and can predict model changes with time. Two experimental case studies of related marine systems were examined. The sway, yaw, and surge motions were involved in one case, while the roll and yaw motions were involved in the second case. This technique successfully predicted regular periodic motions, but performed less well in predicting irregular noisy signals.

Broome and Hall (1998) [119] and Broome (1998) [120] used the linear ARMA filter technique to obtain short-time predictions (10-15 second ahead) of the heave, roll, and pitch motions. The aim of the identification was to aid in the safe landing of aircraft. The identification was applied on-line using data from sensors installed on a real ship. Measurements of the input force were not utilized in the technique. Satisfactory prediction results were obtained. Lainiotis and Plataniotis (1994) [121] utilized neural networks to obtain on-line predictions of ship motions. The ship position estimation is viewed as an adaptive estimation problem with partially unknown parameters. The wave-excitation input is assumed partially or completely unknown. The performance is assessed using simulation experiments. A linear 2D state-space system was tested. The neural network estimator showed excellent performance. The performances of the neural network technique, the adaptive Lainiotis filter (ALF), and the Kalman filter were compared in a study involving the heave motion (Lainiotis et al, 1993 [122]). The results indicated that the ALF and the neural network techniques outperformed

the Kalman filter when the actual model is not completely known. Lainiotis et al (1992) [43] studied the application of the ALF to time-varying and partially unknown linear ship-motion parameters with non-Gaussian initial conditions. The ALF identified the true model even when it was changing and in general outperformed the Kalman filter. Chung et al (1990) [123] presented a new algorithm called "PSIE" for on-line prediction of ship motions. In this algorithm, the wave-excitation force is extracted from the estimated ship-motion data in a deterministic way. The prediction is performed by extrapolating the governing equations of the ship motion. The results of the new algorithm were compared with the standard Kalman filter. Two sets of motions were studied: the surge, sway, and heave and the roll, pitch, and yaw. The PSIE was applied to simulated and real data. It was found that the PSIE enhances the prediction of short-time ship motions. It also has a better ability to correct the modeling error of the governing equations. The method was also tested successfully in conjunction with a moving-target tracking control system mounted on a ship.

Use of Identified Models in Ship Simulators

For training and design purposes, ship simulators are very important. Simulation models are often used to predict a ship's behavior. Some of the previously mentioned ship-prediction techniques are used in such models. Horizontal ship motions are usually simulated using ship-handling simulators, in real-time environment, and including the man-controlled operation (Dallinga, 1986 [124]). Large-, medium-, and small-scale simulators are available. A ship-handling simulator consists of a ship's bridge, a computer, and a large visual screen. The environmental disturbances (waves, wind, etc.) are described mathematically. The equations describing a ship's maneuverability are usually adopted according to experimental test results. Vertical ship motions are simulated using a fast-time simulation model, in which control and environmental disturbances are represented in a numerical way. The motion characteristics are described using transfer functions obtained using 3D diffraction programs. These transfer functions are verified experimentally. Roll damping is calculated

using theoretical/empirical models. The effect of forward speed (sinkage and trim) is calculated using Tuck's formula (Tuck, 1966 [125]).

Chapter 3

Nonlinear Equations of Ship Motion with Forward-Speed Effects

Prediction of ship motions is important because it is directly related to the safe and economic operation of ships. As discussed in Chapter 1, different methods are available for studying and predicting ship motions. These include time-domain, strip-theory, and system-identification-based predictions. With the system-identification-based predictions, one avoids several problems encountered with time-domain and strip-theory predictions. This is, however, true only if the motions and their coupling are accurately modeled. For instance, for small-amplitude motions, one could model each motion (e.g., heave, roll, pitch, etc.) independently or as linearly coupled motions. For large-amplitude motions, one needs an accurate model that takes into consideration all physics of the problem. One issue is the nonlinear coupling among ship motions. Nonlinearities cause resonances, which can amplify certain motions significantly. Besides nonlinearity, other physics effects come into play and must be considered. For instance, it has been established that coupled equations governing ship motions contain coefficients that depend on its forward speed. However, the form of this dependence is not clear, and different theoretical approaches provide different forms of this dependence.

Nayfeh et al (1974) [11] developed the nonlinear equations governing the roll and pitch motions to third order and the equations governing six-degree-of-freedom motions to second order. However, these equations were restricted to ships having no forward speed. Guo (1981) [126] developed a nonlinear theory of ship maneuvering that is based on the hydrodynamics of arbitrary small motions superimposed on a constant forward speed. Equations to second order were presented; however, the effect of forward speed does not appear explicitly in these equations. Marshall et al (1982) [12] used the energy-formulation approach and showed that the linearly coupled coefficients have a different dependence on the forward speed than that predicted by three strip-theory approaches (Korvin-Korvosky and Jacobs, 1957 [5]; Salvesen at al, 1970 [6]; Ogilvie and Tuck, 1969 [7]).

In this chapter, we present a general form of the full nonlinear equations that govern ship motions including the dependence of all parameters on the forward speed. To this end, we utilize the energy formulation to obtain ship-motion models. We extend the work of Nayfeh et al (1974) [11] and Marshall et al (1982) [12] by considering the effect of the forward speed on 6DOF ship motions. We present a method for deriving full nonlinear ship-motion equations using the energy-formulation approach in a moving inertial coordinate system. Six DOF nonlinear equations up to third order are then derived. The method can be easily extended to obtain nonlinear equations of higher orders. The obtained nonlinear equations give explicitly the dependence of the different terms on the forward speed. These equations provide insight into the form of the parameters and their dependence on the forward speed. This insight is important for accurate modeling of ship motions.

3.1 Coordinate Systems and Transformation Equations

The formulation of ship motion is usually established in three coordinate frames. The first one is a moving coordinate frame, which is fixed to the ship and is called the body-fixed reference frame, see Fig. 3.1. The x-axis is oriented along the ship's longitudinal axis and

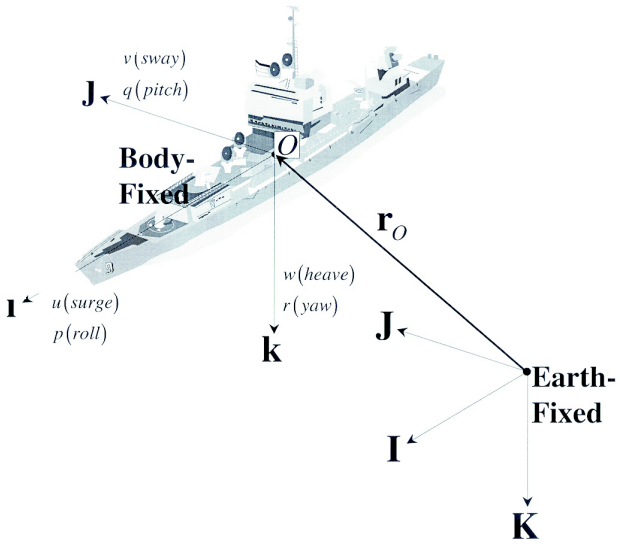

Figure 3.1: Coordinate systems

is directed from stern to bow. The y-axis is oriented along the ship's transverse axis and is directed towards starboard. The z-axis is oriented along the ship's normal axis and is directed from top to bottom. The second frame is an inertial frame, which is fixed to a point on the surface of the earth and is called the earth-fixed reference frame. The third frame is an inertial coordinate system that moves at a constant speed equals the ship's average forward speed U. The initial origin of this frame is located at the origin of the body-fixed frame and its axes are always oriented according to the earth-fixed frame. The position and velocity vectors of the ship motion are then written as (Fossen, 1994 [127])

$$\eta = [x, y, z, \phi, \theta, \psi]^T \tag{3.1}$$

$$\nu = [u, v, w, p, q, r]^T \tag{3.2}$$

where η is the position and orientation vector in the earth-fixed coordinate system, and ν is the linear and angular velocity vector in the body-fixed coordinate system. The variables x, y, and z represent the motions in the x-, y-, and z-directions (surge, sway, and heave), respectively; and the variables ϕ, θ, and ψ are the rotations about the x-, y-, and z-axes (roll, pitch, and yaw), respectively. The variables u, v, and w are the surge, sway, and heave

linear velocities, respectively; and p, q, and r are the roll, pitch, and yaw angular velocities, respectively. The vector η represents the position and orientation of the body-fixed frame with respect to the earth-fixed frame, projected in the earth-fixed frame. The vector ν represents the translational and angular velocities of the body-fixed frame with respect to the earth-fixed frame, projected in the body-fixed frame. The relation between the two velocity vectors can be written as

$$\dot{\eta} = J(\eta)\nu \tag{3.3}$$

$$\nu = E(\eta)\dot{\eta} \tag{3.4}$$

where $J(\eta)$ is a matrix that transforms the velocity vector from the body-fixed coordinate system to the earth-fixed coordinate system and $E(\eta)$ is its inverse. The matrices J and E are given by

$$E(\eta) = \begin{bmatrix} \cos(\psi)\cos(\theta) & \sin(\psi)\cos(\theta) & -\sin(\theta) & 0 & 0 & 0 \\ -\sin(\psi)\cos(\phi) & \cos(\psi)\cos(\phi) & \cos(\theta)\sin(\phi) & 0 & 0 & 0 \\ +\cos(\psi)\sin(\theta)\sin(\phi) & +\sin(\psi)\sin(\theta)\sin(\phi) & & & & \\ \sin(\psi)\sin(\phi) & -\cos(\psi)\sin(\phi) & \cos(\theta)\cos(\phi) & 0 & 0 & 0 \\ +\cos(\psi)\sin(\theta)\cos(\phi) & +\sin(\psi)\sin(\theta)\cos(\phi) & & & & \\ 0 & 0 & 0 & 1 & 0 & -\sin(\theta) \\ 0 & 0 & 0 & 0 & \cos(\phi) & \cos(\theta)\sin(\phi) \\ 0 & 0 & 0 & 0 & -\sin(\phi) & \cos(\theta)\cos(\phi) \end{bmatrix} \tag{3.5}$$

$$J(\eta) = \begin{bmatrix} \cos(\psi)\cos(\theta) & -\sin(\psi)\cos(\phi) & \sin(\psi)\sin(\phi) & 0 & 0 & 0 \\ & +\cos(\psi)\sin(\theta)\sin(\phi) & +\cos(\psi)\sin(\theta)\cos(\phi) & & & \\ \sin(\psi)\cos(\theta) & \cos(\psi)\cos(\phi) & -\cos(\psi)\sin(\phi) & 0 & 0 & 0 \\ & +\sin(\psi)\sin(\theta)\sin(\phi) & +\sin(\psi)\sin(\theta)\cos(\phi) & & & \\ -\sin(\theta) & \cos(\theta)\sin(\phi) & \cos(\theta)\cos(\phi) & 0 & 0 & 0 \\ 0 & 0 & 0 & 1 & \tan(\theta)\sin(\phi) & \tan(\theta)\cos(\phi) \\ 0 & 0 & 0 & 0 & \cos(\phi) & -\sin(\phi) \\ 0 & 0 & 0 & 0 & \frac{\sin(\phi)}{\cos(\theta)} & \frac{\cos(\phi)}{\cos(\theta)} \end{bmatrix} \tag{3.6}$$

The position and orientation vector in the moving inertial coordinate system will be denoted by $\bar{\eta}$ and its components are identical to the components of the vector η except for the first component, which can be expressed as

$$\bar{x} = x + Ut \tag{3.7}$$

where t is time.

3.2 Energy Formulation

One advantage of using the energy formulation to determine the form of the governing equations is that one automatically eliminates the possibility of arriving at self-sustained motions (Nayfeh et al, 1974 [11]). Moreover, the energy approach explicitly yields the dependence of the coefficients on the forward speed (Marshall et al, 1982 [12]). With the energy formulation, one considers the ship and the surrounding water to be a single dynamical system. First, one postulates the forms of the kinetic and potential energies and the dissipation function, giving consideration to the lateral symmetry of the ship. Then, Lagrange's equations are applied to obtain the equations of motion. We note here that due to free-surface effects, both the kinetic energy and dissipation function depend on the position and orientation of the ship; that is z, θ, and ϕ. Also, when postulating the forms of the kinetic and potential energies and the dissipation function, one needs to include all higher-order terms up to quartic nonlinearities to obtain cubic terms in the nonlinear equations.

Lagrange's equations are written as

$$\frac{d}{dt}\left\{\frac{\partial T}{\partial \dot{\eta}}\right\} - \left\{\frac{\partial T}{\partial \eta}\right\} + \left\{\frac{\partial D}{\partial \dot{\eta}}\right\} + \left\{\frac{\partial V}{\partial \eta}\right\} = E^T \tau \tag{3.8}$$

in inertial coordinate systems, and as

$$\frac{d}{dt}\left\{\frac{\partial T}{\partial \nu}\right\} + [\Gamma]\left\{\frac{\partial T}{\partial \nu}\right\} - E^T\left\{\frac{\partial T}{\partial \eta} - \frac{\partial V}{\partial \eta}\right\} + \left\{\frac{\partial D}{\partial \nu}\right\} = \tau \tag{3.9}$$

in quasi coordinate systems. Here, T is the kinetic energy, V is the potential energy, D is the dissipation function, τ represents the external (wave and diffraction) forces and moments vector in the body-fixed frame, and Γ is defined as

$$\Gamma = \begin{bmatrix} 0 & -r & q & 0 & 0 & 0 \\ r & 0 & -p & 0 & 0 & 0 \\ -q & p & 0 & 0 & 0 & 0 \\ 0 & -w & v & 0 & -r & q \\ w & 0 & -u & r & 0 & -p \\ -v & u & 0 & -q & p & 0 \end{bmatrix} \tag{3.10}$$

Since $\partial\eta = \partial\bar{\eta}$ and $\partial\dot{\eta} = \partial\dot{\bar{\eta}}$, we can interchangeably replace η in Eqs. (3.8) and (3.9) with $\bar{\eta}$ and $\dot{\eta}$ in Eq. (3.8) with $\dot{\bar{\eta}}$. The kinetic energy T can be expressed as

$$T = T_{RB} + T_A \tag{3.11}$$

where T_{RB} is the rigid-body kinetic energy and is written as

$$T_{RB} = \nu^T M_{RB} \nu \tag{3.12}$$

and T_A is the kinetic energy of the surrounding fluid and is written as

$$T_A = \nu^T \mathcal{M}_A \nu \tag{3.13}$$

In Eq. (3.12), M_{RB} is the rigid-body mass matrix defined as

$$\mathbf{M}_{RB} = \begin{bmatrix} m & 0 & 0 & 0 & mz_G & -my_G \\ 0 & m & 0 & -mz_G & 0 & mx_G \\ 0 & 0 & m & my_G & -mx_G & 0 \\ 0 & -mz_G & my_G & I_x & -I_{xy} & -I_{xz} \\ mz_G & 0 & -mx_G & -I_{yx} & I_y & -I_{yz} \\ -my_G & mx_G & 0 & -I_{zx} & -I_{zy} & I_z \end{bmatrix} \tag{3.14}$$

where m is the mass of the ship, I_x, I_y, and I_z are the ship moments of inertia about the x-, y-, and z- axes of the body-fixed coordinate system, the I_{ij} are the cross products of inertia, and x_G, y_G, and z_G are the coordinates of the center of gravity in the body-fixed coordinate system. In Eq. (3.13), $\mathcal{M}_A$ is the added mass matrix defined as

$$\mathcal{M}_A = \frac{1}{2} \begin{bmatrix} 2a_1 & a_2 & a_3 & a_4 & a_5 & a_6 \\ a_2 & 2a_7 & a_8 & a_9 & a_{10} & a_{11} \\ a_3 & a_8 & 2a_{12} & a_{13} & a_{14} & a_{15} \\ a_4 & a_9 & a_{13} & 2a_{16} & a_{17} & a_{18} \\ a_5 & a_{10} & a_{14} & a_{17} & 2a_{19} & a_{20} \\ a_6 & a_{11} & a_{15} & a_{18} & a_{20} & 2a_{21} \end{bmatrix} \tag{3.15}$$

The kinetic energy must remain unaltered if the signs of ϕ, v, p, and r are reversed in conjunction. Thus, the elements $a_1, a_3, a_5, a_7, a_9, a_{11}, a_{12}, a_{14}, a_{16}, a_{18}, a_{19}$, and a_{21} are combinations of linear, quadratic, cubic, and quartic functions of z, θ, and ϕ, excluding terms that contain odd powers of ϕ because of symmetry. For example, we write

$$\begin{aligned} a_1 &= a_{1_0} + a_{1z}z + a_{1z^2}z^2 + a_{1z^3}z^3 + a_{1z^4}z^4 \\ &\quad + a_{1\theta}\theta + a_{1\theta^2}\theta^2 + a_{1\theta^3}\theta^3 + a_{1\theta^4}\theta^4 \\ &\quad + a_{1\phi^2}\phi^2 + a_{1\phi^4}\phi^4 \\ &\quad + a_{1z\theta}z\theta + a_{1z\theta^2}z\theta^2 + a_{1z^2\theta}z^2\theta \\ &\quad + a_{1z\phi^2}z\phi^2 + a_{1\theta\phi^2}\theta\phi^2 \\ &\quad + a_{1z\theta^3}z\theta^3 + a_{1z^3\theta}z^3\theta \\ &\quad + a_{1z^2\theta^2}z^2\theta^2 + a_{1z^2\phi^2}z^2\phi^2 \\ &\quad + a_{1\theta^2\phi^2}\theta^2\phi^2 + a_{1z\theta\phi^2}z\theta\phi^2 \end{aligned} \tag{3.16}$$

The remaining elements $a_2, a_4, a_6, a_8, a_{10}, a_{13}, a_{15}, a_{17}$, and a_{20} must contain ϕ or ϕ^3. For example,

$$\begin{aligned} a_2 &= a_{2\phi}\phi + a_{2\phi^3}\phi^3 + a_{2z\phi}z\phi + a_{2\theta\phi}\theta\phi \\ &\quad + a_{2z^2\phi}z^2\phi + a_{2\theta^2\phi}\theta^2\phi \end{aligned} \tag{3.17}$$

The dissipation function can be written as

$$D = \nu^T \mathcal{C} \nu \tag{3.18}$$

where $\mathcal{C}$ is the damping matrix and written as

$$\mathcal{C} = \frac{1}{2}\begin{bmatrix} 2b_1 & b_2 & b_3 & b_4 & b_5 & b_6 \\ b_2 & 2b_7 & b_8 & b_9 & b_{10} & b_{11} \\ b_3 & b_8 & 2b_{12} & b_{13} & b_{14} & b_{15} \\ b_4 & b_9 & b_{13} & 2b_{16} & b_{17} & b_{18} \\ b_5 & b_{10} & b_{14} & b_{17} & 2b_{19} & b_{20} \\ b_6 & b_{11} & b_{15} & b_{18} & b_{20} & 2b_{21} \end{bmatrix} \tag{3.19}$$

The dissipation function must remain unaltered if the signs of ϕ, v, p, and r are reversed in conjunction. Thus, the elements $b_1, b_3, b_5, b_7, b_9, b_{11}, b_{12}, b_{14}, b_{16}, b_{18}, b_{19}$, and b_{21} are combinations of linear, quadratic, cubic functions of z, θ and ϕ, excluding terms that contain odd powers of ϕ because of symmetry. They also contain quadratic functions of the velocities. For example, we write

$$\begin{aligned} b_1 \;=\; & b_1 + b_{1z}z + b_{1z^2}z^2 + b_{1z^3}z^3 + b_{1\phi^2}\phi^2 \\ & + b_{1\theta}\theta + b_{1\theta^2}\theta^2 + b_{1\theta^3}\theta^3 \\ & + b_{1z\theta}z\theta + b_{1z\theta^2}z\theta^2 + b_{1z^2\theta}z^2\theta \\ & + b_{1z\phi^2}z\phi^2 + b_{1\theta\phi^2}\theta\phi^2 \\ & + b_{1\theta^2\phi^2}\theta^2\phi^2 + b_{1z\theta\phi^2}z\theta\phi^2 \\ & + b_{1u^2}u^2 + b_{1v^2}v^2 + b_{1w^2}w^2 + b_{1p^2}p^2 + b_{1q^2}q^2 + b_{1r^2}r^2 \\ & + b_{1vp}vp + b_{1vr}vr + b_{1pr}pr \end{aligned} \tag{3.20}$$

The remaining elements $b_2, b_4, b_6, b_8, b_{10}, b_{13}, b_{15}, b_{17}$, and b_{20} are functions of ϕ and ϕ^3. They also contain quadratic functions of the velocities. For example,

$$\begin{aligned} b_2 \;=\; & b_{2\phi}\phi + b_{2\phi^3}\phi^3 + b_{2z\phi}z\phi + b_{2\theta\phi}\theta\phi \\ & + b_{2z^2\phi}z^2\phi + b_{2\theta^2\phi}\theta^2\phi \\ & + b_{2uv}uv + b_{2up}up + b_{2ur}ur + b_{2uw}uw + b_{2uq}uq + b_{2wp}wp \\ & + b_{2wr}wr + b_{2pq}pq + b_{2qr}qr \end{aligned} \tag{3.21}$$

The potential energy V is expressed as

$$V \;=\; \bar{\eta}^T \mathcal{K} \bar{\eta} \tag{3.22}$$

where $\mathcal{K}$ is the stiffness matrix defined as

$$\mathcal{K} = \frac{1}{2}\begin{bmatrix} 0 & 0 & 0 & 0 & 0 & 0 \\ 0 & 0 & 0 & 0 & 0 & 0 \\ 0 & 0 & 2c_1 & c_2 & c_3 & 0 \\ 0 & 0 & c_2 & 2c_4 & c_5 & 0 \\ 0 & 0 & c_3 & c_5 & 2c_6 & 0 \\ 0 & 0 & 0 & 0 & 0 & 0 \end{bmatrix} \tag{3.23}$$

The potential energy must remain unchanged if the sign of ϕ is reversed. Thus, the elements c_1, c_3, c_4, and c_6 are combinations of linear and quadratic functions of z, θ, and ϕ, excluding terms that contain odd powers of ϕ. For example,

$$c_1 = c_{1_0} + c_{1z}z + c_{1z^2}z^2 + c_{1\theta}\theta + c_{1\theta^2}\theta^2 + c_{1\phi^2}\phi^2 + c_{1z\theta}z\theta \tag{3.24}$$

The elements c_2 and c_5 are functions of ϕ only. For example,

$$c_2 = c_{2\phi}\phi \tag{3.25}$$

3.2.1 Index Notation

In this work, we study the effect of the forward speed on the nonlinear 6DOF equations of ship motion. All nonlinearities up to third order are considered. It is clear from the forms of $\mathcal{M}_{\mathcal{A}}, \mathcal{C}$, and $\mathcal{K}$ that applying Lagrange's equations is very tedious and will yield equations that contain hundreds of terms. This will make it difficult to examine the effects of the forward speed. Also, extending this work to higher-order nonlinearities will be extremely tedious. To overcome these difficulties, we adopt the index notation for the derivation of the nonlinear equations and studying the effect of the forward speed. The components of the system and transformation matrices presented above are defined as

$$\mathbf{M}_{RB} = \left[\, a_{R\mathbf{ij}} \,\right] \tag{3.26}$$

$$\mathcal{M}_A = \left[\, a_{F\mathbf{ij}} \,\right] \tag{3.27}$$

$$\mathcal{M} = \left[a_{\mathbf{ij}} = a_{R\mathbf{ij}} + a_{F\mathbf{ij}} \right] \tag{3.28}$$

$$\mathcal{C} = \left[b_{\mathbf{ij}} \right] \tag{3.29}$$

$$\mathcal{K} = \left[c_{\mathbf{ij}} \right] \tag{3.30}$$

$$J = \left[d_{\mathbf{ij}} \right] \tag{3.31}$$

$$E = \left[e_{\mathbf{ij}} \right] \tag{3.32}$$

$$E^T \tau = \left[f_{\mathbf{i}} \right] \tag{3.33}$$

where the indices **i** and **j** vary from 1 to 6. Lagrange's equations are then expressed as

$$\frac{d}{dt}\left\{\frac{\partial T}{\partial \dot{\eta}_{\mathbf{i}}}\right\} - \left\{\frac{\partial T}{\partial \eta_{\mathbf{i}}}\right\} + \left\{\frac{\partial D}{\partial \dot{\eta}_{\mathbf{i}}}\right\} + \left\{\frac{\partial V}{\partial \eta_{\mathbf{i}}}\right\} = f_{\mathbf{i}} \tag{3.34}$$

in the earth-fixed coordinate system, and as

$$\frac{d}{dt}\left\{\frac{\partial T}{\partial \nu_{\mathbf{i}}}\right\} + \Gamma_{\mathbf{ij}}\frac{\partial T}{\partial \nu_{\mathbf{j}}} - e_{\mathbf{ji}}\left\{\frac{\partial T}{\partial \eta_{\mathbf{j}}} - \frac{\partial V}{\partial \eta_{\mathbf{j}}}\right\} + \frac{\partial D}{\partial \nu_{\mathbf{i}}} = \tau_{\mathbf{i}} \tag{3.35}$$

in the body-fixed coordinate system.

The kinetic and potential energies and the dissipation function are expressed as

$$T = a_{\mathbf{ij}}\nu_{\mathbf{i}}\nu_{\mathbf{j}} \tag{3.36}$$

$$V = c_{\mathbf{ij}}\bar{\eta}_{\mathbf{i}}\bar{\eta}_{\mathbf{j}} \tag{3.37}$$

$$D = b_{\mathbf{ij}}\nu_{\mathbf{i}}\nu_{\mathbf{j}} \tag{3.38}$$

The transformation equations are also expressed as

$$\nu_{\mathbf{i}} = e_{\mathbf{ij}}\dot{\eta}_{\mathbf{j}} \tag{3.39}$$

$$\dot{\eta}_{\mathbf{i}} = d_{\mathbf{ij}}\nu_{\mathbf{j}} \tag{3.40}$$

We expand the components of the transformation matrix E (see Eq. (3.5)) in Taylor series and truncate the terms of order five and higher. In index notation, the components of E are then expressed as

$$\begin{aligned} e_{\mathbf{ij}} &= e_{\mathbf{ij}0} \\ &\quad + e_{\mathbf{ijm}}\bar{\eta}_{\mathbf{m}} \\ &\quad + e_{\mathbf{ijmn}}\bar{\eta}_{\mathbf{m}}\bar{\eta}_{\mathbf{n}} \\ &\quad + e_{\mathbf{ijmno}}\bar{\eta}_{\mathbf{m}}\bar{\eta}_{\mathbf{n}}\bar{\eta}_{\mathbf{o}} \\ &\quad + e_{\mathbf{ijmnop}}\bar{\eta}_{\mathbf{m}}\bar{\eta}_{\mathbf{n}}\bar{\eta}_{\mathbf{o}}\bar{\eta}_{\mathbf{p}} \end{aligned} \tag{3.41}$$

In a more compact form, Eq. (3.41) is written as

$$e_{\mathbf{ij}} = e_{\mathbf{ij}mnop}\bar{\eta}_{mnop} \tag{3.42}$$

where $\bar{\eta}_{mnop}$ is a short notation for $\bar{\eta}_m\bar{\eta}_n\bar{\eta}_o\bar{\eta}_p$. An index with **bold** font implies that it varies from 1 to 6, while an index with an *italic* font implies that it varies from 0 to 6 where $\bar{\eta}_0 = 1$. The matrix $e_{\mathbf{ij}0}$ can be recovered by setting the indices m, n, o, and p equal to zero; that is, keeping only the terms that contain zeros in these indices. The matrix $e_{\mathbf{ijm}}$ can be recovered by setting the indices n, o, and p equal to zero and the index m is set to a nonzero value. Similarly, the matrices $e_{\mathbf{ijmn}}$, $e_{\mathbf{ijmno}}$, and $e_{\mathbf{ijmnop}}$ can be recovered. This convention allows for the representation of Eq. (3.41) in a compact form and is used frequently in this chapter. Utilizing this convention, we rewrite the matrices $a_{\mathbf{ij}}, b_{\mathbf{ij}}$, and $c_{\mathbf{ij}}$ as

$$a_{\mathbf{ij}} = a_{\mathbf{ij}mnop}\bar{\eta}_{mnop} \tag{3.43}$$

$$b_{\mathbf{ij}} = \tilde{b}_{\mathbf{ij}} + \hat{b}_{\mathbf{ij}} \tag{3.44}$$

$$c_{\mathbf{ij}} = c_{\mathbf{ij}mnop}\bar{\eta}_{mnop} \tag{3.45}$$

where

$$\tilde{b}_{\mathbf{ij}} = \tilde{b}_{\mathbf{ij}mnop}\bar{\eta}_{mnop} \tag{3.46}$$

and

$$\hat{b}_{\mathbf{ij}} = \hat{b}_{\mathbf{ijmn}}\nu_{\mathbf{mn}} \tag{3.47}$$

Combining Eqs. (3.42) and (3.39), we express the transformation equation as

$$\nu_{\mathbf{i}} = e_{\mathbf{ij}mnop}\bar{\eta}_{mnop}\dot{\eta}_{\mathbf{j}} \tag{3.48}$$

3.3 Nonlinear Equations of Ship Motion

In this section, we derive third-order nonlinear equations of ship motion. To this end, we apply Lagrange's equations in index notation (Eq. (3.34)). Then, we extract the second-order and first-order equations. To examine the effect of the forward speed, we express the final form of the equations in terms of the moving coordinate system. Since the objective is to derive equations up to finite orders, the matrices a, b, c, and d are expanded in terms of the displacements up to finite orders. Higher-order terms can be truncated because the components of the matrices are small, which is a consequence of the assumption of small nonlinearities.

Combining Eqs. (3.36), (3.43), and (3.48), we write the kinetic energy equation as

$$T = a1_{\mathbf{kl}mnopqrstuvwx}\bar{\eta}_{mnopqrstuvwx}\dot{\eta}_{\mathbf{kl}} \tag{3.49}$$

where

$$a1_{\mathbf{kl}mnopqrstuvwx} = a_{\mathbf{ij}mnop}e_{\mathbf{ik}qrst}e_{\mathbf{jl}uvwx} \tag{3.50}$$

To find the first term on the RHS of Lagrange's equations (Eq. (3.34)), we eliminate the terms in the kinetic energy of order six and higher. This is done by setting the indices $p \ldots x$ equal to zeros. The reduced kinetic energy becomes

$$T = a\acute{1}_{\mathbf{kl}mno}\bar{\eta}_{mno}\dot{\eta}_{\mathbf{kl}} \tag{3.51}$$

where $a\acute{1}_{\mathbf{kl}mno} = a1_{\mathbf{kl}mno000000000}$. By differentiating Eq. (3.51) with respect to $\dot{\eta}_{\mathbf{i}}$, we obtain

$$\frac{\partial T}{\partial \dot{\eta}_{\mathbf{i}}} = a\acute{1}_{\mathbf{kl}mno}\bar{\eta}_{mno}\left(\dot{\eta}_{\mathbf{l}}\delta_{\mathbf{ik}} + \dot{\eta}_{\mathbf{k}}\delta_{\mathbf{il}}\right) \tag{3.52}$$

$$\begin{aligned} &= a\acute{1}_{\mathbf{il}mno}\bar{\eta}_{mno}\dot{\eta}_{\mathbf{l}} + a\acute{1}_{\mathbf{ki}mno}\bar{\eta}_{mno}\dot{\eta}_{\mathbf{k}} \\ &= a\acute{1}_{\mathbf{il}mno}\bar{\eta}_{mno}\dot{\eta}_{\mathbf{l}} + a\acute{1}_{\mathbf{li}mno}\bar{\eta}_{mno}\dot{\eta}_{\mathbf{l}} \\ &= a2_{\mathbf{il}mno}\bar{\eta}_{mno}\dot{\eta}_{\mathbf{l}} \end{aligned}$$

where $a2_{\mathbf{il}mno} = a\acute{1}_{\mathbf{il}mno} + a\acute{1}_{\mathbf{li}mno}$. In Eqs. (3.52), we set $\frac{\partial\dot{\bar{\eta}}_{\mathbf{k}}}{\partial\dot{\bar{\eta}}_{\mathbf{i}}} = \delta_{\mathbf{ki}}$, where $\delta_{\mathbf{ki}}$ is the Kronecker delta. We also made use of the relations $X_{\mathbf{ij}}\delta_{\mathbf{ki}} = X_{\mathbf{kj}}$ and $X_{\mathbf{i}}Y_{\mathbf{i}} = X_{\mathbf{j}}Y_{\mathbf{j}}$. By differentiating Eq. (3.52) with respect to time, we obtain

$$\frac{d}{dt}\left\{\frac{\partial T}{\partial\dot{\eta}_{\mathbf{i}}}\right\} = a2_{\mathbf{il}mno}\bar{\eta}_{mno}\ddot{\eta}_{\mathbf{l}} + a3_{\mathbf{ilm}no}\bar{\eta}_{no}\dot{\bar{\eta}}_{\mathbf{m}}\dot{\eta}_{\mathbf{l}} \tag{3.53}$$

where $a3_{\mathbf{ilm}no} = a2_{\mathbf{ilm}no} + a2_{\mathbf{il}n\mathbf{m}o} + a2_{\mathbf{il}no\mathbf{m}}$. The relation between the velocity vectors in the earth-fixed coordinate system and the moving inertial coordinate system is expressed as

$$\dot{\eta}_{\mathbf{l}} = \dot{\bar{\eta}}_{\mathbf{l}} + U\delta_{1\mathbf{l}} \tag{3.54}$$

Substituting Eq. (3.54) into Eq. (3.53), we obtain

$$\begin{aligned} \frac{d}{dt}\left\{\frac{\partial T}{\partial\dot{\eta}_{\mathbf{i}}}\right\} &= a2_{\mathbf{il}mno}\bar{\eta}_{mno}\ddot{\bar{\eta}}_{\mathbf{l}} + a3_{\mathbf{ilm}no}\bar{\eta}_{no}\dot{\bar{\eta}}_{\mathbf{m}}\left(\dot{\bar{\eta}}_{\mathbf{l}} + U\delta_{1\mathbf{l}}\right) \\ &= a\acute{2}_{\mathbf{il}km}\bar{\eta}_{km}\ddot{\bar{\eta}}_{\mathbf{l}} + a\acute{3}_{\mathbf{ilk}m}\bar{\eta}_{m}\dot{\bar{\eta}}_{\mathbf{lk}} + a4_{\mathbf{il}km}U\bar{\eta}_{km}\dot{\bar{\eta}}_{\mathbf{l}} \end{aligned} \tag{3.55}$$

where $a\acute{2}_{\mathbf{il}km} = a2_{\mathbf{il}km0}$, $a\acute{3}_{\mathbf{ilk}m} = a3_{\mathbf{ilk}m0}$, and $a4_{\mathbf{il}km} = a3_{\mathbf{i}1\mathbf{l}km}$.

To find the second term on the RHS of Lagrange's equations (Eq. (3.34)), we eliminate the terms in the kinetic energy of order seven and higher. This is done by setting the indices $q\ldots x$ in Eq. (3.49) equal to zeros. The reduced kinetic energy becomes

$$T = a\acute{\acute{1}}_{\mathbf{kl}mnop}\bar{\eta}_{mnop}\dot{\eta}_{\mathbf{kl}} \tag{3.56}$$

where $a\acute{\acute{1}}_{\mathbf{kl}mnop} = a1_{\mathbf{kl}mnop00000000}$. By differentiating Eq. (3.56) with respect to $\bar{\eta}_{\mathbf{i}}$, we obtain

$$\frac{\partial T}{\partial\bar{\eta}_{\mathbf{i}}} = a5_{\mathbf{ikl}mno}\bar{\eta}_{mno}\dot{\eta}_{\mathbf{kl}} \tag{3.57}$$

where $a5_{\mathbf{ikl}mno} = a\acute{\acute{1}}_{\mathbf{kli}mno} + a\acute{\acute{1}}_{\mathbf{kl}mi\mathbf{n}o} + a\acute{\acute{1}}_{\mathbf{kl}mn\mathbf{i}o} + a\acute{\acute{1}}_{\mathbf{kl}mno\mathbf{i}}$.

By expanding $\dot{\eta}_{\mathbf{kl}}$ in Eq. (3.57), we obtain

$$\begin{aligned} \frac{\partial T}{\partial\bar{\eta}_{\mathbf{i}}} &= a5_{\mathbf{ikl}mno}\bar{\eta}_{mno}\left[\dot{\bar{\eta}}_{\mathbf{k}}\dot{\bar{\eta}}_{\mathbf{l}} + U\left(\dot{\bar{\eta}}_{\mathbf{k}}\delta_{1\mathbf{l}} + \dot{\bar{\eta}}_{\mathbf{l}}\delta_{1\mathbf{k}}\right) + U^2\delta_{1\mathbf{l}}\delta_{1\mathbf{k}}\right] \\ &= a\acute{5}_{\mathbf{ilk}m}\bar{\eta}_{m}\dot{\bar{\eta}}_{\mathbf{kl}} + a6_{\mathbf{il}km}U\bar{\eta}_{km}\dot{\bar{\eta}}_{\mathbf{l}} + a7_{\mathbf{i}lkm}U^2\bar{\eta}_{lkm} \end{aligned} \tag{3.58}$$

where

$a\acute{5}_{\mathbf{ilk}m} = a5_{\mathbf{ilk}m00}$, $a6_{\mathbf{il}km} = a\acute{5}_{\mathbf{i}11km} + a\acute{5}_{\mathbf{il}1km}$, $a\acute{5}_{\mathbf{ilk}mn} = a5_{\mathbf{ilk}mn0}$, and $a7_{\mathbf{i}lkm} = a5_{\mathbf{i}11lkm}$.

Combining Eqs. (3.58) and (3.55) yields

$$\begin{aligned} \frac{d}{dt}\left\{\frac{\partial T}{\partial \dot{\bar{\eta}}_{\mathbf{i}}}\right\} + \frac{\partial T}{\partial \bar{\eta}_{\mathbf{i}}} &= a\acute{2}_{\mathbf{il}km}\bar{\eta}_{km}\ddot{\bar{\eta}}_{\mathbf{l}} + a8_{\mathbf{ilk}m}\bar{\eta}_m\dot{\bar{\eta}}_{\mathbf{lk}} \\ &\quad + a9_{\mathbf{il}km}U\bar{\eta}_{km}\dot{\bar{\eta}}_{\mathbf{l}} + a10_{\mathbf{i}lkm}U^2\bar{\eta}_{lkm} \end{aligned} \tag{3.59}$$

where $a8_{\mathbf{ilk}m} = a\acute{3}_{\mathbf{ilk}m} - a\acute{5}_{\mathbf{ilk}m}$, $a9_{\mathbf{il}km} = a4_{\mathbf{il}km} - a6_{\mathbf{il}km}$, and $a10_{\mathbf{i}lkm} = -a7_{\mathbf{i}lkm}$.

Now, we turn our attention to the third term on the RHS of Lagrange's equations (Eq. (3.34)). The dissipation function is separated into two parts as follows:

$$D = D1 + D2 \tag{3.60}$$

$$D1 = \tilde{b}_{\mathbf{ij}}\nu_{\mathbf{i}}\nu_{\mathbf{j}} \tag{3.61}$$

$$D2 = \hat{b}_{\mathbf{ij}}\nu_{\mathbf{i}}\nu_{\mathbf{j}} \tag{3.62}$$

$$\frac{\partial D}{\partial \dot{\bar{\eta}}_{\mathbf{i}}} = \frac{\partial D1}{\partial \dot{\bar{\eta}}_{\mathbf{i}}} + \frac{\partial D2}{\partial \dot{\bar{\eta}}_{\mathbf{i}}} \tag{3.63}$$

Using Eqs. (3.46), (3.48), and (3.61), we obtain

$$D1 = b1_{\mathbf{kl}mnopqrstuvwx}\bar{\eta}_{mnopqrstuvwx}\dot{\eta}_{\mathbf{kl}} \tag{3.64}$$

where

$$b1_{\mathbf{kl}mnopqrstuvwx} = \tilde{b}_{\mathbf{ij}mnop}e_{\mathbf{ik}qrst}e_{\mathbf{jl}uvwx} \tag{3.65}$$

By eliminating terms of order six and higher from Eq. (3.65), we obtain

$$D1 = b\acute{1}_{\mathbf{kl}mno}\bar{\eta}_{mno}\dot{\eta}_{\mathbf{kl}} \tag{3.66}$$

where $b\acute{1}_{\mathbf{kl}mno} = b1_{\mathbf{kl}mno00000000}$. By differentiating Eq. (3.66) with respect to $\dot{\eta}_{\mathbf{i}}$, we obtain

$$\begin{aligned} \frac{\partial D1}{\partial \dot{\eta}_{\mathbf{i}}} &= b3_{\mathbf{il}mno}\bar{\eta}_{mno}\dot{\eta}_{\mathbf{l}} \\ &= b3_{\mathbf{il}mno}\bar{\eta}_{mno}\left(\dot{\bar{\eta}}_{\mathbf{l}} + U\delta_{1\mathbf{l}}\right) \\ &= b\acute{3}_{\mathbf{il}km}\bar{\eta}_{km}\dot{\bar{\eta}}_{\mathbf{l}} + b5_{\mathbf{i}lkm}U\bar{\eta}_{lkm} \end{aligned} \tag{3.67}$$

where $b3_{\mathbf{il}mno} = b\acute{1}_{\mathbf{il}mno} + b\acute{1}_{\mathbf{li}mno}$, $b\acute{3}_{\mathbf{il}km} = b3_{\mathbf{li}km0}$, and $b5_{\mathbf{i}lkm} = b3_{\mathbf{i}1lkm}$.

Using Eqs. (3.47), (3.48), and (3.62), we obtain

$$D2 = b2_{\mathbf{mnop}qrstuvwxyzabcdef}\bar{\eta}_{qrstuvwxyzabcdef}\dot{\eta}_{\mathbf{mnop}} \tag{3.68}$$

where

$$b2_{\mathbf{mnop}qrstuvwxyzabcdef} = \hat{b}_{\mathbf{ijkl}}e_{\mathbf{im}qrst}e_{\mathbf{jn}uvwx}e_{\mathbf{ko}yzab}e_{\mathbf{lp}cdef} \tag{3.69}$$

We then eliminate terms of order eight and higher from Eq. (3.69) and obtain

$$D2 = b\acute{2}_{\mathbf{klmn}qrs}\bar{\eta}_{qrs}\dot{\eta}_{\mathbf{klmn}} \tag{3.70}$$

where $b\acute{2}_{\mathbf{klmn}qrs} = b2_{\mathbf{klmn}qrs0000000000000}$. By differentiating Eq. (3.70) with respect to $\dot{\eta}_{\mathbf{i}}$, we obtain

$$\begin{aligned}
\frac{\partial D2}{\partial \dot{\eta}_{\mathbf{i}}} &= b4_{\mathbf{ilkm}qrs}\bar{\eta}_{qrs}\dot{\eta}_{\mathbf{lkm}} \\
&= b4_{\mathbf{ilkm}qrs}\bar{\eta}_{qrs}\left[\dot{\bar{\eta}}_{\mathbf{l}}\dot{\bar{\eta}}_{\mathbf{k}}\dot{\bar{\eta}}_{\mathbf{m}} + U\left(\dot{\bar{\eta}}_{\mathbf{l}}\dot{\bar{\eta}}_{\mathbf{k}}\delta_{1m} + \dot{\bar{\eta}}_{\mathbf{l}}\dot{\bar{\eta}}_{\mathbf{m}}\delta_{1k} + \dot{\bar{\eta}}_{\mathbf{k}}\dot{\bar{\eta}}_{\mathbf{m}}\delta_{1l}\right)\right. \\
&\quad \left. + U^2\left(\dot{\bar{\eta}}_{\mathbf{l}}\delta_{1k}\delta_{1m} + \dot{\bar{\eta}}_{\mathbf{k}}\delta_{1l}\delta_{1m} + \dot{\bar{\eta}}_{\mathbf{m}}\delta_{1l}\delta_{1k}\right) + U^3\delta_{1l}\delta_{1k}\delta_{1m}\right] \\
&= b\acute{4}_{\mathbf{ilkm}}\dot{\bar{\eta}}_{\mathbf{lkm}} + b6_{\mathbf{ilk}m}U\bar{\eta}_m\dot{\bar{\eta}}_{\mathbf{lk}} + b7_{\mathbf{il}km}U^2\bar{\eta}_{km}\dot{\bar{\eta}}_{\mathbf{l}} + b8_{\mathbf{i}lkm}U^3\bar{\eta}_{lkm}
\end{aligned} \tag{3.71}$$

where

$b4_{\mathbf{ilkm}qrs} = b\acute{2}_{\mathbf{ilkm}qrs} + b\acute{2}_{\mathbf{likm}qrs} + b\acute{2}_{\mathbf{lkim}qrs} + b\acute{2}_{\mathbf{lkmi}qrs}$, $b\acute{4}_{\mathbf{ilkm}} = b4_{\mathbf{ilkm}000}$,

$b6_{\mathbf{ilk}m} = b\acute{\acute{4}}_{\mathbf{i1lk}m} + b\acute{\acute{4}}_{\mathbf{il1k}m} + b\acute{\acute{4}}_{\mathbf{ilk1}m}$, where $b\acute{\acute{4}}_{\mathbf{ilkm}q} = b4_{\mathbf{ilkm}q00}$,

$b7_{\mathbf{il}km} = b\acute{\acute{\acute{4}}}_{\mathbf{i11}lkm} + b\acute{\acute{\acute{4}}}_{\mathbf{il1}1km} + b\acute{\acute{\acute{4}}}_{\mathbf{i1l1}km}$, where $b\acute{\acute{\acute{4}}}_{\mathbf{ilkm}qr} = b4_{\mathbf{ilkm}qr0}$, and $b8_{\mathbf{i}lkm} = b4_{\mathbf{i111}lkm}$.

Combining Eqs. (3.63), (3.67), and (3.71) yields

$$\begin{aligned}
\frac{\partial D}{\partial \dot{\eta}_{\mathbf{i}}} &= b\acute{4}_{\mathbf{ilkm}}\dot{\bar{\eta}}_{\mathbf{lkm}} + b6_{\mathbf{ilk}m}U\bar{\eta}_m\dot{\bar{\eta}}_{\mathbf{lk}} \\
&\quad + \left(b\acute{3}_{\mathbf{il}km} + b7_{\mathbf{il}km}\right)U^2\bar{\eta}_{km}\dot{\bar{\eta}}_{\mathbf{l}} + \left(b5_{\mathbf{i}lkm}U + b8_{\mathbf{i}lkm}U^3\right)\bar{\eta}_{lkm}
\end{aligned} \tag{3.72}$$

Now, we calculate the last term of Eq. (3.34). Substituting Eq. (3.45) into Eq. (3.37), we obtain

$$V = c_{\mathbf{kl}mn}\bar{\eta}_{\mathbf{kl}mn} \tag{3.73}$$

Differentiating Eq. (3.73) with respect to $\bar{\eta}_{\mathbf{i}}$ yields

$$\frac{\partial V}{\partial \bar{\eta}_{\mathbf{i}}} = c1_{\mathbf{il}km}\bar{\eta}_{km}\bar{\eta}_{\mathbf{l}} \tag{3.74}$$

where $c1_{\mathbf{il}km} = c_{\mathbf{il}km} + c_{\mathbf{li}km} + c_{\mathbf{lk}im} + c_{\mathbf{lk}m\mathbf{i}}$.

By substituting Eqs. (3.74), (3.72), and (3.59) into Eq. (3.34), we obtain nonlinear equations of ship motion to third order as

$$\begin{aligned} &a\acute{2}_{\mathbf{il}km}\bar{\eta}_{km}\ddot{\bar{\eta}}_{\mathbf{l}} + b\acute{4}_{\mathbf{ilk}m}\dot{\bar{\eta}}_{\mathbf{lk}} + \left(a8_{\mathbf{ilk}m}\bar{\eta}_m + b6_{\mathbf{ilk}m}U\right)\bar{\eta}_m\dot{\bar{\eta}}_{\mathbf{lk}} \\ &+ \left(b\acute{3}_{\mathbf{il}km} + a9_{\mathbf{il}km}U + b7_{\mathbf{il}km}U^2\right)\bar{\eta}_{km}\dot{\bar{\eta}}_{\mathbf{l}} \\ &+ \left(b5_{\mathbf{il}km}U + a10_{\mathbf{il}km}U^2 + b8_{\mathbf{il}km}U^3\right)\bar{\eta}_{lkm} + c1_{\mathbf{il}km}\bar{\eta}_{km}\bar{\eta}_{\mathbf{l}} = f_{\mathbf{i}} \end{aligned} \tag{3.75}$$

By making use of the relations

$b5_{\mathbf{i}lkm} = b5_{\mathbf{il}km} + b5_{\mathbf{i}000}$,

$a10_{\mathbf{i}lkm} = a10_{\mathbf{il}km} + a10_{\mathbf{i}000}$,

and $b8_{\mathbf{i}lkm} = b8_{\mathbf{il}km} + b8_{\mathbf{i}000}$,

we rearrange Eq. (3.75) and obtain

$$\begin{aligned} &b\acute{4}_{\mathbf{ilk}m}\dot{\bar{\eta}}_{\mathbf{lk}} + \left(a8_{\mathbf{ilk}m} + b6_{\mathbf{ilk}m}U\right)\bar{\eta}_m\dot{\bar{\eta}}_{\mathbf{lk}} \\ &\Big[a\acute{2}_{\mathbf{il}km}\ddot{\bar{\eta}}_{\mathbf{l}} + \left(b\acute{3}_{\mathbf{il}km} + a9_{\mathbf{il}km}U + b7_{\mathbf{il}km}U^2\right)\dot{\bar{\eta}}_{\mathbf{l}} \\ &+ \left(c1_{\mathbf{il}km} + b5_{\mathbf{il}km}U + a10_{\mathbf{il}km}U^2 + b8_{\mathbf{il}km}U^3\right)\bar{\eta}_{\mathbf{l}}\Big]\bar{\eta}_{km} \\ &+ b5_{\mathbf{i}000}U + a10_{\mathbf{i}000}U^2 + b8_{\mathbf{i}000}U^3 = f_{\mathbf{i}} \end{aligned} \tag{3.76}$$

The second-order equations can be extracted from Eq. (3.76) by setting $m = 0$. The result is

$$\begin{aligned} &\left(a8_{\mathbf{ilk}0} + b6_{\mathbf{ilk}0}U\right)\dot{\bar{\eta}}_{\mathbf{lk}} \\ &+ \Big[a\acute{2}_{\mathbf{il}k0}\ddot{\bar{\eta}}_{\mathbf{l}} + \left(b\acute{3}_{\mathbf{il}k0} + a9_{\mathbf{il}k0}U + b7_{\mathbf{il}k0}U^2\right)\dot{\bar{\eta}}_{\mathbf{l}} \\ &+ \left(c1_{\mathbf{il}k0} + b5_{\mathbf{il}k0}U + a10_{\mathbf{il}k0}U^2 + b8_{\mathbf{il}k0}U^3\right)\bar{\eta}_{\mathbf{l}}\Big]\bar{\eta}_k \\ &+ b5_{\mathbf{i}000}U + a10_{\mathbf{i}000}U^2 + b8_{\mathbf{i}000}U^3 = f_{\mathbf{i}} \end{aligned} \tag{3.77}$$

The linear equations of motion can be extracted from Eq. (3.76) by setting $k = m = 0$. The result is

$$\begin{aligned} & a\acute{2}_{\mathbf{il00}}\ddot{\bar{\eta}}_{\mathbf{l}} + \left(b\acute{3}_{\mathbf{il00}} + a9_{\mathbf{il00}}U + b7_{\mathbf{il00}}U^2\right)\dot{\bar{\eta}}_{\mathbf{l}} \\ & + \left(c1_{\mathbf{il00}} + b5_{\mathbf{il00}}U + a10_{\mathbf{il00}}U^2 + b8_{\mathbf{il00}}U^3\right)\bar{\eta}_{\mathbf{l}} \\ & + b5_{\mathbf{i000}}U + a10_{\mathbf{i000}}U^2 + b8_{\mathbf{i000}}U^3 = f_{\mathbf{i}} \end{aligned} \tag{3.78}$$

The derivation procedure was programmed using MATLAB. An efficient calculation algorithm was implemented, which takes into account only the nonzero elements of each tensorial quantity. The derivation was validated by comparison with the linear and nonlinear equations of motion provided by Nayfeh et al (1974) [11] and Marshall et al (1982) [12] and with derivations performed by hand.

3.4 Discussion

By examining the above equations, we make several observations. First, the linear ship-motion equations (Eq. (3.78)) derived with the energy approach show that the added mass coefficients are not dependent on the forward speed. On the other hand, the damping and restoring (stiffness) coefficients are speed dependent. In contrast, the linear strip theories of Salvesen et al (1970) [6] and Ogilvie and Tuck (1969) [7] result in equations where the dependence on the forward speed appears in the added mass coefficients and not in the restoring coefficients. In Salvesen et al (1970) [6], the response frequency of the ship is assumed to be equal to the wave encounter frequency Ω. Furthermore, the speed dependent restoring forces have been grouped with the added mass forces by dividing the restoring forces by $-\Omega^2$. The disadvantages of this practice is that the ship response frequency in a given mode is not always equal to Ω. This is especially true when the nonlinear effects are important. Also, transporting the speed dependent terms to the added mass forces changes the linear natural frequencies of the ship and consequently affects the nonlinear problem.

Thus, for nonlinear analyses of ship motions, it is important to use the correct form of the linear ship-motion equations.

Second, the linear equations derived in this chapter are consistent with those derived by Marshall et al (1982) [12] regarding the dependence on forward speed. This is expected since the current derivation is a generalization of their work. However, higher powers of U appear in the current linear equations of motion. For example, the zero-order term provided by Marshall et al (1982) [12] lacks the cubic term. In the current derivation, a more general form of the dissipation function is used, which includes the dependence of the dissipation function on the velocities (see Eqs. (3.20) and (3.21)). This dependence on the velocities resulted in the U^2 term in the damping coefficients and the U^3 term in the restoring and zero-order coefficients.

Third, by examining Eqs. (3.76)-(3.78), we note that the added mass coefficients are always independent of the forward speed and that the restoring coefficients are always dependent on the forward speed. This applies for the linear, second-order, and third-order terms of the equations of motion. The dependence of the restoring forces on the forward speed is linear, quadratic, and cubic, while the dependence of the damping forces on the forward speed is linear and quadratic. Furthermore, the dependence of the zeroth-order term (forward speed force) on the forward speed is in the form of a cubic polynomial with zero y-intercept (see Eq. (3.78)).

Following the derivation in this chapter, we note that higher-order equations (order four and higher) will have forms similar to those of the third-order equations (3.76), with the appearance of higher powers of the forward speed. For example, in the fourth-order equations, the zeroth-order terms will be quartic functions of U, instead of cubic ones. Furthermore, the dependence on the forward speed will be similar; that is, the added mass coefficients do not depend on the forward speed, while the restoring, damping, and zeroth-order terms will depend on the forward speed.

Chapter 4

Linear Parametric Identification with Forward Speed Effects

Besides being important by itself, the identification of the coefficients of the linear terms is a prerequisite for the identification of the coefficients of the nonlinear terms. In previous work, it has been established that the coefficients of the linear terms in the coupled heave and pitch equations are functions of the forward speed. However, the form of this dependence is not very clear. Marshall et al (1982) [12] used the energy-formulation approach and showed that the coupled coefficients have a different dependence on the forward speed than those of three strip-theory approaches (Korvin-Korvosky and Jacobs, 1957 [5]; Salvesen at al, 1970 [6]; Ogilvie and Tuck, 1969 [7]). The generalization of the work by Marshall et al (1982) [12] given in Chapter 3 gives the dependence of all of the coefficients on the forward speed up to cubic terms.

In this chapter, we identify the linear parameters for the coupled ship-motion equations. We determine the correct form of the dependence of the linear terms on the forward speed. To this end, we use the Large Amplitude Motion Program (LAMP) developed by the Science Applications International Corporation (SAIC) (LAMP, 1998 [3]) to generate data for the heave and pitch motions in different sea states and with different forward speeds. Then,

we apply the eigensystem realization algorithm (ERA) (Ho and Kalman, 1965 [45]; Juang and Pappa, 1985 [44]) to the LAMP data to identify the linear coefficients of the coupled heave and pitch equations. The implementation of ERA in this work is part of a MATLAB toolbox called the System/Observer/Controller Identification Toolbox (SOCIT) written by Juang, Horta, and Phan (1991) [128]. For the heave and pitch motions, the identified linear coefficients are fitted against the forward speed using three forms; the first is based on strip theory (Salvesen et al, 1970 [6]), the second is based on the energy approach (Marshall et al, 1982 [12]), and the third is a ninth-order polynomial. The coefficients obtained with the different fitting forms are used to predict ship motions in different sea states with different forward speeds. By comparing these coefficients to LAMP data, we determine the most suitable form of the dependence of the linear coefficients on the forward speed.

The procedure outlined above is repeated to obtain exact fits for the coupled sway, roll, and yaw motions. Finally, exact fits for the full 5 DOF ship motions are provided, and regimes of motions where linear modeling fails are discussed.

4.1 Equations Governing Ship Motions

The equations that govern ship motions involve six degrees of freedom and are linearly and nonlinearly coupled. The identification of the coefficients of the linear terms is a prerequisite for the identification of the coefficients of the nonlinear terms. The surge, heave, and pitch are linearly coupled as one group; and the sway, roll, and yaw are linearly coupled as a second group. Therefore, these two sets can be identified separately.

The formulation of ship motions is usually established in two coordinate frames. The first frame is a moving coordinate frame, which is fixed to the ship and is called body-fixed reference frame. The x-axis is oriented along the ship's longitudinal axis and is directed from aft to fore. The y-axis is oriented along the ship's transverse axis and is directed towards starboard. The z-axis is oriented along the ship's normal axis and is directed from

top to bottom. The second frame is an inertial frame, which is fixed to a point on the surface of the earth and is called earth-fixed reference frame. The position and velocity vectors of the ship motion are then written as (Fossen, 1994 [127])

$$\eta = [x, y, z, \phi, \theta, \psi]^T \tag{4.1}$$

$$\nu = [u, v, w, p, q, r]^T \tag{4.2}$$

$$\dot{\eta} = J(\eta)\nu \tag{4.3}$$

where η represents the position and orientation vector in the earth-fixed coordinate system, ν is the linear and angular velocity vector in the body-fixed coordinate system, and $J(\eta)$ is a matrix that transforms the velocity vector from the body-fixed coordinate system to the earth-fixed coordinate system. The variables x, y, and z represent the motions in the x-, y-, and z-directions (surge, sway, and heave), respectively; and the variables ϕ, θ, and ψ represent the rotations about the x-, y-, and z-axes (roll, pitch, and yaw), respectively. The variables u, v, and w are the surge, sway, and heave linear velocities, respectively; and p, q, and r are the roll, pitch, and yaw angular velocities, respectively.

The forces and moments vector τ acting on the ship in the body-fixed frame are written as

$$\tau = [X, Y, Z, K, M, N]^T \tag{4.4}$$

where X, Y, and Z are the forces in the x-, y-, and z-directions, respectively; and K, M, and N are the moments about the x-, y-, and z-axes, respectively.

The six-degree-of-freedom (6DOF) nonlinear dynamic equations of ship motion can then be expressed in the body-fixed coordinate system as

$$\mathcal{M}_{RB}\dot{\nu} + \mathcal{C}_{RB}(\nu)\nu = \tau \tag{4.5}$$

where $\mathcal{M}_{RB}$ is the rigid-body inertia matrix and $\mathcal{C}_{RB}$ is the rigid-body matrix that contains the Coriolis and centripetal terms. The force vector τ can be divided into several components as

$$\tau = \tau_R + \tau_D + \tau_E \tag{4.6}$$

where τ_R is the radiation-induced hydrodynamic force, which is the force exerted on body due to its own motion with no incident waves; τ_D is the hydrodynamic force due to viscous effects, including skin friction, wave drift damping, and vortex shedding damping; and τ_E is the force exerted on the ship due to external forces including the Froude-Kriloff, diffraction, and forward speed forces.

The radiation-induced forces and moments τ_R can be analyzed as follows:

$$\tau_R = -\mathcal{M}_A\dot{\nu} - \mathcal{C}_A(\nu)\nu - \mathcal{D}_P(\nu)\nu - g(\eta) \tag{4.7}$$

where $\mathcal{M}_A$ is the added mass (inertia) matrix, $\mathcal{C}_A(\nu)$ is the added mass matrix that contains Coriolis and centripetal terms, $\mathcal{D}_P(\nu)$ is the radiation damping matrix, and $g(\nu)$ is a vector of gravitational forces and moments (restoring forces). The first two terms on the right-hand side (RHS) of Eq. (4.7) represent the added mass force due to the inertia of the surrounding fluid. The third term on the RHS represents the radiation-induced potential damping due to the energy carried away by the generated surface waves. The last term on the RHS is the restoring force due to gravity. We note here that sometimes the gravitational force is excluded from the radiation forces and is treated as a separate quantity. The viscous hydrodynamic force can be expressed as

$$\tau_D = -\mathcal{D}_V(\nu)\nu \tag{4.8}$$

where $\mathcal{D}_V(\nu)$ is the viscous damping matrix.

Substituting Eqs. (4.6) through (4.8) into Eq. (4.5), one obtains (Fossen, 1994 [127])

$$\mathcal{M}\dot{\nu} + \mathcal{C}(\nu)\nu + \mathcal{D}(\nu)\nu + g(\eta) = \tau_E \tag{4.9}$$

where

$$\mathcal{M} = \mathcal{M}_{RB} + \mathcal{M}_A \tag{4.10}$$

$$\mathcal{C}(\nu) = \mathcal{C}_{RB}(\nu) + \mathcal{C}_A(\nu) \tag{4.11}$$

$$\mathcal{D}(\nu) = \mathcal{D}_P(\nu) + \mathcal{D}_V(\nu) \tag{4.12}$$

In these equations, $\mathcal{M}$ is the inertia matrix (including the added mass), $\mathcal{C}(\nu)$ is a matrix of the Coriolis and centripetal terms (including the added mass), and $\mathcal{D}(\nu)$ is the damping matrix (including the radiation damping). Equation (4.9) is general in the sense that it is nonlinear and includes all of the forces acting on the ship. Using the transformation matrix $J(\eta)$, we can express Eq. (4.9) in the earth-fixed coordinate system as

$$\mathcal{M}_\eta(\eta)\ddot{\eta} + \mathcal{C}_\eta(\nu,\eta)\dot{\eta} + \mathcal{D}_\eta(\nu,\eta)\dot{\eta} + g_\eta(\eta) = \tau_{\eta E} \tag{4.13}$$

where the subscript η indicates that the quantities are written in the earth-fixed coordinate system. For convenience of notation and reading the subsequent equations, the subscript η is dropped from now on.

Equation (4.13) can be linearized about a steady forward speed U and the associated displacement for the surge motion and about zero velocities and displacements for the other motions to obtain

$$M\ddot{\eta} + C\dot{\eta} + K\eta = \mathbf{f} \tag{4.14}$$

where

$$M = M_{RB} + M_A \tag{4.15}$$

$$C = C_V + C_A \tag{4.16}$$

In these equations, M is the linearized mass (inertia) matrix and is the sum of M_{RB}, the linearized rigid-body mass (inertia) matrix, and M_A, the linearized added mass (inertia) matrix; C is the linearized damping matrix and is the sum of C_V, the linearized viscous damping matrix, and C_A, the linearized added damping matrix; K is the linearized stiffness matrix; $\mathbf{f}$ is the linearized external force vector; and η is redefined such that the surge is measured around the motion due to the steady forward speed of the ship. The Coriolis and centripetal terms disappeared due to linearization about zero angular velocities. It is worth noting here that the matrices M, C, and K are linear in the sense that they do not depend on η or ν, but they may depend on the forward speed U, and this dependence may be linear or nonlinear.

The components of the matrices in Eqs. (4.15) and (4.16) are

$$M_{RB} = \begin{bmatrix} m & 0 & 0 & 0 & mz_G & -my_G \\ 0 & m & 0 & -mz_G & 0 & mx_G \\ 0 & 0 & m & my_G & -mx_G & 0 \\ 0 & -mz_G & my_G & I_x & -I_{xy} & -I_{xz} \\ mz_G & 0 & -mx_G & -I_{yx} & I_y & -I_{yz} \\ -my_G & mx_G & 0 & -I_{zx} & -I_{zy} & I_z \end{bmatrix} \tag{4.17}$$

$$M_A = \left[\; a_{ij} \; \right], i, j = 1..6 \tag{4.18}$$

$$C_A = \left[\; b_{ij} \; \right], i, j = 1..6 \tag{4.19}$$

$$K = \left[\; c_{ij} \; \right], i, j = 1..6 \tag{4.20}$$

$$\mathbf{f} = \left[\; f_j \; \right], j = 1..6 \tag{4.21}$$

where m is the mass of the ship, I_x, I_y, and I_z are the ship moments of inertia about the x-, y-, and z- axes of the body-fixed coordinate system, the I_{ij} are the cross products of inertia, and x_G, y_G, and z_G are the coordinates of the center of gravity in the body-fixed coordinate system.

The equations of ship motion can then be separated into two groups to obtain (assuming that $x_G = y_G = I_{ij} = 0, i \neq j$)

$$(m + a_{11})\ddot{x} + b_{11}\dot{x} + c_{11}x + a_{13}\ddot{z} + b_{13}\dot{z} + c_{13}z + (a_{15} + mz_G)\ddot{\theta} + b_{15}\dot{\theta} + c_{15}\theta = f_1 \tag{4.22}$$

$$(m + a_{33})\ddot{z} + b_{33}\dot{z} + c_{33}z + a_{31}\ddot{x} + b_{31}\dot{x} + c_{31}x + a_{35}\ddot{\theta} + b_{35}\dot{\theta} + c_{35}\theta = f_3 \tag{4.23}$$

$$(I_y + a_{55})\ddot{\theta} + b_{55}\dot{\theta} + c_{55}\theta + (a_{51} + mz_G)\ddot{x} + b_{51}\dot{x} + c_{51}x + a_{53}\ddot{z} + b_{53}\dot{z} + c_{53}z = f_5 \tag{4.24}$$

for the surge, heave, and pitch equations, and

$$(m + a_{22})\ddot{y} + b_{22}\dot{y} + c_{22}y + (a_{24} - mz_G)\ddot{\phi} + b_{24}\dot{\phi} + c_{24}\phi + a_{26}\ddot{\psi} + b_{26}\dot{\psi} + c_{26}\theta = f_2 \tag{4.25}$$

$$(I_x + a_{44})\ddot{\phi} + b_{44}\dot{\phi} + c_{44}\phi + (a_{42} - mz_G)\ddot{y} + b_{42}\dot{y} + c_{42}y + a_{46}\ddot{\psi} + b_{46}\dot{\psi} + c_{46}\theta = f_4 \tag{4.26}$$

$$(I_z + a_{66})\ddot{\psi} + b_{66}\dot{\psi} + c_{66}\psi + a_{62}\ddot{y} + b_{62}\dot{y} + c_{62}y + a_{64}\ddot{\psi} + b_{64}\dot{\psi} + c_{64}\phi = f_6 \tag{4.27}$$

for the sway, roll, and yaw equations.

4.1.1 Effect of Forward Speed on Ship-Motion Parameters

In order to improve the seakeeping prediction and operational procedures, it is important to accurately estimate the ship parameters for different ship speeds. The coefficients a_{ij}, b_{ij}, and c_{ij} of the linear model represented by Eqs. (4.22) through (4.27) are functions of the forward speed. However, the form of this dependence is not clear. Several previous works addressed this problem (Korvin-Korvosky and Jacobs, 1957 [5]; Salvesen at al, 1970 [6]; Ogilvie and Tuck, 1969 [7]; Marshall et al, 1982 [12]). The strip theory of Salvesen et al (1970) [6] resulted in the following form of the dependence of the elements of the matrices on the forward speed:

$$M_A = \begin{bmatrix} m_8 & 0 & m_{22} & 0 & m_{23} + d_2U/\Omega^2 \\ 0 & m_9 & 0 & m_{24} - d_3U/\Omega^2 & 0 \\ m_{22} & 0 & m_{10} & 0 & m_{24} - d_9U \\ 0 & m_{24} + d_3U/\Omega^2 & 0 & m_{11} + m_9U^2/\Omega^2 & 0 \\ m_{23} - d_2U/\Omega^2 & 0 & m_{24} - d_9U/\Omega^2 & 0 & m_{12} + m_8U^2/\Omega^2 \end{bmatrix} \tag{4.28}$$

$$C_A = \begin{bmatrix} d_2 & 0 & d_9 & 0 & d_{10} - m_8U \\ 0 & d_3 & 0 & d_{11} + m_9U & 0 \\ d_9 & 0 & d_4 & 0 & d_{12} - m_{22}U \\ 0 & d_{11} - m_9U & 0 & d_5 + d_3U^2/\Omega^2 & 0 \\ d_{10} + m_8U & 0 & d_{12} + m_{22}U & 0 & d_6 + d_2U^2/\Omega^2 \end{bmatrix} \tag{4.29}$$

and

$$K = \begin{bmatrix} 0 & 0 & 0 & 0 & 0 \\ 0 & V_1 & 0 & V_4 & 0 \\ 0 & 0 & V_2 & 0 & 0 \\ 0 & V_4 & 0 & V_3 & 0 \\ 0 & 0 & 0 & 0 & 0 \end{bmatrix} \tag{4.30}$$

where m_i, d_i, and V_i are constants and Ω is the exciting frequency. We note that the strip-theory formulation does not include the surge motion, which is a consequence of the two-dimensional assumption.

Marshall et al (1982) [12] utilized an energy approach to determine the form of the dependence of the ship parameters on its forward speed. In this approach, the ship and the surrounding water are considered to be a single dynamical system. The forms of the kinetic energy, the potential energy, and the dissipation function of water are then assumed. For example, the kinetic energy is taken to be a function of the position in order to take into account the free-surface effects. Attention is also given to the symmetry properties of the ship and the positive definiteness of the kinetic energy and dissipation. With these assumptions, the possibility of unrealistic self-sustained motions is eliminated (Nayfeh et al, 1974 [11]). Also, the derived formulas of the parameters satisfy the Timman and Newman symmetry conditions (Timman and Newman, 1962 [20]). Based on the work of Marshall et al (1982) [12], the energy approach yields the following forms for the matrices:

$$M_A = \begin{bmatrix} m_1 & 0 & m_{14} & 0 & m_{18} & 0 \\ 0 & m_8 & 0 & m_{22} & 0 & m_{23} \\ m_{14} & 0 & m_9 & 0 & m_{24} & 0 \\ 0 & m_{22} & 0 & m_{10} & 0 & m_{25} \\ m_{18} & 0 & m_{24} & 0 & m_{11} & 0 \\ 0 & m_{23} & 0 & m_{24} & 0 & m_{12} \end{bmatrix} \tag{4.31}$$

$$C_A = \begin{bmatrix} d_1 & 0 & d_7 + m_2U \\ 0 & d_2 & 0 \\ d_7 - m_2U & 0 & d_3 \\ 0 & d_9 - (m_{13} - m_{14})U & 0 \\ {}^M d_8(m_3 + 2m_{14})U & 0 & d_{11} + (m_1 - m_9 - m_{16} + m_{19})U \\ 0 & d_{10} - (m_1 - m_8)U & 0 \end{bmatrix}$$

$$\begin{bmatrix} 0 & d_8 + (m_3 + 2m_{14}U & 0) \\ d_9 + (m_{13} - m_{14})U & 0 & d_{10} + (m_1 - m_8)U \\ 0 & d_{11} - (m_1 - m_9 - m_{16} + m_{19})U & 0 \\ d_4 & 0 & d_{12} - (m_{18} + m_{21} + m_{22})U \\ 0 & d_5 & 0 \\ d_{12} + (m_{18} + m_{21} + m_{22})U & 0 & d_6 \end{bmatrix} \tag{4.32}$$

and

$$K = \begin{bmatrix} 0 & 0 & 0 \\ 0 & 0 & 0 \\ 0 & 0 & V_1 - m_4U^2 \\ 0 & 0 & 0 \\ 0 & 0 & V_4 - (1/2m_6 + m_{15})U^2 \\ 0 & 0 & 0 \end{bmatrix}$$

$$\begin{bmatrix} 0 & 2d_7U & 0 \\ -d_7U & 0 & (d_1 - d_2)U \\ 0 & V_4 - (1/2m_6 + m_{15})U^2 + (d_3 - d_1)U & 0 \\ V_2 - m_7U^2 & 0 & (m_{13} - m_{14})U^2 - d_9U \\ 0 & V_3 + (m_1 - m_5 - m_9 - 2m_{16})U^2 + d_{11}U & 0 \\ (m_{13} - m_{14})U^2 + d_8U & 0 & (m_1 - m_8)U^2 - d_{10}U \end{bmatrix} \tag{4.33}$$

where m_i, d_i, and V_i are constants that appear in the formulas of the kinetic energy, dissipation function, and potential energy. It is clear that, while the energy approach and the strip theory give similar forms for the dependence of many terms on the forward speed, they give different forms for other terms. For example, comparing the coefficients of the heave-pitch equations reveals that the energy-formulation approach predicts that all of the added mass coefficients are not functions of U, c_{33} and c_{53} are functions of U^2, and c_{35} and c_{55} are functions of U and U^2. In contrast, the strip-theory approach predicts that a_{33} is independent of U, a_{35} and a_{53} are functions of U, a_{55} is a function of U^2, and all of the stiffness coefficients are independent of U.

The objective of the work in this chapter is to determine the correct form of the dependence of these coefficients on the forward speed. To achieve our objective, we generate ship-motion data with the LAMP code. Then, we identify the ship motion to determine its parameters as functions of the forward speed. We fit the identified parameters according to both formulations. The results are then compared with the LAMP data to determine the correct dependence on the forward speed. The ship-motion data is identified using a MATLAB toolbox called the System/Observer/Controller Identification Toolbox (SOCIT) written by

Juang et al (1991) [128]. This toolbox calculates the pulse-response functions (Markov parameters) from the time-domain data using a method called the observer/Kalman filter identification (OKID). Then, the ERA is utilized to obtain a linear state-space model from the Markov parameters. The next two sections describe the LAMP code, the formulation of the ship linear identification problem in state-space form, and the application of the ERA to obtain the linear parameters.

4.2 The LAMP Code

In order to identify the parameters of the linear model represented by Eqs. (4.23) and (4.24), we generate numerical ship-motion data using the LAMP code. LAMP is a potential-flow code that can predict time-domain linear and nonlinear motions and loads of floating bodies with and without forward speed in various sea states. LAMP employs two coordinate systems to describe the six DOF motion of a ship in a seaway. One is an earth-fixed coordinate system and the other is a body-fixed coordinate system. LAMP's formulation is based on a panel method and is done in an earth-fixed coordinate system. The submerged body surface at each time step is divided into a number of panels over which linearized transient free-surface sources are distributed. The exact body boundary conditions are applied on the instantaneous submerged hull surface, while a linearized free-surface condition is used. For nonlinear calculations, the position and orientation of the body are updated at each time step and the underwater body surface is repanelized. Several types of formulations are used in LAMP. For the purpose of this work, we utilize the linear hydrodynamics formulation (LAMP2). For this version of LAMP, nonlinearity can arise from the hydrostatics and rigid-body dynamics. In LAMP, a seaway can be prescribed as a linear superposition of sinusoidal components or can be generated from the Pierson-Moskowitz or Brettschneider spectra (Korvin-Kroukovsky, 1961 [129]). LAMP allows the user to constrain some of the degrees of freedom. It also allows modeling of several control systems, including propulsion control, course or track-keeping autopilot, roll stabilization, and external forces. A complete

description of LAMP is given in (LAMP, 1998 [3]).

4.3 Linear Parametric Identification

There are several techniques to fit experimental, analytical, or numerical data with a parametric model. We are interested in a technique that utilizes multiple input and output data to obtain the mode shapes, the poles, and the initial modal amplitudes. We select the ERA because of several reasons. First, it can handle a large number of degrees of freedom. Second, it provides information about the system masses. Third, it does not place any restrictions on the identified roots (eigenvalues) and repeated roots are allowed. Fourth, it can handle noisy data. Finally, it does not involve iterations.

4.3.1 State-Space Formulation

The ERA provides the linear system parameters in a state-space form. Hence, it is essential to transform the linear model of Eqs. (4.22) through (4.27) into that form in order to interpret the results of the ERA. A discrete state-space model of the ship motion is constructed using the following definitions (Juang, 1994 [29]):

$$x = \begin{bmatrix} \eta \\ \dot{\eta} \end{bmatrix} \tag{4.34}$$

$$A_c = \begin{bmatrix} \emptyset_{\frac{n}{2}\times\frac{n}{2}} & I_{\frac{n}{2}\times\frac{n}{2}} \\ -M^{-1}K & -M^{-1}C \end{bmatrix} \tag{4.35}$$

$$B_c = \begin{bmatrix} \emptyset_{\frac{n}{2}\times r} \\ M^{-1}F \end{bmatrix} \tag{4.36}$$

$$\mathbf{f} = Fu \tag{4.37}$$

where $\frac{1}{2}n$ is the number of independent variables, n is the system order, x is an n by 1 state vector, A_c is an n by n state matrix, B_c is an n by r input influence matrix, where r is

the number of inputs (forces), $\emptyset_{\frac{n}{2}\times\frac{n}{2}}$ is an $\frac{n}{2}$ by $\frac{n}{2}$ zero matrix, $I_{\frac{n}{2}\times\frac{n}{2}}$ is an $\frac{n}{2}$ by $\frac{n}{2}$ identity matrix, F is an $\frac{n}{2}$ by r matrix characterizing the locations and types of inputs, and u is an r by 1 input vector. The superscript -1 denotes a matrix inverse and the subscript c denotes continuous time systems.

Using Eqs. (4.34) through (4.37), we transform Eq. (4.14) into

$$\dot{x}(t) = A_c x(t) + B_c u(t) \tag{4.38}$$

where t is time. The output of the system can then be expressed as

$$y = C_a \ddot{\eta} + C_v \dot{\eta} + C_d \eta \tag{4.39}$$

where C_a, C_v, and C_d are m by $\frac{n}{2}$ output influence matrices for acceleration, velocity, and displacement, respectively, with m being the number of outputs, and y is an m by 1 output vector. Equation (4.39) can be transformed into

$$y(t) = Cx(t) + Du(t) \tag{4.40}$$

$$C = \left[\begin{array}{cc} C_d - C_a M^{-1} K & C_v - C_a M^{-1} C \end{array} \right] \tag{4.41}$$

$$D = C_a M^{-1} F \tag{4.42}$$

where C is as an m by n output influence matrix for the state vector x, including the effect of velocity and displacement only, and D is an m by r direct transmission matrix.

It is necessary to transform Eqs. (4.38) and (4.40) into discrete forms in order to handle the discrete ship data of LAMP. The discrete form of these equations can be written as

$$x(k+1) = Ax(k) + Bu(k) \tag{4.43}$$

$$y(k) = Cx(k) + Du(k) \tag{4.44}$$

where A is the state matrix in discrete form, B is the input influence matrix in discrete form, and k is the time index. The relations between A_c and B_c and A and B are given by

$$A = e^{A_c \Delta t} \tag{4.45}$$

$$B = \int_0^{\Delta t} e^{A_c \xi} \, d\xi B_c \tag{4.46}$$

where Δt is the time step and ξ is a dummy variable of integration. It should be noted here that for a 6 DOF ship motion, $m = r = \frac{n}{2} = 6$, while for the 2 DOF coupled heave and pitch equations, $m = r = \frac{n}{2} = 2$. Also, $D = [\emptyset]_{2\times 2}$ and $F = [I]_{2\times 2}$.

4.3.2 Eigensystem Realization Algorithm

The eigensystem realization algorithm (ERA) is a multiple-reference (input), multiple-response (output) algorithm (Juang and Pappa, 1985 [44]; Juang, 1994 [29]). We begin the presentation of this technique by considering a sequence of pulse-response matrices Y_{pq} constructed as

$$Y_{pq}(k) = \begin{bmatrix} y_{11}(k) & y_{12}(k) & \dots & y_{1q}(k) \\ y_{21}(k) & y_{22}(k) & \dots & y_{2q}(k) \\ \vdots & \vdots & \ddots & \vdots \\ y_{p1}(k) & y_{p2}(k) & \dots & y_{pq}(k) \end{bmatrix} \tag{4.47}$$

where p, q, and k are response, reference, and time indices, respectively, and $y_{pq}(k)$ is the pulse response of degree of freedom p due to a pulse input of degree of freedom q at time index k. The constant matrices in the pulse-response sequence are called the Markov parameters, which are unique for a given system. It can be shown that the pulse-response matrices can be compactly expressed as (Juang, 1994 [29])

$$Y_{pq}(k) = CA^{k-1}B \tag{4.48}$$

Without loss of generality, we consider the case when A is diagonal. In this case, A contains the information about the modal damping rate and the damped natural frequencies, B defines the initial modal amplitudes, and C defines the mode shapes at the sensor points. Other forms of A like the form given by Eq. (4.35) can be found by applying the appropriate transformation to the diagonal form of A. All of the different forms of A have the same eigenvalues. Thus, any nonsingular linear transformation of the state-space system produces the same input-output description of the system.

A realization is the computation of a triplet $[A, B, C]$ from the Markov parameters such that Eq. (4.48) holds for all values of k. The objective of ERA is to find a minimum realization. Minimum realization means a model with the smallest state-space dimensions; that is, A, B, and C have the smallest dimensions possible. Generally, the sizes of p and q are the number of response and reference measures, while the size of n need not be related to p or q. However, in the case of a 6 DOF ship motion, $p = q = \frac{n}{2} = 6$, while for the coupled heave and pitch equations, $p = q = \frac{n}{2} = 2$. We proceed by considering the following $r \times s$ *block* matrix ($rp \times sq$ matrix)

$$H_{rs}(k-1) = \begin{bmatrix} Y_{pq}(k) & Y_{pq}(k+1) & \dots & Y_{pq}(k+s-1) \\ Y_{pq}(k+1) & Y_{pq}(k+2) & \dots & Y_{pq}(k+s) \\ \vdots & \vdots & \ddots & \vdots \\ Y_{pq}(k+r-1) & Y_{pq}(k+r) & \dots & Y_{pq}(k+s+r-2) \end{bmatrix} \tag{4.49}$$

which is called the generalized Hankel matrix whose entries are matrices themselves, explained by the term *block*. The choices of the integer values for s and r are arbitrary. However, the smallest dimension of the block Hankel matrix must be equal to or greater than n. The matrix $H_{rs}(k-1)$ can be related to the response matrix according to

$$Y_{pq}(k) = E_p^T H_{rs}(k-1) E_q \tag{4.50}$$

where $E_p^T = [I_{p\times p}, \emptyset_{p\times p}, \dots, \emptyset_{p\times p}]_{p\times rp}$ and $I_{p\times p}$ and $\emptyset_{p\times p}$ are identity and null matrices of order p, respectively. Similarly, $E_q^T = [I_{q\times q}, \emptyset_{q\times q}, \dots, \emptyset_{q\times q}]_{q\times sq}$.

The zero-lag block matrix is resolved using the singular value decomposition as

$$\begin{aligned} H_{rs}(0) &= [P|P_0] \begin{bmatrix} [\backslash D \backslash] & \emptyset \\ \emptyset & [\backslash D_0 \backslash] \end{bmatrix} \left[\begin{array}{c} Q^T \\ \hline Q_0^T \end{array}\right] \\ &\approx [P][\backslash D \backslash][Q]^T \end{aligned} \tag{4.51}$$

where the augmented matrices on the right-hand side are $rp \times sq$, $sq \times sq$, and $sq \times sq$ from left to right when $rp \geq sq$. However, if the dynamics of a limited bandwidth signal are dominated by $\frac{n}{2}$ so-called normal modes, then only n singular values and vectors are

physically significant. By advocacy, the smallest singular values are truncated. One speaks of D, P, and Q as the significant singular values and the left and right singular vectors, respectively.

The system eigenvalues can be uncovered by finding A. In accordance with Eqs. (4.48), (4.50), and (4.51),

$$H_{rs}(1) = PD^{1/2}\tilde{A}D^{1/2}Q^T \tag{4.52}$$

where $\tilde{A}$ is defined, within a rotation of A given as the solution of the eigenvalue problem $\tilde{A}\psi = \psi A$, as

$$\tilde{A} = D^{-1/2}P^T H_{rs}(1)QD^{-1/2} \tag{4.53}$$

$$\psi^{-1}[D^{-1/2}P^T H_{rs}(1)QD^{-1/2}]\psi = [\backslash A \backslash] \tag{4.54}$$

The matrix A is given as $[\backslash z_1 \dots z_k \dots z_n \backslash]$ in the desired diagonal form, where the z_k are the system poles in the z-domain. The frequency-domain pole estimates λ_k can be found as

$$\lambda_k = \frac{1}{\Delta t}\ln(z_k) \tag{4.55}$$

in radians per second (for time in seconds).

The mode shapes and initial modal amplitudes are determined by constructing two identity matrices as

$$\left[D^{1/2}\psi\psi^{-1}D^{-1/2}P^T P\right] = I_{n\times n}, \qquad \left[Q^T Q D^{-1/2}\psi\psi^{-1}D^{1/2}\right] i = I_{n\times n} \tag{4.56}$$

where we utilized the properties that P and Q are self orthogonal ($P^T P = I, Q^T Q = I$), which do not extend to PP^T or QQ^T. These matrices can be inserted into the right-hand side of Eq. (4.52) to produce

$$P\left[D^{1/2}\psi\psi^{-1}D^{-1/2}P^T P\right]D^{1/2}\tilde{A}D^{1/2}\left[Q^T Q D^{-1/2}\psi\psi^{-1}D^{1/2}\right]Q^T$$

which when combined with Eqs. (4.48), (4.50), (4.52), and (4.54) yields

$$\left[E_p^T P D^{1/2}\psi\right][\backslash z \backslash]\left[\psi^{-1}D^{1/2}Q^T E_q\right] = [C][\backslash A \backslash][B] \tag{4.57}$$

Equation (4.57) represents the mode shapes, poles, and initial modal amplitudes, respectively. In the next section, we present the results of identifying the linearly coupled heave and pitch equations.

4.4 Identification of the Heave and Pitch Equations

For the data used here, we use the linear version of the LAMP code (LAMP2). Only the heave and pitch motions are considered with all of the other motions constrained. In order to estimate the matrices A, B, and C of Eqs. (4.43) and (4.44), we apply the ERA to the motion (input) and force (output) data of sea state 3 runs. The nondimensional forward speed U, which is also the Froude number, is varied between 0.05 and 0.5. The discrete system matrices A and B are transformed into a continuous form using the relations given by Eqs. (4.45) and (4.46). Given the matrices A_c, B_c, and C, the linear system matrices M, C, and K are found using the definitions given by Eqs. (4.35) and (4.36). Knowing M, C, and K, we find all of the coefficients of the linear model represented by Eqs. (4.23) and (4.24) (excluding the effects of the surge motion) using the definitions given by Eqs. (4.17) and (4.21). Then, each of the coefficients (for example b_{33}) is fitted against U using three different forms. The first form is an exact fit, using a polynomial of order nine. The second form is an energy-formulation fit (Marshall et al, 1982 [12]), and the last form is a strip-theory fit (Salvesen et al, 1970 [6]). As an example, Fig. 4.1 shows the calculated data and the corresponding fits of the damping coefficients b_{33}, b_{35}, b_{53}, and b_{55} using the three aforementioned forms. In general, the results can be fitted to obtain relatively good agreement. Similar fits were obtained for all of the parameters using the three different forms. The results of the energy-formulation fit are

$$a_{33} = 0.0046257 \qquad a_{35} = a_{53} = -0.000036406 \qquad \text{and} \qquad a_{55} = 0.0001723 \tag{4.58}$$

for the added mass coefficients,

$$b_{33} = 0.0088364 \qquad b_{35} = 0.00066 + 0.0036372U \tag{4.59}$$

$$b_{53} = 0.00066 - 0.0036372U \quad \text{and} \quad b_{55} = 0.00020942 \tag{4.60}$$

for the damping coefficients, and

$$c_{33} = 0.11189 - 0.060993U^2 \quad c_{35} = 0.005079 + 0.0088364U - 0.0047567U^2 \tag{4.61}$$

$$c_{53} = 0.005079 - 0.0047567U^2 \quad \text{and} \quad c_{55} = 0.0066298 + 0.00066U - 2.3615e{-}05U^2 \tag{4.62}$$

for the stiffness coefficients.

The results of the strip-theory fit are

$$a_{33} = 0.0046257 \quad a_{35} = -0.0001062 + 0.00057883U \tag{4.63}$$

$$a_{53} = -0.0001062 - 0.00057883U \quad \text{and} \quad a_{55} = 0.00016508 + 7.5623e - 05U^2 \tag{4.64}$$

for the added mass coefficients,

$$b_{33} = 0.0088364 \quad b_{35} = 0.00066 + 0.0041043U \tag{4.65}$$

$$b_{53} = 0.00066 - 0.0041043U \quad \text{and} \quad b_{55} = 0.00032636 - 0.0012139U^2 \tag{4.66}$$

for the damping coefficients, and

$$c_{33} = 0.11776 \quad c_{35} = c_{53} = 0.0058883 \quad \text{and} \quad c_{55} = 0.0068091 \tag{4.67}$$

for the stiffness coefficients. The lengthy exact-fit polynomials are not presented.

Given the coefficients of the linear model obtained with the different fits, Eqs. (4.23) and (4.24) can be integrated to predict the heave and pitch motions. The validity of all fits, however, should be examined by comparing the predictions obtained using the identified coefficients with the original data from the LAMP simulations. The accuracy of the results (based on the normal variance) for sea state 3 and forward speeds that range from 0.05 to 0.5 and sea states 2 through 7 with a forward speed of 0.25 are summarized in Table 4.1. The results show that the accuracy level of the exact fit varies between 92% and 99%. The accuracy level of the energy-formulation fit varies between 72% and 99%. On the other hand, the accuracy level of the strip-theory fit varies between 41% and 96%.

Figure 4.2 compares the ship-motion predictions obtained with the three different fits to the original LAMP data for sea state 3 and forward speed $U = 0.4$. The pitch response is in degrees, while the time and the heave displacement are nondimensional. The length L of the ship is used as the length scale and $\sqrt{\frac{L}{g}}$ is used as the time scale, where g is the gravitational acceleration The simulation data is sampled at a nondimensional rate of 0.02. It is obvious that the exact fit is the most accurate and that the energy-formulation fit gives more accurate predictions than the strip-theory fit. Similar observations can be obtained from Fig. 4.3, which presents comparisons for sea state 7 and $U = 0.25$. It is worth noting here that as the sea state increases, the validity of the linear formulation becomes questionable since the nonlinear terms in the equations of motion become important. This explains the relatively less accurate results for all fits at higher sea states.

By examining the results of this section, it is established that the ERA is capable of extracting the linear system coefficients for a variety of sea conditions and forward speeds. It is also established that the models for the effect of the forward speed provided by the energy-formulation approach produce more accurate predictions than those provided by the strip-theory approach.

4.5 Identification of the Sway, Roll, and Yaw Equations

The same methodology discussed with respect to the heave and pitch motions is applied for the identification of the coefficients of the sway, roll, and yaw motions. Data for these motions is generated with the LAMP code. ERA is applied with the motion (input) and force (output) data of sea state 3 runs. The nondimensional forward speed U is varied between 0.05 to 0.5 with a step of 0.05. The discrete system matrices A and B are transformed into a continuous form and the linear system matrices $\mathbf{M}$, $\mathbf{C}$, and $\mathbf{K}$ are found. All of the coefficients of the linear model represented by Eqs. (4.25), (4.26), and (4.27) are found.

Table 4.1: Accuracy of the predicted data as compared with the LAMP data

Sea state	U	Exact (order 9 polynomial)		Energy formulation		Strip theory	
		Heave	Pitch	Heave	Pitch	Heave	Pitch
3	0.05	0.96602	0.96806	0.72158	0.94965	0.73844	0.94282
3	0.1	0.99088	0.98015	0.84919	0.97542	0.87306	0.84571
3	0.15	0.9735	0.98099	0.92614	0.95657	0.92655	0.82385
3	0.2	0.95741	0.92284	0.91576	0.87953	0.76328	0.65192
3	0.25	0.95297	0.95162	0.9586	0.94671	0.70487	0.82308
3	0.3	0.97498	0.95228	0.96086	0.92217	0.66441	0.84349
3	0.35	0.96946	0.96664	0.95801	0.94732	0.61252	0.92466
3	0.4	0.98316	0.98744	0.98517	0.9768	0.60387	0.95661
3	0.45	0.98587	0.99595	0.9979	0.99035	0.50458	0.9443
3	0.5	0.90289	0.94985	0.97839	0.96849	0.42184	0.86806
2	0.25	0.93388	0.97401	0.90188	0.97378	0.90749	0.95816
3	0.25	0.95297	0.95162	0.9586	0.94671	0.70487	0.82308
4	0.25	0.96303	0.93964	0.97498	0.9415	0.83057	0.79756
5	0.25	0.97255	0.88156	0.94327	0.83625	0.77409	0.49162
6	0.25	0.97022	0.85061	0.93239	0.77016	0.76014	0.41324
7	0.25	0.9587	0.86707	0.96631	0.8479	0.86205	0.62279

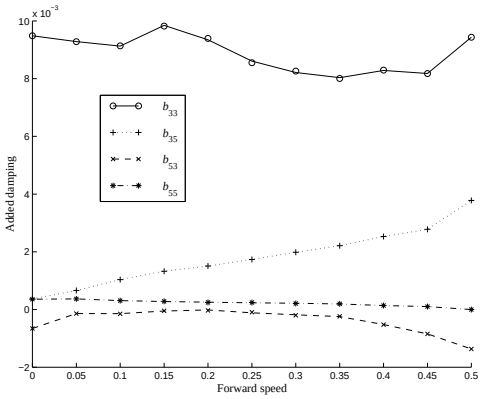

(a) Exact fit

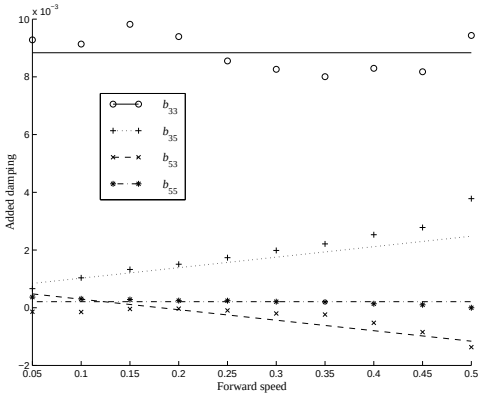

(b) Energy-formulation fit

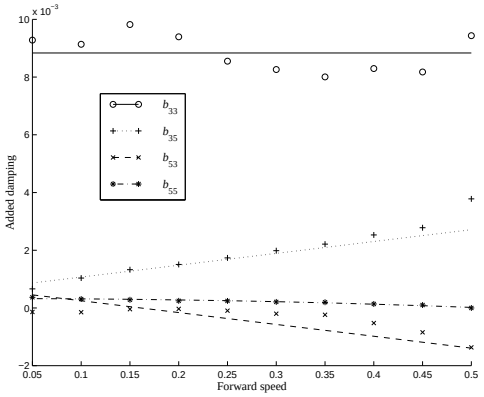

(c) Strip-theory fit

Figure 4.1: Fitting of the calculated damping coefficients using three different methods

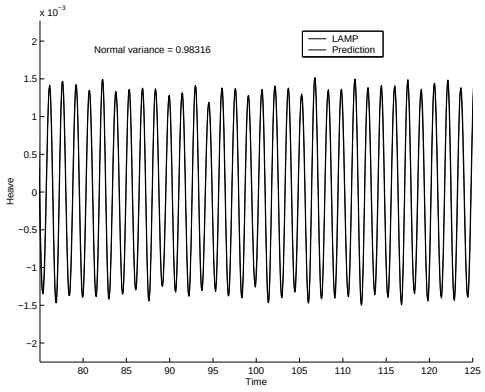

(a) Exact-fit (heave)

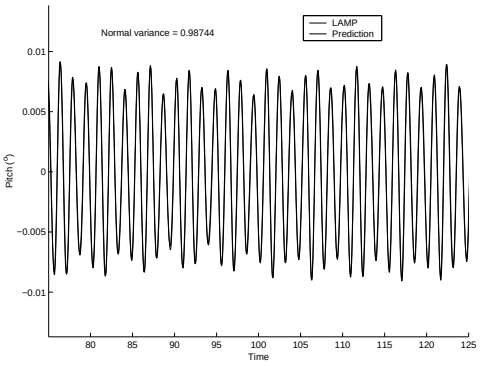

(b) Exact-fit (pitch)

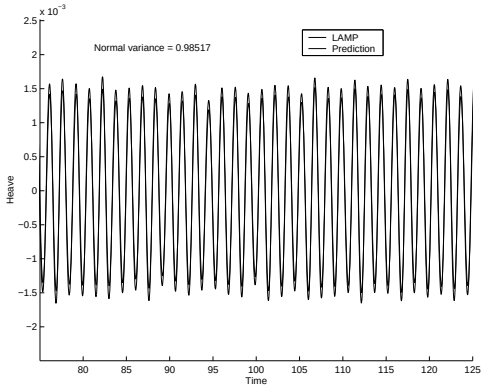

(c) Energy-formulation fit (heave)

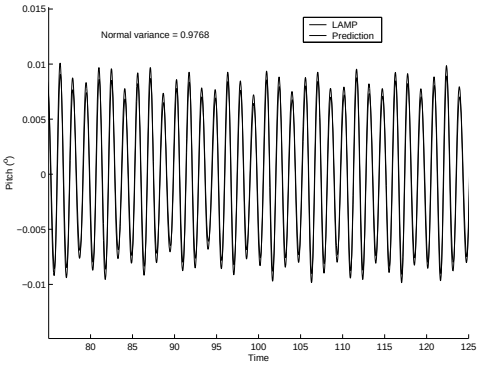

(d) Energy-formulation fit (pitch)

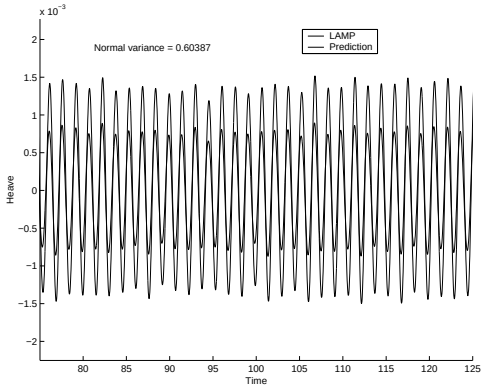

(e) Strip-theory fit (heave)

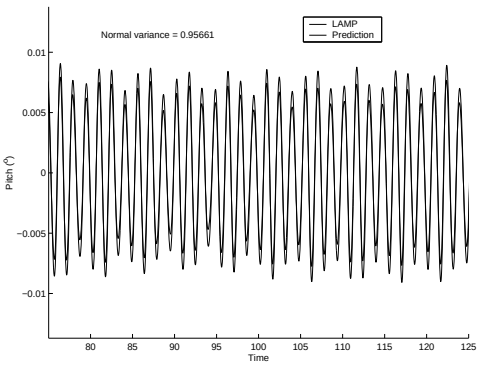

(f) Strip-theory fit (pitch)

Figure 4.2: Prediction of ship motion for sea state 3 and $U = 0.4$

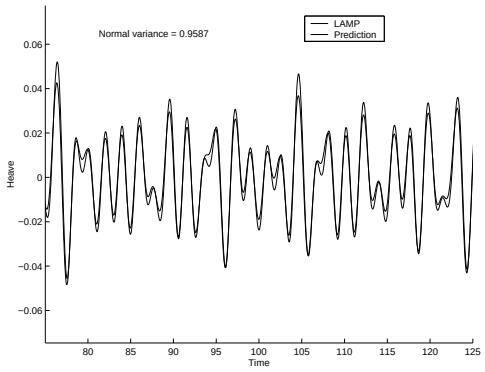

(a) Exact-fit (heave)

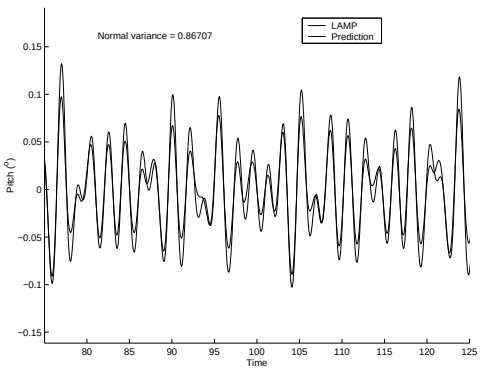

(b) Exact-fit (pitch)

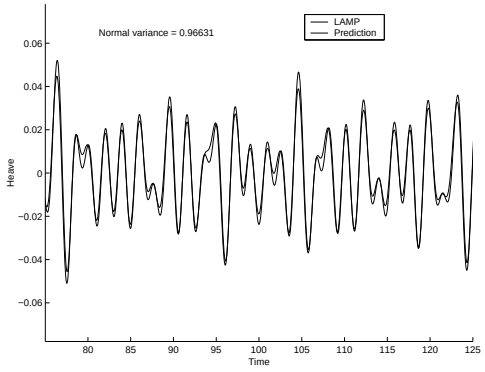

(c) Energy-formulation fit (heave)

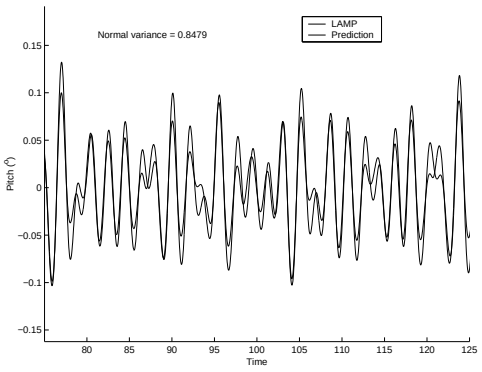

(d) Energy-formulation fit (pitch)

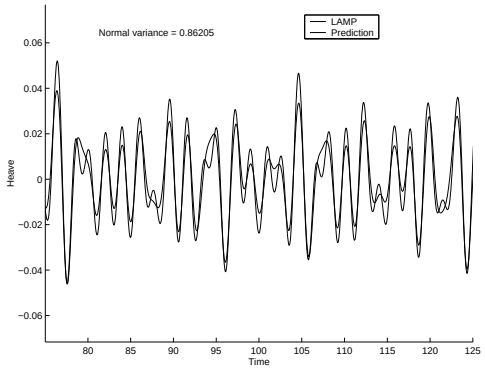

(e) Strip-theory fit (heave)

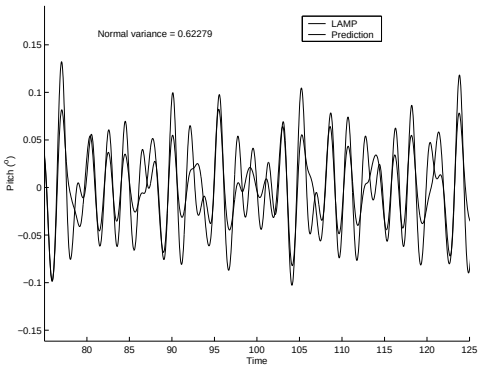

(f) Strip-theory fit (pitch)

Figure 4.3: Prediction of ship motion for sea state 7 and $U = 0.25$

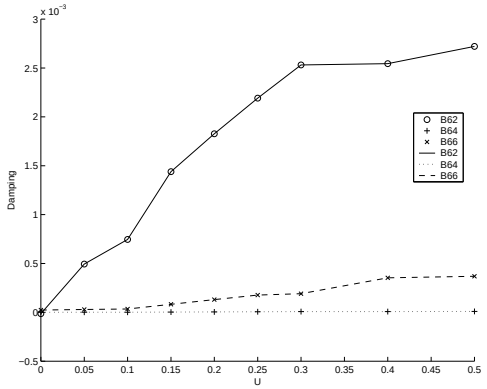

Figure 4.4: Polynomial fits of the calculated damping coefficients

Then, each of the coefficients is fitted against U using a polynomial of order 9. Figure 4.4 shows fits of the damping coefficients b_{62}, b_{64}, and b_{66} as function of the forward speed. The lengthy polynomial fits are not given here.

Given the coefficients of the linear model obtained with the these fits, Eqs. (4.25), (4.26) and (4.27) can be integrated to predict the sway, roll, and yaw motions. The validity of the fits is examined by comparing the predictions obtained using the identified coefficients with the original data from the LAMP simulations. The LAMP data are for sea state 3 and forward speeds that range from 0.05 to 0.5 and sea states 2 through 4 with a forward speed of 0.25. The accuracy of the results (based on the normal variance) are summarized in Table 4.2. The accuracy level of the fits is between 86% and 99%. Again, it is established that the ERA is capable of extracting the linear system coefficients for a variety of sea conditions. Figure 4.5 compares the ship-motion predictions to the original LAMP data for sea state 3 and $U = 0.4$. The roll and yaw responses are in degrees, while the time and the sway displacement are nondimensional. The nondimensionalization parameters are the same as described in the previous section. The simulation data is sampled at a nondimensional rate of 0.02. It is obvious that the fits are accurate. Similar observations can be obtained from Fig. 4.6 which presents the comparisons for sea state 4 and $U = 0.25$. It is worth noting here that the linear model fails for states 5 and above. This is attributed to the nonlinear effects, as will be discussed in more detail in Chapter 6.

Table 4.2: Accuracy of the predicted data as compared with the LAMP data

Sea state	U	Accuracy		
		Sway	Roll	Yaw
2	0.25	0.8923	0.876	0.8828
3	0.0	0.8672	0.9986	0.9953
3	0.05	0.9809	0.9963	0.995
3	0.1	0.9426	0.9618	0.9631
3	0.15	0.9642	0.9912	0.9862
3	0.2	0.9674	0.997	0.9848
3	0.25	0.98	0.9974	0.9812
3	0.3	0.9757	0.9987	0.9745
3	0.35	0.9858	0.9917	0.99
3	0.4	0.9915	0.9888	0.9835
3	0.45	0.9923	0.9825	0.9726
3	0.45	0.9923	0.9825	0.9726
3	0.5	0.9719	0.9523	0.9108
4	0.25	0.8797	0.8594	0.8686

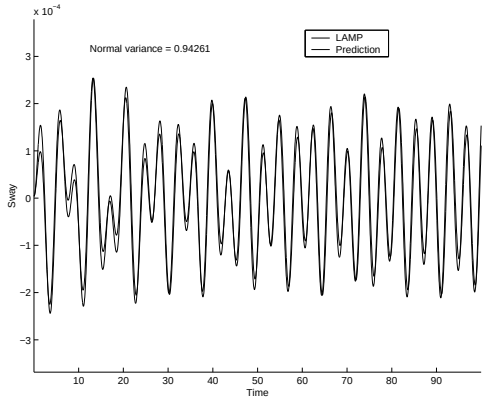

(a) sway

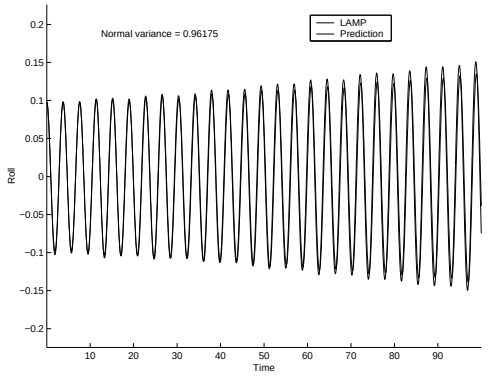

(b) roll

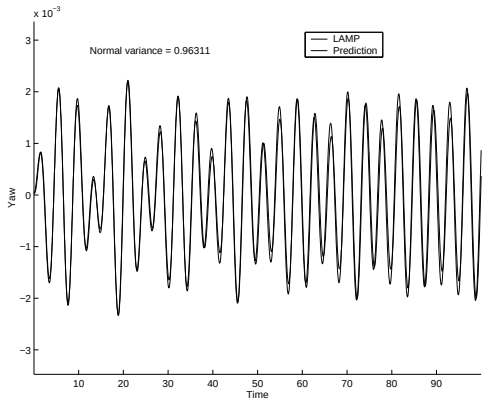

(c) yaw

Figure 4.5: Prediction of ship motion for sea state 3 and $U = 0.4$

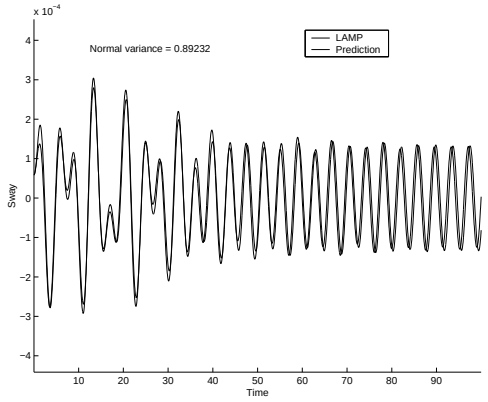

(a) sway

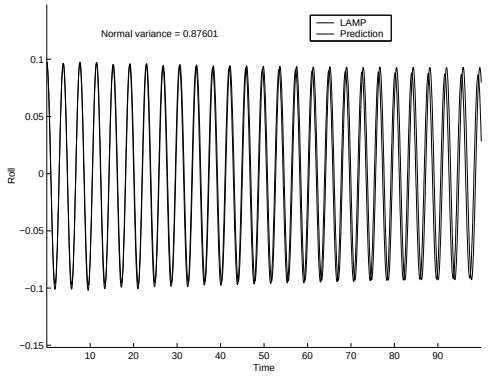

(b) roll

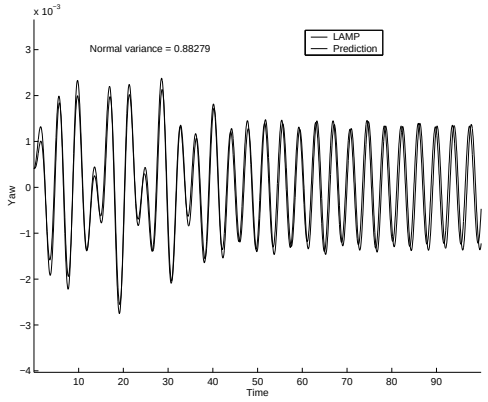

(c) yaw

Figure 4.6: Prediction of ship motion for sea state 4 and $U = 0.25$

4.6 Identification of 5 DOF Ship Motion

In this part, we apply the linear parametric identification methodology to 5 DOF ship motion. The LAMP code is used to generate the heave, pitch, sway, roll, and yaw motions. Then, ERA is applied separately to the heave and pitch motions as one group and to the sway, roll, and yaw motions as another group. The nondimensional forward speed U is varied between 0.05 to 0.35. Exact fits are used for the identified parameters. The results of the two identification groups are combined and used to predict the 5 DOF ship motion. The prediction results for different sea states and forward speeds are summarized in Figs. 4.7a and 4.7b. Figure 4.7a shows the accuracy of the ERA prediction in comparison to the LAMP data for different forward speeds and sea state 3. It is evident that the ERA provides good predictions for all motions and for all values of forward speed. Figure 4.7b shows the accuracy of the ERA prediction for different sea states and a forward speed of 0.2. It can be seen that the accuracy of the heave and pitch predictions are excellent for all sea states. On the other hand, the accuracy of the sway, roll, and yaw predictions is good up to sea state 4, and then the accuracy deteriorates for higher sea states. It can be concluded that the linear model of the heave and pitch motions is applicable for all sea states, where the nonlinear effects are negligible. On the other hand, the linear model of the sway, roll, and yaw motions fails above sea state 4 since the nonlinear effects are strong. The worst accuracy occurs at sea state 5 because, at this sea state, and forward speed of 0.2, a nonlinear parametric resonance in the roll motion is excited (Sanchez and Nayfeh, 1990 [130]; Oh at al, 1993 [78]; Oh et al, 2000 [131]). Such a resonance can be exploited to find the nonlinear parameters, as explained in Chapter 6.

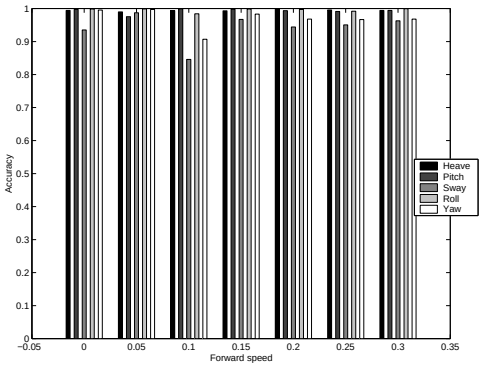

(a) Sea sate 3

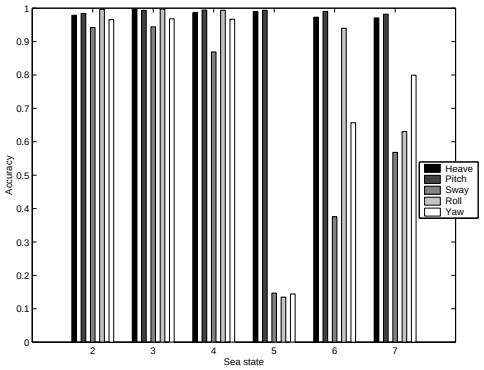

(b) U=0.2

Figure 4.7: Prediction of ship motion for different forward speeds and sea states

Chapter 5

Linear Nonparametric Identification of Ship Motion

Nonparametric identification is usually done in the frequency domain and is commonly based on transfer functions. Yet, when the interest is in the amplitude and statistics of the ship responses, some practitioners base their predictions on the response amplitude operators (RAOs). RAOs are functions that are used to analyze ship motions in irregular seaways from the wave spectrum. The RAO is defined as the ratio of the amplitude of the response (ship motion) to the amplitude of the sea waves for all involved frequency components. It can be defined for each of the ship responses, such as the heave, pitch, roll, and relative bow motion. As such, the RAOs serve to linearly relate the frequency components of one or more of the ship responses to the same components in the wave spectrum. Other functions that have been used to predict ship responses to sea waves include frequency-domain transfer functions (frequency-response functions). In fact, the RAO is equal to the amplitude of the transfer function.

Frequency-domain analysis is commonly performed using the discrete Fourier transform (DFT). Yet, one of the problems encountered in applying the DFT is leakage, which results from using finite records and causes errors in the power distribution among frequency

components (Harris, 1978 [132]). The severity of leakage can be reduced by using long records and/or applying data windows. Also, leakage can be eliminated by choosing a record length that is a multiple of the period of the signal. However, this can only be achieved when the frequency content of the signal is known *a priori* and when these frequencies are rational multiples of each other. In many experimental setups or practical applications, this may not be possible. Fahey et al (2000) [52] proposed the circular-hyperbolic decomposition (CHD) to determine the frequency components of a signal. This decomposition is closely related to Prony's method. The Prony family of algorithms provides a means to estimate the frequency components of a signal without some of the limitations of the DFT. These algorithms provide the amplitude, phase, frequency, and decay (or growth) information in the signal. The CHD can be used to study signals consisting of a combination of circular and hyperbolic sine and cosine functions. However, only the circular functions are physically significant for stationary signals, as considered in this dissertation. For stationary signals, the CHD is applicable to signals that neither decay nor grow with time. The decomposition technique has advantages over the DFT in that prior knowledge of the system frequencies is not required and the leakage problem is eliminated.

In this part of our work, we apply the CHD to determine the RAOs of the coupled heave and pitch motions of a Series 60 ship. The data is generated using the linear version of LAMP (LAMP, 1998 [3]; Lin et al, 1999 [133]). In the next section, we provide a general background of Prony-based algorithms and introduce the CHD. Then, we define the RAO and the steps used to obtain the response spectra. We also compare the RAOs obtained with the DFT with those obtained with the CHD.

5.1 Signal Processing Background

The Prony family of algorithms (Prony, 1795 [49]), including the complex exponential algorithm (Spitznogle and Quazi, 1970 [50]; Brown et al, 1979 [51]), has been shown to be

very useful in the representation of discrete time-limited signals by one or more complex exponentials. This representation is achieved by expressing a real signal v_s as

$$v_s(t_\ell) = \sum_{i=1}^{m} A_{si} \exp(\lambda_i t_\ell) \tag{5.1}$$

in the absence of noise, and as

$$y_s(t_\ell) = v_s(t_\ell) + \epsilon_s(t_\ell) \tag{5.2}$$

in the presence of Gaussian noise, where m, λ_i, A_{si}, $v_s(t_\ell)$, $y_s(t_\ell)$, $\epsilon_s(t_\ell)$, the subscript s, and t_ℓ are, respectively, the number of poles, poles (frequencies and decay rates), residues (amplitudes and phases), signals, signals with noise, noise, signal index, and evenly sampled control variable (often taken as time or distance along a path) with the associated index ℓ. Because $v_s(t_\ell)$ is real, a complex pole λ_i must have a complex conjugate $\lambda_k = \lambda_i^*$ and its corresponding complex conjugate residue $A_{sk} = A_{si}^*$. On the other hand, the poles of hyperbolic functions are real and occur in reciprocal pairs (e.g., $\lambda_2 = 1/\lambda_1$). In practice, we often make the restriction that m is an even number. Yet, there can be unpaired real poles in which case m could be odd. Here, we restrict m to be an even number $2n$ for notational purpose. We note that, although not all data can be expressed in terms of either Eq. (5.1) or Eq. (5.2), they encompass a very large class of signals.

Prony hereditary algorithms can be used to fit data with circular and hyperbolic sine and cosine functions because they represent a special case of complex exponentials. However, unless the signal is noiseless, one must contend with non-zero decay rates for circular sine and cosine functions and unpaired exponentials for hyperbolic sine and cosine functions, which can cause a dilemma in the interpretation of signal parameter estimates. Thus, we consider the special case of the circular-hyperbolic functions expressed as

$$\begin{aligned} v_s(t_\ell) = & \sum_{i=1}^{n_\omega} p_{si}\cos(\omega_i t_\ell) + q_{si}\sin(\omega_i t_\ell) \\ & + \sum_{i=1}^{n_\kappa} a_{si}\cosh(\kappa_i t_\ell) + b_{si}\sinh(\kappa_i t_\ell) \\ & + (-1)^{\ell-1} \sum_{i=1}^{n_\eta} c_{si}\cosh(\eta_i t_\ell) + d_{si}\sinh(\eta_i t_\ell) \end{aligned} \tag{5.3}$$

$$
\begin{aligned}
&+\sum_{i=1}^{n_\lambda}\{e_{si}\cos[\mathrm{Im}(\lambda_i)t_\ell]\cosh[\mathrm{Re}(\lambda_i)t_\ell] \\
&\quad +f_{si}\sin[\mathrm{Im}(\lambda_i)t_\ell]\cosh[\mathrm{Re}(\lambda_i)t_\ell] \\
&\quad +g_{si}\cos[\mathrm{Im}(\lambda_i)t_\ell]\sinh[\mathrm{Re}(\lambda_i)t_\ell] \\
&\quad +h_{si}\sin[\mathrm{Im}(\lambda_i)t_\ell]\sinh[\mathrm{Re}(\lambda_i)t_\ell]\} \\
y_s(t_\ell) &= v_s(t_\ell) + \epsilon_s(t_\ell)
\end{aligned} \tag{5.4}
$$

where the n_ω, n_κ, n_η, and n_λ are the number of the frequencies ω_i, κ_i, η_i, and λ_i, respectively; and the p_{si}, q_{si}, a_{si}, b_{si}, c_{si}, d_{si}, e_{si}, f_{si}, g_{si}, and h_{si} are the amplitudes. The parameters ω_i, κ_i, η_i, p_{si}, q_{si}, a_{si}, b_{si}, c_{si}, d_{si}, e_{si}, f_{si}, g_{si}, and h_{si} are real-valued for real signals, whereas λ_i is complex. The transition from Eq. (5.1) to Eq. (5.3) provides $n = n_\omega + n_\kappa + n_\eta + 2n_\lambda$ constraints that can be integrated into the estimation procedure as explained below. For stationary signals, however, Eq. (5.3) simplifies to

$$
v_s(t_\ell) = \sum_{i=1}^{n_\omega} p_{si}\cos(\omega_i t_\ell) + q_{si}\sin(\omega_i t_\ell)
$$

which is the case in this dissertation. A brief review of the complex exponential algorithm and details of the CHD are given below.

5.1.1 Complex Exponential Algorithm

The complex exponential algorithm (Spitznogle and Quazi, 1970 [50]; Brown et al, 1979 [51]) is also known as the least-squares Prony method, the autoregressive technique, and the maximum entropy method. In its implementation, we assume that N evenly sampled data points are known to contain exactly $2n$ distinct complex exponentials in the presence of Gaussian noise, as in Eq. (5.2). The solution is carried out in two stages. In the first stage, the poles λ_i are obtained. In the second stage, the residues A_{si} are determined. However, it is helpful to first consider the problem without noise in order to illustrate some concepts involved in the first stage.

In the absence of noise, the following expressions hold:

$$\begin{aligned} v_s(\ell) &= \sum_{i=1}^{2n} A_{si} \exp(\lambda_i[\ell-1]\Delta t) \\ &= \sum_{i=1}^{2n} A_{si}[z_i]^{\ell-1} \\ &= [A_{s1}, A_{s2}, \ldots, A_{s(2n)}] \begin{bmatrix} z_1 & & & 0 \\ & z_2 & & \\ & & \ddots & \\ 0 & & & z_{2n} \end{bmatrix}^{\ell-1} \begin{Bmatrix} 1 \\ 1 \\ \vdots \\ 1 \end{Bmatrix} \end{aligned} \tag{5.5}$$

where $t_\ell = [\ell - 1]\Delta t$ is time in seconds. The parameters z_i and λ_i represent the ith pole in the z-domain and frequency domain, respectively. These parameters are related by

$$\lambda_i = \frac{1}{\Delta t} \ln(z_i) \tag{5.6}$$

where λ_i has units of radians per second. For the noiseless case, the problem reduces to finding the z_i and A_i such that Eq. (5.5) holds for all $\ell \in \{1, 2, \ldots, N\}$.

Under the condition that all $|\lambda_i| < \frac{\pi}{\tau \Delta t}$, the z-domain characteristic polynomial is given by

$$\prod_{i=1}^{2n} [z - z_i^\tau] = \sum_{k=0}^{2n} \alpha_k [z]^k \tag{5.7}$$

where τ is a real positive integer called the decimation parameter, $\alpha_{2n} = 1$, and the z_i are the poles that need to be uncovered. The decimation parameter is useful for improving the numerical condition of the problem for oversampled signals. For oversampled records, any two consecutive columns of the Hankel matrix (defined below) become close to each other. Thus, the condition number of the Hankel matrix becomes large and its inverse becomes inaccurate. Consequently, the accuracy of the results deteriorates. This problem can be overcome by using decimation, where some of the data points in each row of the Hankel matrix are skipped to improve its condition number. As a rule of thumb, we recommend that $\tau \approx \frac{\pi}{2\Delta t \lambda_i}$. We note that the characteristic polynomial has the special property

$$\sum_{k=0}^{2n} \alpha_k [z]^k = 0 \tag{5.8}$$

whenever $z \in \{z_1^\tau, z_2^\tau, \ldots, z_{2n}^\tau\}$.

Next, we introduce the Hankel matrix $V_s(i,k) \equiv v_s(i+\tau k-1)$ for the noiseless case, which can be expressed in verbose form as

$$V_s(1:N-2n, 1:2n+1) = \begin{bmatrix} v_s(1) & v_s(1+\tau) & \ldots & v_s(1+2n\tau) \\ v_s(2) & v_s(2+\tau) & \ldots & v_s(2+2n\tau) \\ \vdots & \vdots & \ddots & \vdots \\ v_s(N-2n\tau) & v_s(N-2n\tau+\tau) & \ldots & v_s(N) \end{bmatrix} \tag{5.9}$$

In this case, the column length of V_s is $N-2n\tau$ and is chosen so that the index ℓ does not exceed N. As a consequence of Eq. (5.5), every row in the Hankel matrix can be written as

$$V_s(\ell, 1:2n+1) = [A_1, A_2, \ldots, A_{2n}] \times \begin{bmatrix} z_1 & & & 0 \\ & z_2 & & \\ & & \ddots & \\ 0 & & & z_{2n} \end{bmatrix}^{\ell-1} \begin{bmatrix} 1 & z_1^\tau & \ldots & z_1^{2n\tau} \\ 1 & z_2^\tau & \ldots & z_2^{2n\tau} \\ \vdots & \vdots & \ddots & \vdots \\ 1 & z_{2n}^\tau & \ldots & z_{2n}^{2n\tau} \end{bmatrix} \tag{5.10}$$

However, it follows from Eq. (5.8) that

$$\begin{bmatrix} 1 & z_1^\tau & \ldots & z_1^{2n\tau} \\ 1 & z_2^\tau & \ldots & z_2^{2n\tau} \\ \vdots & \vdots & \ddots & \vdots \\ 1 & z_{2n}^\tau & \ldots & z_{2n}^{2n\tau} \end{bmatrix} \begin{Bmatrix} \alpha_0 \\ \alpha_1 \\ \vdots \\ \alpha_{2n} \end{Bmatrix} = \begin{Bmatrix} 0 \\ 0 \\ \vdots \\ 0 \end{Bmatrix} \tag{5.11}$$

Therefore, $V_s(\ell, 1:2n+1)[\alpha_0, \alpha_1, \ldots, \alpha_{2n}]^T = 0$, and $V_s(1:2n, 1:2n+1)[\alpha_0, \alpha_1, \ldots, \alpha_{2n}]^T$ results in the null vector $[0, 0, \ldots, 0]^T$. Hence, the entries in each row of the noiseless Hankel matrix are related by the coefficients of the characteristic polynomial. The characteristic polynomial can be determined by setting $\alpha_{2n} = 1$ and choosing any $2n$ rows of the Hankel matrix. These $2n$ rows represent $2n$ linear equations in $2n$ unknown signal parameters that can be solved via the Gaussian elimination or other applicable techniques.

For a signal with noise, the Hankel matrix $Y_s(i,k) \equiv y_s(i+\tau k-1)$ can be expressed in verbose form as

$$Y_s(1:N-2n, 1:2n+1) = \begin{bmatrix} y_s(1) & y_s(1+\tau) & \dots y_s(1+2n\tau) \\ y_s(2) & y_s(2+\tau) & \dots y_s(2+2n\tau) \\ \vdots & \vdots & \ddots \quad \vdots \\ y_s(N-2n\tau) & y_s(N-2n\tau+\tau) & \dots \quad y_s(N) \end{bmatrix} \tag{5.12}$$

where $y_s(\ell) = v_s(\ell) + \epsilon_s(\ell)$. Each row of the Hankel matrix $Y_s(\ell, 1:2n+1)$ can still be related by the coefficients of the characteristic polynomial in Eq. (5.7), with an associated error $e_s(\ell)$ given by

$$e_s(\ell) = Y_s(\ell, 1:2n+1) \begin{Bmatrix} \alpha_0 \\ \alpha_1 \\ \vdots \\ \alpha_{2n} \end{Bmatrix} \tag{5.13}$$

This error must be equal to $\sum_{k=0}^{2n} \alpha_k \epsilon_s(\ell + k\tau)$ according to the definition of $y_s(\ell)$ in Eq. (5.2).

The first stage of the least-squares solution is obtained by summing the squares of the errors and minimizing the primary objective function

$$SSE_1(\alpha_0, \dots, \alpha_{2n-1}; \alpha_{2n}) = \sum_{s=1}^{S} \sum_{\ell=1}^{N-2n+1} e_s(\ell)^2 \tag{5.14}$$

where S is the total number of signals under consideration. The solution is then expressed as

$$[\alpha_0, \alpha_1, \dots, \alpha_{2n-1}]^T = -\begin{bmatrix} Y_1(1:N-2n, 1:2n) \\ Y_2(1:N-2n, 1:2n) \\ \vdots \\ Y_S(1:N-2n, 1:2n) \end{bmatrix}^+ \begin{Bmatrix} Y_1(1:N-2n, 2n+1) \\ Y_2(1:N-2n, 2n+1) \\ \vdots \\ Y_S(1:N-2n, 2n+1) \end{Bmatrix} \tag{5.15}$$

where α_{2n} is equal to unity and the matrix pseudo-inverse operator $[\ ]^+ \equiv [[\ ]^T[\ ]]^{-1}[\ ]^T$ for real quantities and $[\ ]^+ \equiv [[\ ]^H[\ ]]^{-1}[\ ]^H$ for complex ones. As a minimum requirement, the solution of Eq. (5.15) demands that $N \geq 2n\tau + 1$ and $S(N - 2n\tau) \geq 2n$. However, we recommend choosing $N \gg 2n\tau + 2n$ as a rule of thumb. The poles z_i are determined from Eq. (5.8).

In the second stage, the residues A_{si} are determined by defining a secondary objective function for each signal y_s as

$$SSE_2(A_{s1}, \ldots, A_{s(2n)}) = \sum_{\ell=1}^{N} \epsilon_s(\ell)^2 \tag{5.16}$$

The minimum of this function is realized when

$$\begin{Bmatrix} A_{s1} \\ A_{s2} \\ \vdots \\ A_{s(2n)} \end{Bmatrix} = \begin{bmatrix} 1 & 1 & \ldots & 1 \\ z_1 & z_2 & \ldots & z_{2n} \\ \vdots & \vdots & \ddots & \vdots \\ z_1^{N-1} & z_2^{N-1} & \ldots & z_{2n}^{N-1} \end{bmatrix}^+ \begin{Bmatrix} y_s(1) \\ y_s(2) \\ \vdots \\ y_s(N) \end{Bmatrix} \tag{5.17}$$

We note also that the matrix pseudo-inverse operation in Eq. (5.17) needs to be calculated only once for all of the signals y_s under consideration.

5.1.2 Circular-Hyperbolic Decomposition

In this section, we describe how to constrain the complex exponential algorithm to decompose a signal in terms of circular-hyperbolic functions in the presence of noise, as expressed in Eqs. (5.3) and (5.4). This section also provides two important extensions of the work of Fahey et al (2000) [52], namely, how to contend with data decimation and multiple signals. By implementation of CHD to multiple signals, it is meant to simultaneously determine the same frequency components in more than one signal.

We begin by examining the structure of the characteristic polynomial for circular and hyperbolic functions; that is, $p\cos(\omega t_\ell)+q\sin(\omega t_\ell)$, $a\cosh(\kappa t_\ell)+b\sinh(\kappa t_\ell)$, or $(-1)^{\ell-1}[c\cosh(\eta t_\ell)+$

$d\sinh(\eta t_\ell)]$. We observe that each of these functions has two poles $\{z_1, z_2\}$ with the property

$$z_1^\tau z_2^\tau = 1 \tag{5.18}$$

As for the function

$$\begin{aligned} &e\cos[\mathrm{Im}(\lambda)t_\ell]\cosh[\mathrm{Re}(\lambda)t_\ell] + f\sin[\mathrm{Im}(\lambda)t_\ell]\cosh[\mathrm{Re}(\lambda)t_\ell] \\ &+g\cos[\mathrm{Im}(\lambda)t_\ell]\sinh[\mathrm{Re}(\lambda)t_\ell] + h\sin[\mathrm{Im}(\lambda)t_\ell]\sinh[\mathrm{Re}(\lambda)t_\ell] \end{aligned}$$

it has four poles $\{z_1, z_2, z_3, z_4\}$ with the property

$$z_1^\tau z_2^\tau = z_3^\tau z_4^\tau = 1 \tag{5.19}$$

Hence, the characteristic polynomial for either a circular or a hyperbolic function always takes the form

$$z^2 + (z_1^\tau + z_2^\tau)z + 1 = z^2 + r_1 z + 1 \tag{5.20}$$

where r_1 is real. Subsequently, the characteristic polynomial for n circular-hyperbolic functions can be expressed as

$$\begin{aligned} \prod_{i=1}^{n}[z^2 + r_i z + 1] &= z^{2n} + \sum_{i=1}^{n} r_i z^{2n-1} \\ &+ \sum_{i=1}^{n}\sum_{k=1}^{n} r_i r_k z^{2n-2} + \ldots + \sum_{i=1}^{n} r_i z + 1 = \\ &z^{2n} + \alpha_{2n-1} z^{2n-1} + \alpha_{2n-2} z^{2n-2} + \ldots + \alpha_1 z + 1 \end{aligned} \tag{5.21}$$

Examining the structure of Eq. (5.21), we note that the polynomial coefficients exhibit the symmetries

$$\alpha_{n-i} = \alpha_{n+i} \text{ for } i \in \{1, 2, \ldots, n\} \tag{5.22}$$

which provide n constraints.

Next, we consider the matrix

$$\tilde{Y}_s(1 : N - 2n, 1 : n + 1) = \tag{5.23}$$

$$\left[\begin{array}{c|c|c} y_s(1+n\tau) & y_s(1+[n-1]\tau)+y_s(1+[n+1]\tau) & \dots \\ y_s(2+n\tau) & y_s(2+[n-1]\tau)+y_s(2+[n+1]\tau) & \dots \\ \vdots & \vdots & \ddots \\ y_s(N-n\tau) & y_s(N-[n+1]\tau)+y_s(N-[n-1]\tau) & \dots \end{array}\right.$$
$$\left.\begin{array}{cc} \dots & y_s(1)+y_s(1+2n\tau) \\ \dots & y_s(2)+y_s(2+2n\tau) \\ \ddots & \vdots \\ \dots & y_s(N-2n\tau)+y_s(N) \end{array}\right]$$

Due to the symmetries in Eq. (5.22), the objective function, expressed in Eq. (5.14), has a constrained minimum when

$$[\alpha_n, \alpha_{n+1}, \dots, \alpha_{2n-1}]^T = \tag{5.24}$$
$$-\left[\begin{array}{c} \tilde{Y}_1(1:N-2n, 1:n) \\ \tilde{Y}_2(1:N-2n, 1:n) \\ \vdots \\ \tilde{Y}_S(1:N-2n, 1:n) \end{array}\right]^+ \left\{\begin{array}{c} \tilde{Y}_1(1:N-2n, n+1) \\ \tilde{Y}_2(1:N-2n, n+1) \\ \vdots \\ \tilde{Y}_S(1:N-2n, n+1) \end{array}\right\}$$

where $\alpha_{2n} = 1$. Here, we note that the minimum number of data points required is reduced; Eq. (5.24) can be executed when $N \geq 2n\tau + 1$ and $S(N - 2n\tau) \geq n$, whereas Eq. (5.15) requires that $S(N-2n\tau) \geq 2n$. However, we recommend choosing $N \gg 2n\tau + n$ as a rule of thumb. Then, the polynomial coefficients $\{\alpha_0, \alpha_1, \dots, \alpha_{n-1}\}$ are given by Eq. (5.22), and the poles are calculated by solving Eq. (5.8) as before. The residues can be calculated according to Eq. (5.17).

If the results can be presented in exponential form, the decomposition is complete. When the results are desired in the form of Eq. (5.3), some additional algebra is required. We collect the poles on the unit circle and pair complex conjugate poles and residues. The circular frequencies ω_i and amplitudes p_{si} and q_{si} associated with the pole pair $\{z, z^*\}$ and corresponding residues $\{A, A^*\}$ are

$$\omega = |\arg(z)|/\Delta t \tag{5.25}$$

$$p = 2 \text{ Real}(A) \tag{5.26}$$

$$q = -2 \text{ Imag}(A) \tag{5.27}$$

where $\arg(z)$ denotes the argument of z (the polar angle of z in the z-domain). If there are pole estimates that are not on the unit circle, this suggests that the signal is not stationary. For nonstationary signals, a similar procedure is required to collect the remaining hyperbolic parameters of Eq. (5.3). The noise part can be obtained by generating Eq. (5.3) from the parameter estimates and subtracting the result from the original data. The effect of noise on the data analysis using the CHD and the collection of the hyperbolic parameters have been discussed by Fahey et al (2000) [52]. Equations (5.17), (5.22), and (5.24) represent the basic formulation of the circular-hyperbolic decomposition.

5.2 Application to RAO Estimation

The RAO is a function by which the spectra of a ship response can be determined. The determination of the spectra consists of the following steps (Bhattacharyya, 1976 [134]; Korvin-Korvosky, 1955 [19]). First, the ship response is found in a regular seaway for various wave frequencies. The ship response can be found either analytically, experimentally, or via numerical simulations. The RAO is then constructed as the motion amplitude divided by the wave amplitude for each of the involved frequency components. The RAO may be expressed as a function of the encounter frequencies; that is, wave frequencies as seen by an observer riding on the ship. Second, a seaway wave spectrum where the ship will operate is expressed as a function of the absolute or encounter frequencies. The motion response spectrum is then obtained by multiplying the wave spectrum by the square of the RAO at the corresponding absolute/encounter frequencies. In this work, all of the frequency domain results are calculated in terms of the encounter input frequencies. However, the results are presented in terms of the absolute input frequencies.

The numerically simulated data, used to find the RAOs of the coupled heave and pitch

motions, are generated by using the linear version of the LAMP code written by SAIC (Lin et al, 1999 [133]). LAMP has the capability of predicting in the time-domain the linear and nonlinear motions and loads of floating bodies with and without forward speed in various sea states. We considered only the steady-state parts of the signals because the transients, would introduce errors in the amplitudes and phases of the circular components. The simulated data is for a Series 60 ship with a Froude number of 0.2. Figures 5.1 and 5.2 show the coupled heave and pitch motions of the ship in response to 16 input frequencies of unit amplitude. Because the problem considered is linear, the ship response can be obtained by multiplying the transfer functions by the amplitude of each frequency component in the input spectrum. The pitch response is in degrees, while the time and the heave displacement are nondimensional. The length L of the ship is used as the length scale and $\sqrt{\frac{L}{g}}$ is used as the time scale, where g is the gravitational acceleration. The simulation data is sampled at a nondimensional rate of 0.02. In the data used here, the encounter frequencies of the input waves range from $\pi/6$ to $8\pi/3$ with a step of $\pi/6$ in radians per nondimensional time. We note that the input frequencies are chosen to be rational multiples of each other. Since the data is oversampled, decimation, as explained above, has been utilized to improve the accuracy of the results.

The amplitudes and phases of the frequency components of the heave motion are, respectively, shown in Figs. 5.3 and 5.4. Figures 5.3a and 5.4a show the exact frequency-domain amplitude and phase of the heave motion. They were generated using the DFT with the record length properly chosen to avoid the effect of leakage. A record length of multiples of 600 samples makes the encounter input frequencies integer multiples of the frequency resolution. It is important to note here that *a priori* knowledge of the system frequencies was required in order to eliminate the leakage problem. Also, this could not have been achieved if the wave frequencies were not rational multiples of each other. Figures 5.3b and 5.4b show the amplitude and phase of the frequency components of the heave motion without properly choosing the record length to avoid leakage. The record length involves 750 samples, which causes the input frequencies not to be integer multiples of the frequency resolution. The

leakage effects caused an erroneous amplitude and phase, with the effects on the phase being much more pronounced.

Figures 5.3c and 5.4c show the frequency-domain amplitude and phase of the heave motion using the CHD discussed above. Although no prior information about the system frequencies has been used, the CHD provides frequency-domain results that are very close to those provided by the DFT without the effect of leakage; that is, the exact decomposition. It is worth noting here that in many practical cases, the exact system frequencies are not known in advance or they are not rational multiples of each other, which renders the leakage problem inevitable. It should be noted here that in the implementation procedure, both circular and hyperbolic terms were permitted. However, as expected, no hyperbolic components were found because they were not part of the signal. For an example where hyperbolic components are present, the readers are referred to Fahey et al (2000) [135]. The amplitudes and phases of the frequency components of the pitch motion are, respectively, shown in Figs. 5.5 and 5.6. Again, it is seen that using the CHD gives results that are very close to those obtained using the DFT without the effect of leakage.

Figure 5.7 shows the RAO of the heave motion computed using the DFT with the exact record length to eliminate leakage, the DFT with a record length that results in leakage effects, and the CHD. The RAO was generated by dividing the response amplitude over the input amplitude at the corresponding frequencies. The exact RAO is the one obtained using the DFT with no leakage effects in both input and output signals. The results of Fig. 5.7 show that the RAO obtained using the DFT with the effect of leakage in both input and output signals deviates significantly from the exact RAO. With the CHD, the resulting RAO is close to the exact RAO. This demonstrates the ability of the CHD to uncover the signal characteristics without *a priori* knowledge of the system frequencies or having to worry about the record length.

Figure 5.8 shows the RAO of the pitch motion computed using the aforementioned three different methods. Again, it is clear that the RAO found using the CHD is close to the exact

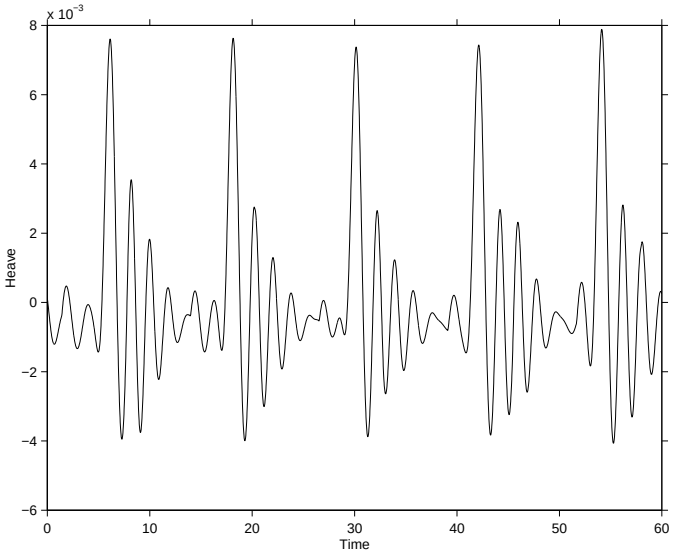

Figure 5.1: The heave motion of a Series 60 ship

RAO, while the RAO found using the DFT with a record length that results in leakage deviates significantly from the exact RAO. In real applications or in model experiments, it is usually hard to control the input frequencies to be exact rational multiples of each other. Even if one frequency at a time is used to excite the ship, it is almost impossible to set the wave frequency exactly at a desired value. Because of these limitations, the CHD is superior to the DFT in uncovering system characteristics in situations where the system frequencies are not known in advance.

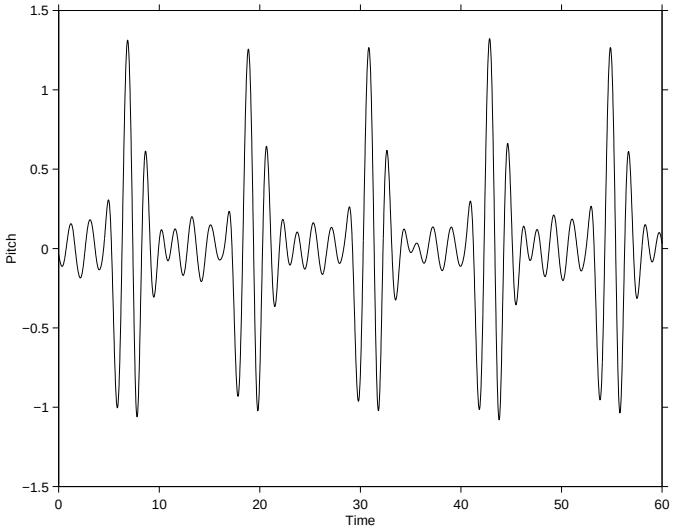

Figure 5.2: The pitch motion of a Series 60 ship

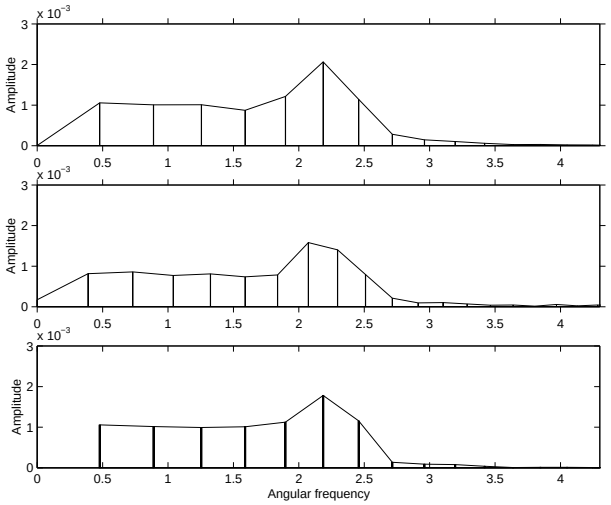

Figure 5.3: Amplitude of the heave motion

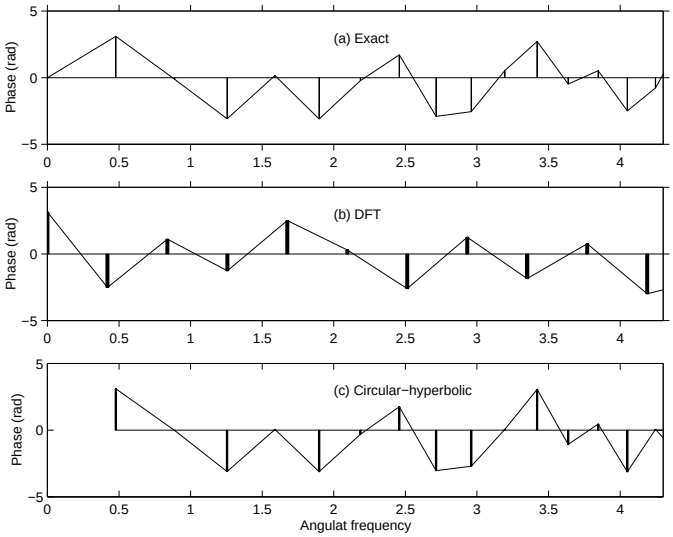

Figure 5.4: Phase of the heave motion

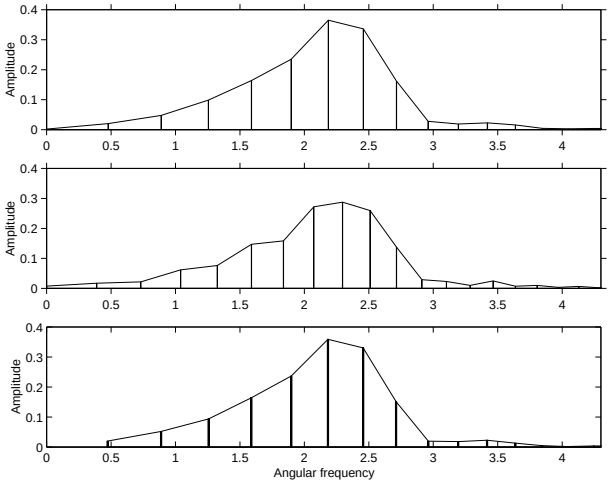

Figure 5.5: Amplitude of the pitch motion

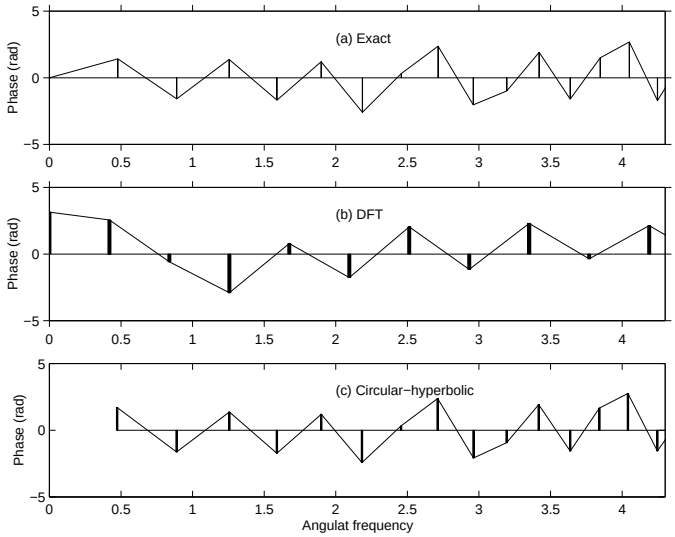

Figure 5.6: Phase of the pitch motion

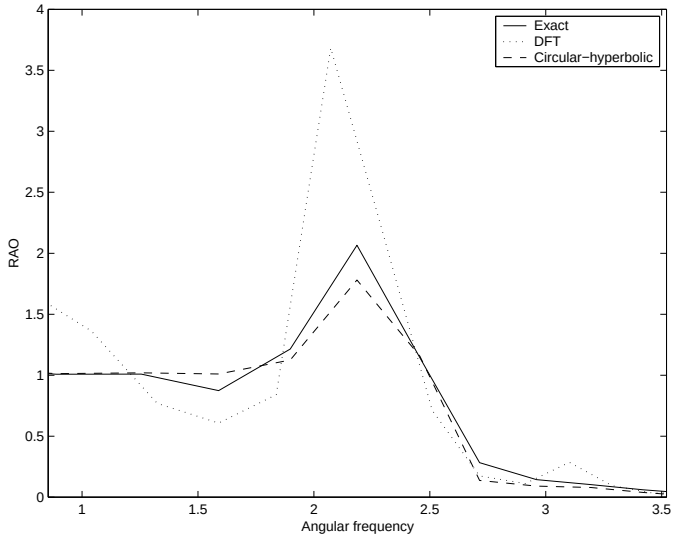

Figure 5.7: The RAO for the heave motion

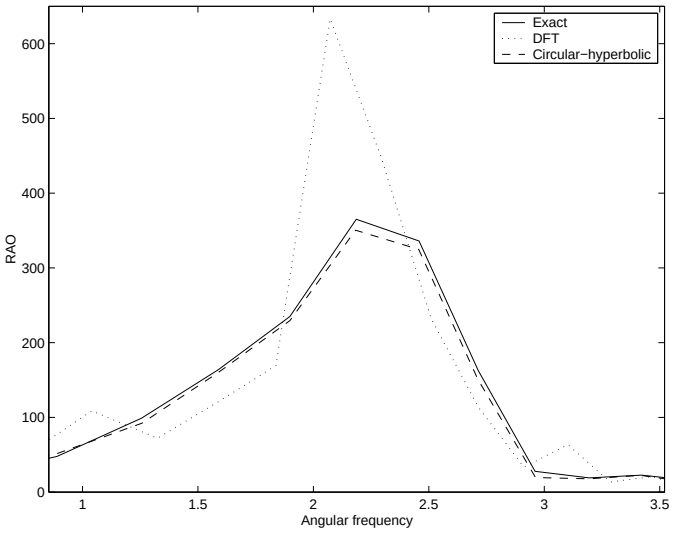

Figure 5.8: The RAO for the pitch motion

Chapter 6

Nonlinear Parametric System Identification

Using a traditional "brute-force" technique to identify the nonlinear parameters requires solving for a large number of unknown parameters simultaneously. This approach reduces the accuracy of the identified parameters. Moreover, special care must be taken to monitor and eliminate the cancellation effect. By the cancellation effect, it is meant that two or more parameters may be inaccurate but the effects of their contributions to the response cancel one another. The prediction will be accurate for the specific response although the identified parameters are not accurate. In this work, we use an identification procedure that eliminates these problems. This procedure is based on exploiting the ship motion nonlinear resonances (Nayfeh, 1985 [71]). The procedure combines the method of multiple scales and higher-order spectral moments. The reason for adopting this technique is that few parameters are identified by setting up a simulation that stresses their role.

In this chapter, we discuss the nonlinear effects in ship motions in general and in the LAMP code in particular. Then, we present the adopted nonlinear system-identification methodology and apply it to identify the parameters that contribute to the nonlinear parametric roll resonance. Results for the identified parameters as function of the forward speed are then

presented and discussed in light of the results presented in Chapter 3.

6.1 Nonlinear Effects in Ship Motions

The fluid flow around ships is assumed to be potential; that is, inviscid and irrotational. This assumption is reasonable since the effects of viscous damping on ship motions are small. One exception is the roll motion, where the viscous damping has a significant effect and must be considered for accurate predictions. The potential flow is governed by Laplace's equation, which is linear. Although Laplace's equation is linear, nonlinearities are introduced through Bernoulli's equation and through the nonlinear free-surface and body boundary conditions. Two kinds of boundary conditions are involved in the problem of ship motions in seas. The first is the body boundary condition, which represents the fact that the fluid cannot penetrate the solid surface, which is moving, and must slide along the surface. The second is the free-surface boundary condition, which represents the fact that the air and water pressures on both sides of the interface must be equal and that the water particles cannot penetrate the free surface. Nonlinearity is involved in applying both boundary conditions. The main difficulty in treating these boundary conditions is that the shape of the free surface is not known in advance and that the wetted part of ship changes with time. For an accurate solution, the shape of the free surface should be calculated as part of the solution and the updated wetted surface should be taken into account.

The potential flow around the ship can be divided into several components. One component is due to the oscillatory motion of the ship and is called the radiation potential. The radiation potential includes the effects of the added mass and damping. A second component is the incident wave potential, which is constructed using wave kinematics, assuming no interference occurs between the wave and the ship's body. The diffraction potential results from the interaction between the waves and the body of the ship. Finally, a potential is formed due to the steady forward speed of the ship. It is worth noting here that the radiation and diffraction

potentials depend on the forward speed. The total potential is the summation of all of the above mentioned potentials. Once the potential-flow equation is solved, Bernoulli's equation is applied to find the pressure distribution over the ship's hull. The pressure distribution is then integrated to yield the total hydrodynamic forces and moments exerted on the ship.

Besides the hydrodynamic forces and moments, there is a need to account for the hydrostatic forces and moments, which result from the hydrostatic pressures caused by a displacement of the water volume (buoyancy). They should be calculated with the ship at its exact position, taking into account the real wetted surface. This requirement introduces nonlinearities. Adding the hydrodynamic and hydrostatic forces and moments yields the total forces and moments acting on the ship. These total forces and moments cause the ship motions and determine the position and orientation of the ship.

Solving the full nonlinear problem with exact boundary conditions is extremely difficult, if not impossible. Many simplifications are usually made for engineering applications. One of the simplifications is to linearize the body boundary condition at the mean wetted surface. Another simplification is to linearize the free-surface condition at the mean free surface. Also, the hydrostatic and Froude-Kriloff (incident wave) forces can be calculated considering the mean wetted surface of the ship, which renders them linear.

6.1.1 Nonlinear Effects in LAMP

In this section, we discuss the formulation of the different versions of the LAMP code, namely, LAMP-1 and LAMP-2, which were used as the data generation tools for this work. In both versions, linearized free-surface and body boundary conditions are implemented. The linearization of the body boundary conditions involves the use of "m-terms". Both linear and nonlinear version of the Bernoulli equation can be used to calculate the pressure.

The steady forward-speed potential is denoted as ϕ_0 (zeroth-order solution). Perturbations to the forward speed potential are added due to the existence of the body- and free- surface

boundary conditions. The nonlinear potential solution ϕ is then expressed as

$$\phi = \phi_0 + \epsilon\phi_1 + \epsilon^2\phi_2 + \epsilon^3\phi_3 \tag{6.1}$$

where ϵ is a bookkeeping device that indicates the order of magnitude of the corresponding terms, ϕ_1 is the first-order perturbation potential due to the linearized boundary conditions, ϕ_1 is the second-order perturbation due to the nonlinear boundary conditions, and ϕ_2 is the third-order perturbation due to the nonlinear boundary conditions.

The unsteady Bernoulli equation is written as

$$-\frac{p}{\rho} = \frac{\partial\phi}{\partial t} + \frac{1}{2}\nabla\phi\cdot\nabla\phi \tag{6.2}$$

Substituting Eq. (6.1) into Eq. (6.2) yields

$$\begin{aligned} -\frac{p}{\rho} = {} & \frac{1}{2}\nabla\phi_0\cdot\nabla\phi_0 \\ & +\epsilon[\frac{\partial\phi_1}{\partial t} + \nabla\phi_0\cdot\nabla\phi_1] \\ & +\epsilon^2[\frac{\partial\phi_2}{\partial t} + \frac{1}{2}\nabla\phi_1\cdot\nabla\phi_1 + \nabla\phi_0\cdot\nabla\phi_2] \\ & +\epsilon^3[\frac{\partial\phi_3}{\partial t} + \nabla\phi_0\cdot\nabla\phi_3 + \nabla\phi_1\cdot\nabla\phi_2] + O(\epsilon^4) \end{aligned} \tag{6.3}$$

If linearized boundary conditions are used to obtain the potential solution and the linearized Bernoulli equation is used to calculate the pressure, then Eq. (6.3) is reduced to

$$\begin{aligned} -\frac{p}{\rho} = {} & \frac{1}{2}\nabla\phi_0\cdot\nabla\phi_0 \\ & \epsilon[\frac{\partial\phi_1}{\partial t} + \nabla\phi_0\cdot\nabla\phi_1] \end{aligned} \tag{6.4}$$

If linearized boundary conditions are used to obtain the potential solution and the nonlinear Bernoulli equation is used to calculate the pressure, then then Eq. (6.3) is reduced to

$$\begin{aligned} -\frac{p}{\rho} = {} & \frac{1}{2}\nabla\phi_0\cdot\nabla\phi_0 \\ & +\epsilon[\frac{\partial\phi_1}{\partial t} + \nabla\phi_0\cdot\nabla\phi_1] \\ & +\epsilon^2[\frac{1}{2}\nabla\phi_1\cdot\nabla\phi_1] \end{aligned} \tag{6.5}$$

We should note that using linearized boundary conditions with the nonlinear Bernoulli equation can account for some of the nonlinearities that exist in the system, but not all of them. While some of the quadratic nonlinearities are accounted for, none of the cubic nonlinearities are accounted for. The above argument regarding the nonlinearity in the hydrodynamic forces and moments applies for both LAMP-1 and LAMP-2.

Regarding the hydrostatic and incident wave (Froude-Kriloff) forces and moments, LAMP-1 calculates them at the mean wetted surface. On the other hand, LAMP-2 calculates them at the instantaneous wetted surface. Thus, the hydrostatic forces and moments are linear in LAMP-1, while quadratic and cubic hydrostatic nonlinearities are introduced in LAMP-2. It should be noted here that the radiation, forward speed, and diffraction potentials are solved for as one quantity in LAMP-1 and LAMP-2. In the special version of LAMP-2 that implements the IRF formulation, these three quantities are solved for as separate quantities, where the forward-speed potential is calculated first, then the diffraction and radiation potentials are calculated. In both LAMP-1 and LAMP-2, and for both the regular and IRF formulations, the hydrostatic forces are found separately from the hydrodynamics forces. The rigid-body dynamics are nonlinear in both LAMP-1 and LAMP-2, with nonlinearities being quadratic.

In this work, we restrict ourselves to identifying the nonlinearities that exist in the LAMP code. Although these nonlinearities do not include all of the real physical ones, the identification methodology can be applied for any motion data, whether it was generated with numerical codes, model tests, or full-scale experiments.

6.1.2 Nonlinear LAMP Results

In this section, we present some LAMP data that show the effect of nonlinearities on the different ship motions. Figures 6.1 and 6.2 show the heave and pitch data as one set and the sway, roll, and yaw data as another set. The data shown are for sea state 3 and $U = 0.2$. In each figure, data from three different LAMP runs are presented. These are

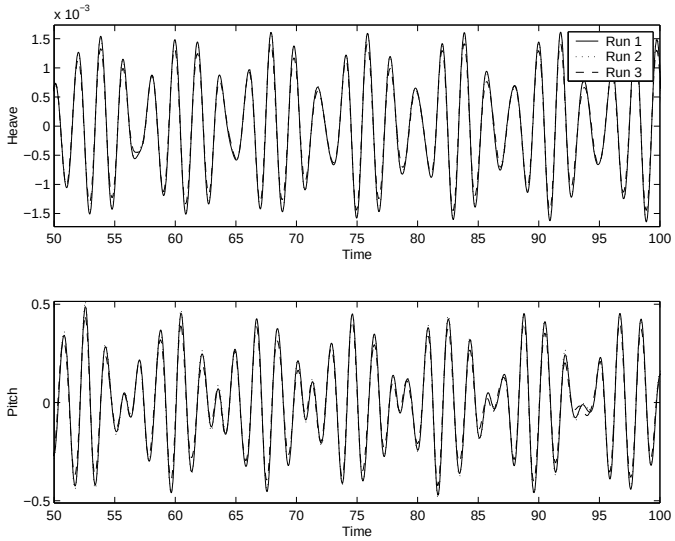

Figure 6.1: The heave and pitch motions for sea state 3 and $U = 0.2$

- Run 1 where LAMP-1 is used with the linearized Bernoulli equation; that is, linear hydrostatics, linear hydrodynamics, and nonlinear rigid-body motions.
- Run 2 where LAMP-2 is used with the linearized Bernoulli equation; that is, nonlinear hydrostatics, linear hydrodynamics, and nonlinear rigid-body motions, and
- Run 3 where LAMP-2 is used with the nonlinear Bernoulli equation; that is, nonlinear hydrostatics, nonlinear hydrodynamics, and nonlinear rigid-body motions.

By examining Fig. 6.1, we note that the different LAMP runs give virtually identical results for the heave and pitch data. This means that the heave and pitch responses are approximately linear and that the effect of nonlinearity on these motions is small. We should note here that small DC values of the heave and pitch motions were removed when plotting the results of the nonlinear cases (Runs 2 and 3). Those small DC values are attributed to small quadratic nonlinearities. On the other hand, by examining Fig. 6.2, we see that the different LAMP runs give different results for the sway, roll, and yaw data. This means that the sway, roll, and yaw motions are greatly affected by the nonlinearities that exist in the ship system. Figures 6.3 and 6.4 show similar data sets for sea state 7 and $U = 0.2$, with the exception

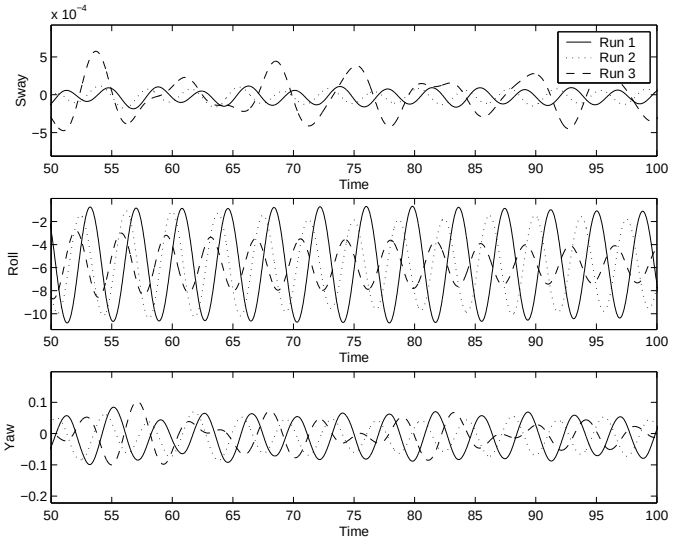

Figure 6.2: The sway, roll, and yaw motions for sea state 3 and $U = 0.2$

that only runs of type 1 and 3 are presented. It can be seen that the same trends observed for sea state 3 are noted for sea state 7. Thus, it can be concluded that for all sea states, the effects of nonlinearity are minor on the heave and pitch motions, while they are significant on the sway, roll, and yaw motions. This conclusion is important for modeling the parametric roll resonance, where the heave and pitch motions are represented using linear models, while the roll motion is represented using a nonlinear model, as described below. Also, it should be noted that the linear models of the sway, roll, and yaw motions, as discussed in Chapter 4, were found to be accurate for sea states 2 through 4. Since the run type 1 (linear hydrostatics and hydrodynamics) was used to identify and validate the linear models, it is evident that the linear models break down for the sway, roll, and yaw motions due to the effects of the nonlinearities in the rigid-body motion. On the contrary, this type of nonlinearity is not important for the heave and pitch motions.

The linear behavior of the heave and pitch motions was further investigated by generating amplitude-response and frequency-response curves of the heave and pitch equations. These functions were generated using LAMP runs with the other motions constrained. LAMP-2 with the nonlinear Bernoulli equation was utilized to find these functions. In other words, the

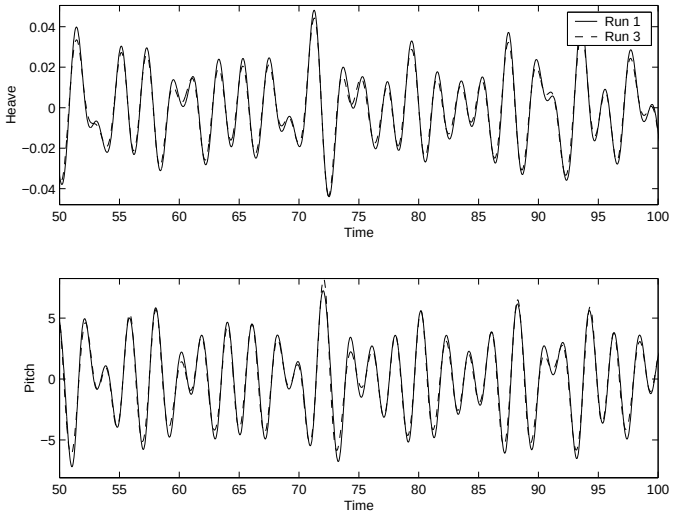

Figure 6.3: The heave and pitch motions for sea state 7 and $U = 0.2$

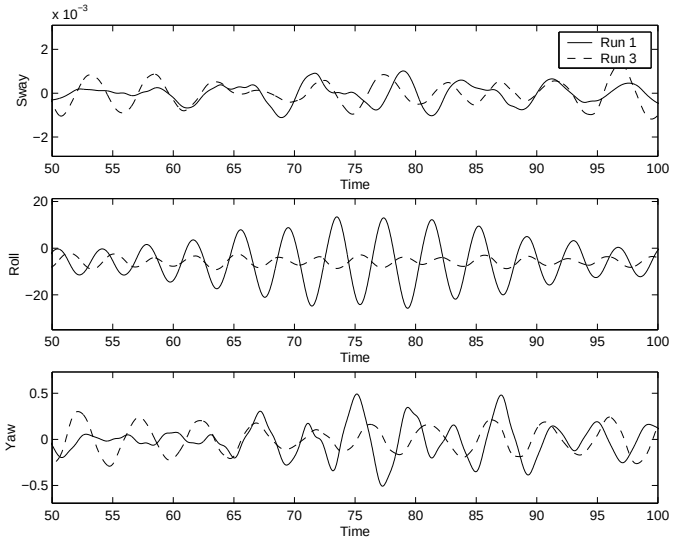

Figure 6.4: The sway, roll, and yaw motions for sea state 7 and $U = 0.2$

runs include nonlinear rigid-body motions, nonlinear hydrostatics, and partially nonlinear hydrodynamics.

For a linear system, it is expected that the response amplitude increases linearly with the forcing amplitude. On the other hand, for a nonlinear system with an excitation near one of its natural frequencies, one expects jumps in the amplitude-response and frequency response curves for large-amplitude excitations. These jumps are unique to nonlinear systems and occur at saddle-node or turning points. Figure 6.5 shows the amplitude-response curves generated for the heave and pitch motions. They were generated by running LAMP with six input-wave frequencies that are close to the two natural frequencies of the heave and pitch motions. The input amplitudes were increased from 0.01 to 0.085. Further increases in the input amplitudes were not possible because the heave and pitch amplitudes became unrealistically very high and the LAMP calculations became unstable. The amplitude of the heave and pitch at one of the exciting frequencies is plotted in Fig. 6.5. It is clear that the response amplitude varies approximately linearly with the wave amplitude. Although the amplitude-response curves do not exhibit jumps, the effect of the nonlinearity was evident when the linear models we used to predict the heave and pitch motions. It was found that for input amplitudes up to 0.03, the predictions were very accurate (above 95%); while for input amplitudes above 0.03, the accuracy of the linear prediction was reduced ($70\% - 85\%$).

Figure 6.6 shows the frequency-response curves generated for the heave and pitch motions. Again, for linear systems, as the frequency is swept across the natural frequencies of the system, no jumps are expected in the response. On the other hand, for nonlinear systems, jumps are expected in the frequency-response curves, which occur at saddle-node bifurcation points. To generate the frequency-response curves, we performed two series of LAMP runs. In the first series, a harmonic input wave was used with an amplitude of 0.01. In the second series, the amplitude was increased to 0.1. The frequencies were varied between 0.41 to 0.65, where this range of frequencies encompasses the two natural frequencies of the heave and pitch motions. The frequency-response curves at the amplitude 0.01 are shown in Fig.

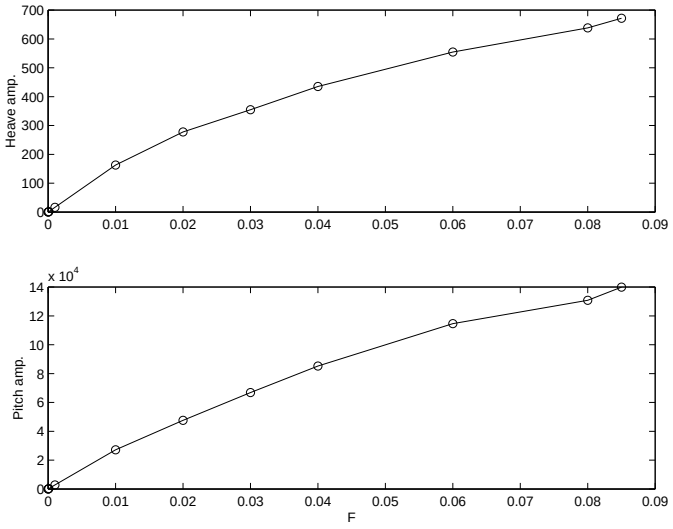

Figure 6.5: Amplitude-response curves of the heave and pitch motions

6.6a. It can be seen there are no jumps in the response and that the frequency-response curves are representative of those corresponding to linear systems. As the input amplitude was increased by an order of magnitude, similar frequency-response curves were obtained, as shown in Fig. 6.6b. It is clear the frequency-response curves are single-valued, again a characteristic of linear behavior. However, the nonlinear effects are manifested in a shift in the peak (resonant) frequency; the first peak in the pitch motion occurs at around 0.49 in Fig. 6.6a, while it occurs at around 0.44 in the Fig. 6.6b. This behavior is a characteristic of nonlinear systems. We note that the nondimensional significant wave amplitude of sea state 7 is 0.0615. Thus, in light of the results presented in Figs. 6.5 and 6.6, we expect the heave and pitch motions to behave linearly for this sea state and all of the sea states below it.

In summary, we conclude that the effect of the nonlinearity is small on the heave and pitch motions. One term that appears in the heave motion due to the rigid-body dynamics is $z_G\dot{\theta^2}$, where z_G is the nondimensional vertical location of the center of gravity of the ship. For the ship used here, $z_G = -0.00518$, which is small. As mentioned before, LAMP includes some of the physical nonlinearities that occur in real ship motions. LAMP can totally account for the rigid-body and hydrostatic nonlinearities, while it partially accounts for the hydrodynamic

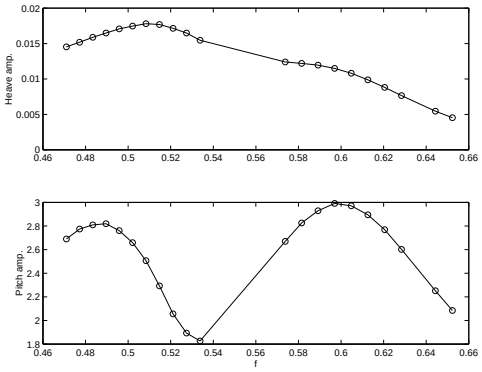

(a) F=0.01

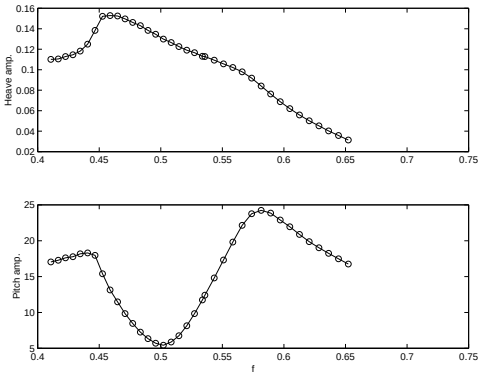

(b) F=0.1

Figure 6.6: Frequency-response curves of the heave and pitch motions

nonlinearities. So, the scope of the aforementioned remarks should be restricted to the physics that is represented in LAMP and in particular to physics that applies for Series 60 ships. In other words, if a better nonlinear modeling in LAMP is utilized, the effect of nonlinearity in the heave and pitch motions may have been more pronounced. Also, using other ship geometries may lead to a different ship-motion behavior.

6.2 Methodology for Nonlinear System Identification

The nonlinear system-identification methodology used in this work consists of the following steps. First, we adopt a nonlinear model for ship motions based on the results of Chapter 3. The model accounts for the coupling among the different degrees of freedom and explicitly expresses the dependence of the parameters on the forward speed. Second, we generate ship-motion data with LAMP-2 that exploit different resonance mechanisms. Having the linear parameters as determined in Chapter 4, we identify the nonlinear ship parameters using higher-order spectra and the method of multiple scales. Finally, we validate the generated model using LAMP data.

6.3 Higher-Order Spectra

The frequency components of a system can be calculated using the Fourier transforms of the first and second moments. For real-valued, zero-mean stationary time series, $x(t)$ and $y(t)$, the auto power spectrum $P_{xx}(f)$ and the cross power spectrum P_{xy} are estimated as

$$P_{xx}(f) = \lim_{T\to\infty} \frac{1}{T} E[X(f)X^*(f)] \tag{6.6}$$

$$P_{xy}(f) = \lim_{T\to\infty} \frac{1}{T} E[X(f)Y^*(f)] \tag{6.7}$$

and the linear coherence $\gamma_{xy}(f)$ is defined as

$$\gamma_{xy}(f) = \frac{|P_{xy}|^2}{|P_{xx}||P_{yy}|} \tag{6.8}$$

where $X(f)$ is the complex Fourier amplitude of $x(t)$ defined as

$$X(f) = \int_{-\infty}^{\infty} x(t) e^{-2\pi i f t} dt \tag{6.9}$$

Similarly, we define $Y(f)$ as the complex Fourier amplitude of $y(t)$. The notation $E[\ldots]$ denotes the expected value. The power spectrum of a signal provides a measure of the distribution of energy among the frequency components of the signal. The linear coherence provides a measure of the linear relationship between the frequency modes of $x(t)$ and $y(t)$. However, these tools provide no means for the identification or the quantization of the system parameters when the modes are nonlinearly coupled. On the other hand, higher-order spectra have been employed to characterize nonlinear behavior in many fields (Hajj et al, 1997 [136]).

According to Kim and Powers (1979) [137], the auto-bispectrum is estimated as

$$B_{xxx}(f_i, f_j) = \lim_{T \to \infty} \frac{1}{T} E[X(f_i + f_j) X^*(f_i) X^*(f_j)] \tag{6.10}$$

which establishes a measure of the level of nonlinear coupling by determining the variations in its phase. The auto-bispectrum preserves the phase information between the coupled modes of a nonlinear system. It provides a measure of the nonlinear coupling among the frequency components f_i and f_j and $f_i + f_j$ in the signal $x(t)$. It can be normalized to to obtain the auto-bicoherence as

$$b^2_{xxx}(f_i, f_j) = \frac{|B_{xxx}(f_i, f_j)|^2}{E[|X(f_i)X(f_j)|^2] E[|X(f_i + f_j)|^2]} \tag{6.11}$$

which is bounded by zero and one. For quadratically coupled modes with frequencies f_i, f_j, and $f_i + f_j$, the auto-bicoherence $b^2(f_i + f_j)$ equals one. Uncoupled modes will yield a zero value for the auto-bicoherence. Values between zero and one indicate partial coupling.

The cross-bispectrum and the cross-bicoherence are defined as

$$B_{xxy}(f_i, f_j) = \lim_{T \to \infty} \frac{1}{T} E[Y(f_i + f_j) X^*(f_i) X^*(f_j)] \tag{6.12}$$

and

$$b^2_{xxy}(f_i, f_j) = \frac{|B_{xxy}(f_i, f_j)|^2}{E[|X(f_i)X(f_j)|^2] E[|Y(f_i + f_j)|^2]} \tag{6.13}$$

respectively. The cross-bispectrum provides a measure of the nonlinear coupling among the frequency components f_i and f_j in signal $x(t)$ and the component $f_i + f_j$ in signal $y(t)$. Like the auto-bicoherence, the cross-bicoherence also takes on values between zero and one, depending on the strength of the nonlinear coupling between the components f_i and f_j in signal $x(t)$ and component $f_i + f_j$ in signal $y(t)$.

6.4 Approximate Solutions to Equations of Ship Motions with Perturbation Techniques

6.4.1 Solvability Condition

In this section, we discuss the solvability condition for a system in the form

$$AX = b \tag{6.14}$$

where A is an n by n matrix and b is an n by 1 vector. If the the matrix A is nonsingular ($|A| \neq 0$), then the solution of Eq. (6.14) exists and unique for all values of b and can be written as

$$X = A^{-1}b \tag{6.15}$$

In cases where b is the null vector, then the only possible solution is the trivial one. If the matrix A is singular ($|A| = 0$), then the system

$$AX = 0 \tag{6.16}$$

may have nontrivial solutions. They belong to the null space of the matrix A; that is, the space spanned by the eigenvectors associated with the zero eigenvalues of A. In other words, one needs to solve the eigenvalue problem and find the zero eigenvalues and the associated eigenvectors. The solution is a linear combination of these eigenvectors. If there is one zero eigenvalue, then the solution consists of its associated eigenvector multiplied by a constant.

The eigenvalue problem can be expressed as

$$(A - \lambda_j I)X_j = 0 \tag{6.17}$$

where λ_j is the j^{th} eigenvalue and X_j is its associated eiegnevector. For zero λ_j, Eq. (6.17) reduces to Eq. (6.16). For a singular matrix A, the nonhomogeneous system as given by Eq. (6.14), has a solution if and only if a certain condition is satisfied. This condition is referred to as the solvability condition. It can be shown that the solvability condition can be expressed as (Nayfeh, 1981 [68])

$$b^T u = 0 \tag{6.18}$$

where u is a solution to the homogeneous adjoint problem

$$A^* X = 0 \tag{6.19}$$

where A^* is the adjoint matrix, defined as the complex conjugate of the transpose of A. Thus, u is an eigenvector of A^* that is associated with a zero eigenvalue of A^*. For a Hermitian matrix or a real symmetric matrix, $A^* = A$, which is referred to as a self-adjoint matrix. In this case, the solvability condition leads to X being normal to the eigenvectors of A that are associated with zero eigenvalues; that is, X is normal to all of the solutions of the homogeneous system represented by Eq. (6.16).

Application to a second-order system

A homogeneous second-order system with real and symmetric matrices given by

$$M\ddot{X} + KX = 0 \tag{6.20}$$

has an associated eigenvalue problem, which can be expressed as

$$(-\omega_j^2 M + K)\phi_j = 0 \tag{6.21}$$

where ω_j is the j^{th} eigenvalue (natural frequency) of the system and ϕ_j is its associated eigenvector. The system represented by Eq. (6.21) has a nontrivial solution when

$$| - \omega_j^2 M + K| = 0 \tag{6.22}$$

This equation gives the eigenvalues (assumed distinct here) of the system represented by Eq. (6.20). Substituting the ω_j into Eq. (6.21), one can solve for the eigenvectors of the system. The solution of Eq. (6.20) is then given by

$$X = \phi_j e^{\mathbf{i}\omega_j} C_j \tag{6.23}$$

where the C_j are arbitrary constants that are determined from the initial conditions and $\mathbf{i}$ is $\sqrt{-1}$. We note that, in Eq. (6.23), an index summation over the index j was used. The summation is unconventional because the index j appears more than two times in one term. The summation applies only when all of the quantities having the j index appear together in the same term. If a partial term is considered, for example $\phi_j e^{\mathbf{i}\omega_j}$, then no summation applies over the j index. This convention is used throughout this chapter, and an effort will be made to clarify which of the indices is summed and which is not.

A nonhomogeneous second-order system given by

$$M\ddot{X} + KX = Fe^{\mathbf{i}\Omega t} + cc \tag{6.24}$$

where cc stands for complex conjugate of $Fe^{\mathbf{i}\Omega t}$, has a particular solution that can be expressed in the form

$$X = Ce^{\mathbf{i}\Omega t} + cc \tag{6.25}$$

Substituting Eq. (6.25) into Eq. (6.24) leads to the following system:

$$(-\Omega^2 M + K)C = F \tag{6.26}$$

If $\Omega \neq \omega_j$, where ω_j is any of the eigenvalues of the system, then $| - \Omega^2 M + K| \neq 0$ and C can be expressed as

$$C = (-\Omega^2 M + K)^{-1} F \tag{6.27}$$

If $\Omega = \omega_j$, then $|-\Omega^2 M + K| = 0$ and the solvability condition requires that F be normal to the solution of the homogeneous system

$$(-\omega_j^2 M + K)\phi_j = 0 \tag{6.28}$$

if M and K are real and symmetric. In other words, F must be normal to the system eigenvector associated with ω_j.

A more general representation of the system can be written as

$$M_{nl}\ddot{X}_l + K_{nl}X_l = F_{nk}e^{\mathbf{i}\Omega_k t} + cc \tag{6.29}$$

where the indices l and n represent the degrees of freedom and the summation applies. If one of the excitation frequencies Ω_p is equal to one of the natural frequencies ω_q, the following solvability condition applies:

$$F_{np}\phi_{nq} = 0 \tag{6.30}$$

The solution corresponding to the other (nonresonant) frequencies can be expressed as

$$X_n = e^{\mathbf{i}\Omega_k t}C_{nk} + cc \tag{6.31}$$

where

$$C_{nk} = (-\Omega_k^2 M + K)^{-1}_{nm}F_{mk} \tag{6.32}$$

6.4.2 Approximate Solutions for Parametric Resonance

In this section, we apply the method of multiple scales (Nayfeh, 1973 [67]; Nayfeh, 1981 [68]) to derive approximate solutions of the equations of ship motions derived in Chapter 3, and hence obtain modulation equations of the amplitudes and phases. The third-order equations of ship motion are expressed in index notation as

$$M_{nl}\ddot{\eta}_l + K_{nl}\eta_l = -\epsilon^2 C_{nl}\dot{\eta}_l + \epsilon F_n \tag{6.33}$$

$$
\begin{aligned}
&-\epsilon\left[P_{nlk}\eta_k\ddot{\eta}_l + Q_{nlk}\eta_k\dot{\eta}_l + R_{nlk}\eta_k\eta_l + S_{nlk}\dot{\eta}_k\dot{\eta}_l\right] \\
&-\epsilon^2\left[T_{nlkm}\eta_m\eta_k\ddot{\eta}_l + U_{nlkm}\eta_m\eta_k\dot{\eta}_l + V_{nlkm}\eta_m\eta_k\eta_l\right. \\
&\left.+W_{nlkm}\eta_m\dot{\eta}_k\dot{\eta}_l + X_{nlkm}\eta_m\dot{\eta}_k\dot{\eta}_l\right]
\end{aligned}
$$

where ϵ is a bookkeeping device that indicates the order of magnitude of the corresponding terms. We expand the displacement variable η_l as

$$\eta_l = \epsilon_i\eta_{il} \tag{6.34}$$

where $\epsilon_i = \epsilon^i(\epsilon_0 = 1, \epsilon_1 = \epsilon, \epsilon_2 = \epsilon^2)$. Since we are seeking expansions up to second order, the values of i can be 0, 1, or 2. We define several time scales as

$$T_i = \epsilon_i t \tag{6.35}$$

and express the corresponding time derivatives as $D_i = \frac{d}{dT_i}$, which relate to the ordinary time derivatives as

$$\frac{d}{dt} = \epsilon_i D_i \tag{6.36}$$

$$\frac{d^2}{dt^2} = \epsilon_i\epsilon_j D_i D_j \tag{6.37}$$

The displacements, velocities, accelerations, and their multiplications are expressed as

$$\dot{\eta}_l = \epsilon_i\epsilon_j D_i\eta_{jl} \tag{6.38}$$

$$\ddot{\eta}_l = \epsilon_i\epsilon_j\epsilon_s D_i D_j\eta_{sl} \tag{6.39}$$

$$\eta_k\eta_l = \epsilon_i\epsilon_j\eta_{ik}\eta_{jl} \tag{6.40}$$

$$\eta_k\dot{\eta}_l = \epsilon_i\epsilon_j\epsilon_s\eta_{ik}D_j\eta_{sl} \tag{6.41}$$

$$\eta_k\ddot{\eta}_l = \epsilon_i\epsilon_j\epsilon_s\epsilon_p\eta_{ik}D_j D_s\eta_{pl} \tag{6.42}$$

$$\dot{\eta}_k\dot{\eta}_l = \epsilon_i\epsilon_j\epsilon_s\epsilon_p D_i\eta_{jk}D_s\eta_{pl} \tag{6.43}$$

$$\eta_m\eta_k\ddot{\eta}_l = \epsilon_i\epsilon_j\epsilon_s\epsilon_p\epsilon_r\eta_{im}\eta_{jk}D_s D_p\eta_{rl} \tag{6.44}$$

$$\eta_m\eta_k\dot{\eta}_l = \epsilon_i\epsilon_j\epsilon_s\epsilon_p\eta_{im}\eta_{jk}D_s\eta_{pl} \tag{6.45}$$

$$\eta_m\eta_k\eta_l = \epsilon_i\epsilon_j\epsilon_s\eta_{im}\eta_{jk}\eta_{sl} \tag{6.46}$$

$$\eta_m\dot{\eta}_k\dot{\eta}_l = \epsilon_i\epsilon_j\epsilon_s\epsilon_p\epsilon_r\eta_{im}D_j\eta_{sk}D_p\eta_{rl} \tag{6.47}$$

$$\dot{\eta_m}\dot{\eta}_k\dot{\eta}_l = \epsilon_i\epsilon_j\epsilon_s\epsilon_p\epsilon_r\epsilon_q D_i\eta_{jm}D_s\eta_{pk}D_r\eta_{ql} \tag{6.48}$$

$$\tag{6.49}$$

Substituting Eqs. (6.38) through (6.48) into Eq. (6.33) and separating terms of different orders leads to the following equations:

Order ϵ^0

$$(M_{nl}D_0^2 + K_{nl})\eta_{0l} = 0 \tag{6.50}$$

Order ϵ

$$\begin{aligned}(M_{nl}D_0^2 + K_{nl})\eta_{1l} = {} & F_n - 2M_{nl}D_0D_1\eta_{0l} - P_{nlk}\eta_{0k}D_0^2\eta_{0l} \\ & -Q_{nlk}\eta_{0k}D_0\eta_{0l} - R_{nlk}\eta_{0k}\eta_{0l} - S_{nlk}D_0\eta_{0k}D_0\eta_{0l}\end{aligned} \tag{6.51}$$

Order ϵ^2

$$\begin{aligned}(M_{nl}D_0^2 + K_{nl})\eta_{2l} = {} & -2M_{nl}\left[(D_0D_2 + \frac{1}{2}D_1^2)\eta_{0l} - D_0D_1\eta_{1l}\right] \\ & -C_{nl}D_0\eta_{0l} - 2R_{nlk}\eta_{0k}\eta_{1l} \\ & -P_{nlk}\left[\eta_{0k}D_0^2\eta_{1l} + 2\eta_{0k}D_0D_1\eta_{0l} + \eta_{1k}D_0^2\eta_{0l}\right] \\ & -Q_{nlk}\left[\eta_{0k}D_1\eta_{0l} + \eta_{1k}D_0\eta_{0l} + \eta_{0k}D_0\eta_{1l}\right] \\ & -2S_{nlk}\left[D_0\eta_{0k}D_0\eta_{1l} + D_0\eta_{0k}D_1\eta_{0l}\right] \\ & -T_{nlkm}\eta_{0m}\eta_{0k}D_0^2\eta_{0l} - U_{nlkm}\eta_{0m}\eta_{0k}D_0\eta_{0l} - V_{nlkm}\eta_{0m}\eta_{0k}\eta_{0l} \\ & -W_{nlkm}\eta_{0m}D_0\eta_{0k}D_0\eta_{0l} - X_{nlkm}D_0\eta_{0m}D_0\eta_{0k}D_0\eta_{0l}\end{aligned} \tag{6.52}$$

In Eq. (6.52), we used the symmetry properties $P_{nlk} = P_{nkl}$ and $S_{nlk} = S_{nkl}$.

The solution of Eq. (6.50) can be expressed as

$$\eta_{0l} = \psi_{lj}e^{\mathbf{i}\omega_j T_0}A_j(T_1, T_2) + cc \tag{6.53}$$

where ψ_{lj} is the eigenvector associated with the eigenvalue ω_j and A_j is a complex function. It should be noted again that the summation over j is unconventional. To solve Eq. (6.51),

we write the derivatives of Eq. (6.53) and their products as

$$D_0\eta_{0l} = \mathbf{i}\omega_j\psi_{lj}e^{\mathbf{i}\omega_j T_0}A_j + cc \tag{6.54}$$

$$D_0^2\eta_{0l} = -\omega_j^2\psi_{lj}e^{\mathbf{i}\omega_j T_0}A_j + cc \tag{6.55}$$

$$D_0D_1\eta_{0l} = \mathbf{i}\omega_j\psi_{lj}e^{\mathbf{i}\omega_j T_0}\acute{A}_j + cc \tag{6.56}$$

$$\eta_{0k}\eta_{0l} = E_{rjkl} + \grave{E}_{rjkl} + cc \tag{6.57}$$

$$\eta_{0k}D_0\eta_{0l} = \mathbf{i}\omega_j(E_{rjkl} + \grave{E}_{rjkl}) + cc \tag{6.58}$$

$$D_0\eta_{0k}D_0\eta_{0l} = -w_r\omega_j(E_{rjkl} - \grave{E}_{rjkl}) + cc \tag{6.59}$$

$$\eta_{0k}D_0^2\eta_{0l} = -\omega_j^2(E_{rjkl} + \grave{E}_{rjkl}) + cc \tag{6.60}$$

$$\eta_{0m}\eta_{0k}\eta_{0l} = F_{srjmkl} + F_{s\grave{r}jmkl} + F_{sr\grave{j}mkl} + F_{srj\grave{m}kl} + cc \tag{6.61}$$

$$\eta_{0m}\eta_{0k}D_0^2\eta_{0l} = -\omega_j^2(F_{srjmkl} + F_{s\grave{r}jmkl} + F_{sr\grave{j}mkl} + F_{srj\grave{m}kl}) + cc \tag{6.62}$$

$$\eta_{0m}\eta_{0k}D_0\eta_{0l} = \mathbf{i}\omega_j(F_{srjmkl} + F_{s\grave{r}jmkl} + F_{sr\grave{j}mkl} - F_{srj\grave{m}kl}) + cc \tag{6.63}$$

$$\eta_{0m}D_0\eta_{0k}D_0\eta_{0l} = -\omega_r\omega_j(F_{srjmkl} + F_{s\grave{r}jmkl} - F_{sr\grave{j}mkl} - F_{srj\grave{m}kl}) + cc \tag{6.64}$$

$$D_0\eta_{0m}D_0\eta_{0k}D_0\eta_{0l} = -\mathbf{i}\omega_s\omega_r\omega_j(F_{srjmkl} - F_{s\grave{r}jmkl} - F_{sr\grave{j}mkl} - F_{srj\grave{m}kl}) + cc \tag{6.65}$$

where

$$\acute{A}_j = \frac{dA_j}{dT_1} \tag{6.66}$$

$$E_{rjkl} = \psi_{kr}\psi_{lj}e^{\mathbf{i}(\omega_j+\omega_r)T_0}A_jA_r \tag{6.67}$$

$$\grave{E}_{rjkl} = \psi_{kr}\psi_{lj}e^{\mathbf{i}(\omega_j-\omega_r)T_0}A_j\bar{A}_r \tag{6.68}$$

$$F_{srjmkl} = \psi_{lj}\psi_{kr}\psi_{ms}e^{\mathbf{i}(\omega_j+\omega_r+\omega_s)T_0}A_jA_rA_s \tag{6.69}$$

$$F_{s\grave{r}jmkl} = \psi_{lj}\psi_{kr}\psi_{ms}e^{\mathbf{i}(\omega_j+\omega_r-\omega_s)T_0}A_jA_r\bar{A}_s \tag{6.70}$$

$$F_{sr\grave{j}mkl} = \psi_{lj}\psi_{kr}\psi_{ms}e^{\mathbf{i}(\omega_j-\omega_r+\omega_s)T_0}A_j\bar{A}_rA_s \tag{6.71}$$

$$F_{srj\grave{m}kl} = \psi_{lj}\psi_{kr}\psi_{ms}e^{\mathbf{i}(-\omega_j+\omega_r+\omega_s)T_0}\bar{A}_jA_rA_s \tag{6.72}$$

The overbar denotes the complex conjugate. Equations (6.67) and (6.72) involve no summation, while Eqs. (6.54) through (6.65) involve summation over j, r, and s in an unconventional manner.

For a periodic excitation, the forcing term is expressed as

$$F_n = \frac{1}{2} f_{np} e^{\mathbf{i}(\Omega_p T_0 + \tau_{np})} + cc \tag{6.73}$$

where Ω_p is the p^{th} excitation frequency and f_{np} and τ_{np} are the associated amplitude and phase of excitation to the n^{th} degree of freedom. Also, in Eq. (6.73), the summation is over p only (no summation over n). Substituting Eqs. (6.54) through (6.60), (6.67), (6.68), and (6.73) into Eq. (6.51) yields

$$\begin{aligned}(M_{nl} D_0^2 + K_{nl})\eta_{1l} &= -\mathbf{i}\omega_j \left[2M_{nl}\acute{A}_j\right] \psi_{lj} e^{\mathbf{i}\omega_j T_0} + \frac{1}{2} f_{np} e^{\mathbf{i}(\Omega_p T_0 + \tau_{np})} \\ &\quad -W_{nrjkl} E_{rjkl} - \grave{W}_{nrjkl} \grave{E}_{rjkl} + cc\end{aligned} \tag{6.74}$$

where

$$W_{nrjkl} = -\omega_j^2 P_{nlk} + \mathbf{i}\omega_j Q_{nlk} + R_{nlk} - \omega_r \omega_j S_{nlk} \tag{6.75}$$

$$\grave{W}_{nrjkl} = -\omega_j^2 P_{nlk} + \mathbf{i}\omega_j Q_{nlk} + R_{nlk} + \omega_r \omega_j S_{nlk} \tag{6.76}$$

In Eqs. (6.75) and (6.76), there is no summation, while in Eq. (6.74), there is a summation over r, j, k, and l. In the absence of primary external resonances (i.e., $\Omega_p \neq \omega_i$ for all values of p and i) and internal resonances (i.e., $\omega_r + \omega_j \neq \omega_i$ for all values of r, j, and i), the only terms that may produce secular terms on the RHS of Eq. (6.74) are the first terms. The solvability condition is then written as

$$-\mathbf{i}\omega_j \left[2M_{nl}\acute{A}_j\right] \psi_{lj} \psi_{nj} = 0 \tag{6.77}$$

or

$$\hat{M}_j \acute{A}_j = 0 \tag{6.78}$$

where $\hat{M}_j$ is the modal mass associated with the j^{th} natural frequency, defined as

$$\hat{M}_j = \psi_{nj} M_{nl} \psi_{lj} \tag{6.79}$$

where the index j is used unconventionally in Eqs. (6.77), (6.78), and (6.79); it appears more than once in one term although no summation is taken over it. This means that each

of the j-terms that appears in Eq. (6.78) must be equal to zero. Then Eq. (6.78) leads to

$$\acute{A}_j = 0 \tag{6.80}$$

or

$$A_j = A_j(T_2) \tag{6.81}$$

Then, solving Eq. (6.74), we have

$$\begin{aligned} \eta_{1k} &= \frac{1}{2} g_{kp} e^{\mathbf{i}(\Omega_p T_0 + \tau_{kp})} \\ &\quad + \psi_{sr}\psi_{pj}\left[H_{krjsp} e^{\mathbf{i}(\omega_j+\omega_r)T_0} A_j A_r + \grave{H}_{krjsp} e^{\mathbf{i}(\omega_j-\omega_r)T_0} A_j \bar{A}_r\right] + cc \end{aligned} \tag{6.82}$$

where

$$g_{kp} = \left[-\Omega_p^2 M + K\right]^{-1}_{kn} f_{np} \tag{6.83}$$

$$H_{krjsp} = \left[-(\omega_j+\omega_r)^2 M + K\right]^{-1}_{kn} W_{nrjsp} \tag{6.84}$$

$$\grave{H}_{krjsp} = \left[-(\omega_j-\omega_r)^2 M + K\right]^{-1}_{kn} \grave{W}_{nrjsp} \tag{6.85}$$

In Eqs. (6.83) through (6.85), a summation is taken over n only, while in Eq. (6.82), summation is taken over j, r, s, and p.

For the case where one of the input frequencies Ω_r is near twice one of the natural frequencies ω_q, we introduce a detuning parameter σ defined as

$$\Omega_r = 2\omega_q + \epsilon^2 \sigma \tag{6.86}$$

The modulation equations are obtained by substituting Eqs. (6.53) and (6.82) into Eq. (6.52). We keep the quantities that may produce secular terms. These are

$$D_0 D_2 \eta_{0l} = \mathbf{i}\omega_j \psi_{lj} e^{\mathbf{i}\omega_j T_0} \acute{A}_j + cc \tag{6.87}$$

$$\eta_{1k} D_0 \eta_{0l} = -\mathbf{i}\omega_j G_{pjlk} + cc + NST \tag{6.88}$$

$$\eta_{1k} D_0^2 \eta_{0l} = -\omega_j^2 G_{pjlk} + cc + NST \tag{6.89}$$

$$\eta_{0k} D_0 \eta_{1l} = \mathbf{i}\Omega_p G_{pjlk} + cc + NST \tag{6.90}$$

$$\eta_{0k} \eta_{1l} = G_{pjlk} + cc + NST \tag{6.91}$$

$$D_0\eta_{0k} D_0 \eta_{1l} = \omega_j \Omega_p G_{pjlk} + cc + NST \tag{6.92}$$

$$\eta_{0k} D_0^2 \eta_{1l} = -\Omega_p^2 G_{pjlk} + cc + NST \tag{6.93}$$

$$\eta_{0m}\eta_{0k}\eta_{0l} = 3\grave{F}_{jjjmkl} + cc \tag{6.94}$$

$$\eta_{0m}\eta_{0k} D_0^2 \eta_{0l} = -3\omega_j^2 \grave{F}_{jjjmkl} + cc \tag{6.95}$$

$$\eta_{0m}\eta_{0k} D_0 \eta_{0l} = \mathbf{i}\omega_j \grave{F}_{jjjmkl} + cc \tag{6.96}$$

$$\eta_{0m} D_0\eta_{0k} D_0 \eta_{0l} = \omega_i^2 \grave{F}_{jjjmkl} + cc \tag{6.97}$$

$$D_0\eta_{0m} D_0\eta_{0k} D_0 \eta_{0l} = 3\mathbf{i}\omega_j^3 \grave{F}_{jjjmkl} + cc \tag{6.98}$$

where NST stands for terms that do not produce secular terms and

$$G_{pjlk} = \frac{1}{2}\psi_{kj} g_{lp} \bar{A}_j e^{\mathbf{i}[(\Omega_p - \omega_j)T_0 + \tau_{lp}]} \tag{6.99}$$

$$\grave{F}_{jjjmkl} = \psi_{lj}\psi_{kj}\psi_{mj} A_j^2 \bar{A}_j e^{\mathbf{i}\omega_j T_0} \tag{6.100}$$

In Eqs. (6.99) and (6.100), there is no summation, while in Eqs. (6.87) through (6.98), there is summation over j and p. Substituting Eqs. (6.87) through (6.100) into Eq. (6.52) yields

$$\begin{aligned}(M_{nl} D_0^2 + K_{nl})\eta_{2l} = {} & \left\{-\mathbf{i}\omega_j \psi_{lj}[2M_{nl}\acute{A}_j + C_{nl} A_j]\right. \\ & \left. + N_{nlkmj}\psi_{lj}\psi_{kj}\psi_{mj} A_j^2 \bar{A}_j\right\} e^{\mathbf{i}\omega_j T_0} \\ & + \frac{1}{2} L_{nlkpj} g_{lp}\psi_{kj}\bar{A}_j e^{\mathbf{i}[(\Omega_p - \omega_j)T_0 + \tau_{lp}]}\end{aligned} \tag{6.101}$$

where

$$d\acute{A}_j = \frac{dA_j}{T_2} \tag{6.102}$$

$$L_{nlkpj} = (\Omega^2 P_{nlk} + \omega_j^2 P_{nkl}) - \mathbf{i}(-\Omega_p Q_{nlk} + \omega_j Q_{nkl}) - 2R_{nlk} - 2\omega_j\Omega_p S_{nlk} \tag{6.103}$$

$$N_{nlkmj} = 3\omega_j^2 T_{nlkm} - \mathbf{i}\omega_j U_{nlkm} - 3V_{nlkm} - \omega_j^2 W_{nlkm} - 3\mathbf{i}\omega_j^3 X_{nlkm} \tag{6.104}$$

In Eqs. (6.103) and (6.104), there is no index summation, while in Eq. (6.101), there is summation over l and k, p, m, and j.

Next, the solvability condition is obtained for two different cases. The first is the case where $j \neq q$. Under these conditions, secular terms are only produced by the first two terms on the RHS of Eq. (6.101). So these terms should be normal to the j^{th} eigenvector of the system, hence

$$\left\{-\mathbf{i}\omega_j\psi_{lj}[2M_{nl}\acute{A}_j + C_{nl}A_j] + N_{nlkmj}\psi_{lj}\psi_{kj}\psi_{mj}A_j^2\bar{A}_j\right\}\psi_{nj} = 0 \tag{6.105}$$

where no summation is taken over the index j. After some manipulation, this solvability condition can be written as

$$-\mathbf{i}\omega_j[\acute{A}_j + \mu_j A_j] + \alpha_j A_j^2\bar{A}_j = 0 \tag{6.106}$$

where μ_j is the j^{th} modal damping coefficient defined as

$$\mu_j = \frac{\psi_{nj}C_{nl}\psi_{lj}}{2\psi_{nj}M_{nl}\psi_{lj}} \tag{6.107}$$

and α_j is the effective cubic coefficient of the natural frequency j, defined as

$$\alpha_j = \frac{\psi_{nj}N_{nlkmj}\psi_{lj}\psi_{kj}\psi_{mj}}{2\psi_{nj}M_{nl}\psi_{lj}} \tag{6.108}$$

Again, in Eqs. (6.107) and (6.108), no summation is taken over the index j. Defining $A_j(T_2) = \frac{1}{2}a_j(T_2)e^{\mathbf{i}\beta_j(T_2)}$ (no summation involved), we write the modulation equations (6.106) as

$$\acute{a_j} = -\mu_j a_j + \frac{1}{4\omega_j}a_j^3\Im(\alpha_j) \tag{6.109}$$

$$a_j\acute{\beta_j} = -\frac{1}{4\omega_j}a_j^3\Re(\alpha_j) \tag{6.110}$$

where $\Im$ stands for the imaginary part of a complex quantity and $\Re$ stands for the real part of a complex quantity. For steady-state response ($\acute{a_j} = \acute{\beta_j} = 0$), the modulation equations reduce to

$$a_j = 0 \tag{6.111}$$

The second case is for $j = q$. In this case , secular terms are produced by all terms on the RHS of Eq. (6.101). So, the solvability condition is written as

$$\begin{aligned}\Big\{-\mathbf{i}\omega_q\psi_{lq}[2M_{nl}\acute{A}_q + C_{nl}A_q] + N_{nlkmq}\psi_{lq}\psi_{kq}\psi_{mq}A_q^2\bar{A}_q \\ +\frac{1}{2}L_{nlkpq}g_{lp}\psi_{kq}\bar{A}_q e^{\mathbf{i}(\sigma T_2+\tau_{lr})}\Big\}\psi_{nq} &= 0\end{aligned} \tag{6.112}$$

where there is no summation over the index q. We manipulate Eq. (6.112) and obtain

$$-\mathbf{i}\omega_q[\acute{A}_q + \mu_q A_q] + \alpha_q A_q^2\bar{A}_q + \frac{1}{2}\nu_{lrq}\bar{A}_q e^{\mathbf{i}(\sigma T_2+\tau_{lr})} = 0 \tag{6.113}$$

where

$$\nu_{lrq} = \frac{\psi_{nq}L_{nlkrq}\psi_{kq}}{2\psi_{nq}M_{nk}\psi_{kq}}g_{lr} \tag{6.114}$$

In Eq. (6.114), the summation applies for the indices n and k, while in Eq. (6.113), the summation applies for the index l. The quantity ν_{lrq} is the effective forcing amplitude due to the degree of freedom l, which excites the q^{th} mode of the system at the input frequency Ω_r (resonant frequency). The effective amplitude due to all degrees of freedom f_{rq} can be expressed as

$$f_{rq} = \nu_{lrq}e^{\mathbf{i}\tau_{lr}} \tag{6.115}$$

where the summation is taken over index l only.

Defining $A_j(T_2) = \frac{1}{2}a_j(T_2)e^{\mathbf{i}\beta_j(T_2)}$ (no summation involved), we write the modulation equations (6.113) as

$$\acute{a_q} = -\mu_q a_q + \frac{1}{4\omega_q}a_q^3\Im(\alpha_q) + \frac{1}{2\omega_q}a_q[\Im(\nu_{lrq})\cos(\gamma_{lrq}) + \Re(\nu_{lrq})\sin(\gamma_{lrq})] \tag{6.116}$$

$$a_q\acute{\gamma_{lrq}} = a_q\sigma + \frac{1}{2\omega_q}a_q^3\Re(\alpha_q) - \frac{1}{\omega_q}a_q[\Re(\nu_{lrq})\cos(\gamma_{lrq}) - \Im(\nu_{lrq})\sin(\gamma_{lrq})] \tag{6.117}$$

$$\tag{6.118}$$

where the summation applies for the index l only, and

$$\gamma_{lrq} = \sigma T_2 + \tau_{lr} - 2\beta_q \tag{6.119}$$

For steady-state response ($\acute{a_q} = \acute{\gamma_{lrq}} = 0$), Eqs. (6.116) and (6.117) reduce to

$$\frac{1}{4\omega_q}a_q^2 = \frac{\mu_q}{\Im(\alpha_q)} - \frac{\Im(\nu_{lrq})}{2\Im(\alpha_q)\omega_q}\cos(\gamma lrq) - \frac{\Re(\nu_{lrq})}{2\Im(\alpha_q)\omega_q}\sin(\gamma lrq) \tag{6.120}$$

$$\frac{1}{2\omega_q}a_q^2 = -\frac{\sigma}{\Re(\alpha_q)} - \frac{\Re(\nu_{lrq})}{\Re(\alpha_q)\omega_q}\cos(\gamma lrq) + \frac{\Im(\nu_{lrq})}{\Re(\alpha_q)\omega_q}\sin(\gamma lrq) \tag{6.121}$$

The general approximate solution can then be constructed as

$$\begin{aligned}\eta_l = {} & \psi_{lj}e^{\mathbf{i}w_jT_0}A_j(T_2) + \epsilon\left\{\frac{1}{2}g_{lp}e^{\mathbf{i}(\Omega_pT_0+\tau_{lp})}\right. \\ & \left.+\psi_{sr}\psi_{pj}\left[H_{lrjsp}e^{\mathbf{i}(\omega_j+\omega_r)T_0}A_jA_r + \grave{H_{lrjsp}}e^{\mathbf{i}(\omega_j-\omega_r)T_0}A_j\bar{A}_r\right]\right\} + cc\end{aligned} \tag{6.122}$$

In Eq. (6.122), there is a summation over the indices j, r, and p. For steady-state response, it was shown that $A_j(T_2) = 0$ when $j \neq q$. So, Eq. (6.122) can be rewritten as

$$\begin{aligned}\eta_l &= \psi_{lq}e^{\mathbf{i}\omega_qT_0}A_q(T_2) + \epsilon\left\{\frac{1}{2}g_{lp}e^{\mathbf{i}(\Omega_pT_0+\tau_{lp})} + cc\right\} \\ &= \psi_{lq}a_q\cos(\omega_qt+\beta_q) + \epsilon\left\{g_{lp}\cos(\Omega_pt+\tau_{lp})\right\} \\ &= \psi_{lq}a_q\cos[\frac{1}{2}(\Omega_rt - \bar{\gamma_{lrq}} + \bar{\tau_{lr}})] + \epsilon\left\{g_{lp}\cos(\Omega_pt+\tau_{lp})\right\}\end{aligned} \tag{6.123}$$

where the overbar denotes the average of the associated quantity. In Eqs. (6.123), there is a summation over p. The amplitude a_q and phase γ_{lrq} are controlled by Eqs. (6.120) and (6.121). The quantity γ_{lrq} can be interpreted as the difference between the phase of the degree of freedom l at the excitation frequency Ω_r and double the phase of the degree of freedom q at $\frac{1}{2}\Omega_r$, half the excitation frequency. Using the concepts of higher-order spectra, we note that this quantity is given by the phase of the cross-bispectrum B_{lqq} between the degrees of freedom l and q (Hajj et al, 1995 [75]; Nayfeh et al, 1997 [76]; Hajj et al, 2000 [85]; Nayfeh et al, 1998 [109]); that is, $\gamma_{lrq} = \angle B_{lqq}(\frac{1}{2}\Omega_r, \frac{1}{2}\Omega_r)$

6.4.3 Parametric Roll Resonance

In this section, we examine the nonlinear parametric roll resonance, which occurs due to the nonlinear interaction between the heave and/or pitch motions on one hand and the roll

motion on the other hand (Sanchez and Nayfeh, 1990 [130]; Oh et al, 1993 [78]; Oh et al, 2000 [131]). In this resonance, the heave and pitch motions are coupled linearly. However, they are coupled nonlinearly with the roll motion, with the nonlinear coupling terms appearing in the roll equation. The equations governing the heave, pitch, and roll equations are taken as special cases of the general equations of ship motion derived in Chapter 3 and written as

$$m_{33}\ddot{z} + m_{35}\ddot{\theta} + k_{33}z + k_{35}\theta = -c_{33}\dot{z} + c_{35}\dot{\theta} + \epsilon f_{zp}\cos(\Omega_p t + \tau_{zp}) \tag{6.124}$$

$$m_{53}\ddot{z} + m_{55}\ddot{\theta} + k_{53}z + k_{55}\theta = -c_{53}\dot{z} + c_{55}\dot{\theta} + \epsilon f_{\theta p}\cos(\Omega_p t + \tau_{\theta p}) \tag{6.125}$$

$$\begin{aligned} m_{44}\ddot{\phi} + k_{44}\phi = & -c_{44}\dot{\phi} + \epsilon f_{\phi p}\cos(\Omega_p t + \tau_{\phi p}) \\ & -\epsilon\left[2R_{434}z\phi + 2R_{454}\theta\phi\right] \\ & -\epsilon^2\left[V_{4444}\phi^3 + X_{4444}\dot{\phi}^3\right] \end{aligned} \tag{6.126}$$

where z is the heave motion, θ is the pitch motion, and ϕ is the roll motion; Ω_p is the p^{th} input frequency, f_{zp} and τ_{zp} are the amplitude and phase of the heave force associated with Ω_p, respectively; $f_{\theta p}$ and $\tau_{\theta p}$ are the amplitude and phase of the pitch force associated with Ω_p, respectively; and $f_{\phi p}$ and $\tau_{\phi p}$ are the amplitude and phase of the roll force associated with Ω_p, respectively. We only include the static quadratic coefficients R_{434} and R_{454} in Eq. (6.126) because they can represent the effects of other quadratic coefficients, such as $K_{\dot{\phi}\dot{z}}$ and $K_{\dot{\phi}\dot{\theta}}$, respectively. Thus, these coefficients are considered as the effective quadratic coefficients in the roll equation.

Following the work of Oh et al (1993) [78] and Oh et al (2000) [131], we include quadratic and cubic terms that contribute to the parametric roll resonance. In this work, we advance the previous formulation by considering the linear coupling between the heave and pitch equations and by considering an input that represents sea states (several frequencies). Also, we allow the roll motion to be excited by the sea wave. The resonance condition can be expressed as

$$\Omega_r = 2\omega_\phi + \epsilon^2\sigma \tag{6.127}$$

where ω_ϕ is the roll natural frequency defined as $\sqrt{\frac{k_{44}}{m_{44}}}$.

Following the solution presented in Section 6.4.2, we obtain

$$z = \epsilon \{g_{zp} \cos(\Omega_p T_0 + \tau_{zp})\} \tag{6.128}$$

$$\theta = \epsilon \{g_{\theta p} \cos(\Omega_p T_0 + \tau_{\theta p})\} \tag{6.129}$$

and

$$\phi = a_\phi \cos\{\frac{1}{2}[\Omega_r t - \frac{1}{2}(\gamma_{zr\phi} + \gamma_{\theta r\phi}) + \frac{1}{2}(\tau_{zr} + \tau_{\theta r})]\} + O(\epsilon) \tag{6.130}$$

where g_{zp} is the amplitude of the heave motion at the excitation frequency Ω_p and τ_{zp} is its associated phase, $g_{\theta p}$ is the amplitude of the pitch motion at the excitation frequency Ω_p and $\tau_{\theta p}$ is its associated phase, and a_ϕ is the steady-state amplitude of the roll motion at half the excitation frequency Ω_r. We note that, in Eqs. (6.128) and (6.129), a summation is taken over the index p. On the other hand, Eq. (6.130) involves no summation.

The steady-state modulation equations governing the amplitude of the roll motion are obtained as special cases of Eqs. (6.120) and (6.121) as

$$\begin{aligned} \frac{3}{4}\omega_\phi^2 a_\phi^2 &= -\frac{\mu_\phi}{X_{4444}/2m_{44}} - \frac{1}{2\omega_\phi}\frac{R_{434}/m_{44}}{X_{4444}/2m_{44}} g_{zr}\sin(\gamma_{zr\phi}) \\ &\quad -\frac{1}{2\omega_\phi}\frac{R_{454}/m_{44}}{X_{4444}/2m_{44}} g_{\theta r}\sin(\gamma_{\theta r\phi}) \end{aligned} \tag{6.131}$$

$$\begin{aligned} \frac{3}{4\omega_\phi}a_\phi^2 &= -\frac{\sigma}{V_{4444}/m_{44}} - \frac{1}{\omega_\phi}\frac{R_{434}/m_{44}}{V_{4444}/m_{44}} g_{zr}\sin(\gamma_{zr\phi}) \\ &\quad -\frac{1}{\omega_\phi}\frac{R_{454}/m_{44}}{V_{4444}/m_{44}} g_{\theta r}\sin(\gamma_{\theta r\phi}) \end{aligned} \tag{6.132}$$

where μ_ϕ is the linear damping parameter of the roll motion, defined as $\mu_\phi = c_{44}/2m_{44}$,

6.4.4 Nonlinear Identification Procedure

Equations (6.131) and (6.132) constitute two equations with four unknowns. The unknown coefficients are X_{4444}, V_{4444}, R_{434}, and R_{454}. The quantities $\gamma_{zr\phi}$ and $\gamma_{\theta r\phi}$ represent the phase relations between the different motions. They can be obtained from the phases of the

cross-bispectrum given by

$$\gamma_{zr\phi} = \angle B_{z\phi\phi}(\frac{1}{2}\Omega_r, \frac{1}{2}\Omega_r) \tag{6.133}$$

and

$$\gamma_{\theta r\phi} = \angle B_{\theta\phi\phi}(\frac{1}{2}\Omega_r, \frac{1}{2}\Omega_r) \tag{6.134}$$

The quantities a_ϕ, g_{zr}, and $g_{\theta r}$ are the amplitudes of the roll, heave, and pitch motions, respectively. The natural frequency of the roll motion ω_ϕ and the linear damping μ_ϕ are obtained using the linear techniques described in Chapter 4.

One way to identify the unknown coefficients is to separate the problem into two parts. One part includes the effects of the heave motion only and the other includes the effects of the pitch motion only. Redefining the coefficients as

$$\mu_3 = \frac{X_{4444}}{2M_{44}} \tag{6.135}$$

$$\alpha_3 = \frac{V_{4444}}{M_{44}} \tag{6.136}$$

$$K_{\phi z} = -4\frac{R_{434}}{M_{44}} \tag{6.137}$$

and

$$K_{\phi\theta} = -4\frac{R_{454}}{M_{44}} \tag{6.138}$$

we rewrite Eqs. (6.131) and (6.132) for the heave component only as

$$\frac{3}{4}\omega_\phi^2 a_\phi^2 = -\frac{\mu_\phi}{\mu_3} + \frac{1}{8\omega_\phi}\frac{K_{\phi z}}{\mu_3} g_{zr}\sin(\gamma_{zr\phi}) \tag{6.139}$$

$$\frac{3}{4\omega_\phi}a_\phi^2 = -\frac{\sigma}{\alpha_3} - \frac{1}{4\omega_\phi}\frac{K_{\phi z}}{\alpha_3} g_{zr}\cos(\gamma_{zr\phi}) \tag{6.140}$$

$$\tag{6.141}$$

and for the pitch component only as

$$\frac{3}{4}\omega_\phi^2 a_\phi^2 = -\frac{\mu_\phi}{\mu_3} + \frac{1}{8\omega_\phi}\frac{K_{\phi\theta}}{\mu_3} g_{\theta r}\sin(\gamma_{\theta r\phi}) \tag{6.142}$$

$$\frac{3}{4\omega_\phi}a_\phi^2 = -\frac{\sigma}{\alpha_3} - \frac{1}{4\omega_\phi}\frac{K_{\phi\theta}}{\alpha_3} g_{\theta r}\cos(\gamma_{\theta r\phi}) \tag{6.143}$$

Equations (6.139) through (6.143) are consistent with the modulation equations derived by Oh et al (1993) [78]. By examining Eqs. (6.139) through (6.143), we can see that a_ϕ^2 varies linearly with $g_{zr}\sin(\gamma_{zr\phi})$, $g_{zr}\cos(\gamma_{zr\phi})$, $g_{\theta r}\sin(\gamma_{\theta r\phi})$, and $g_{\theta r}\cos(\gamma_{\theta r\phi})$, respectively. All of these quantities can be determined from the LAMP runs and spectral analysis. By plotting $\frac{3}{4}\omega_\phi^2 a_\phi^2$, $\frac{3}{4\omega_\phi}$, $\frac{3}{4}\omega_\phi^2 a_\phi^2$, and $\frac{3}{4\omega_\phi}a_\phi^2$ versus $g_{zr}\sin(\gamma_{zr\phi})$, $g_{zr}\cos(\gamma_{zr\phi})$, $g_{\theta r}\sin(\gamma_{\theta r\phi})$, and $g_{\theta r}\cos(\gamma_{\theta r\phi})$, respectively, we can use the slopes and the y-intercepts to determine the unknown parameters μ_3, α_3, $K_{\phi z}$, and $K_{\phi\theta}$. It should be noted here that some of the coefficients can be found using more than one set of information, which provides a means to double check the identified coefficients. We should also note that the identification procedure outlined above will allow us to determine if the modeling parameters are satisfactory. For instance, if the relation between $\frac{3}{4}\omega_\phi^2 a_\phi^2$ and $g_{zr}\sin(\gamma_{zr\phi})$ is not linear, that would imply that other parameters need to be included in the governing equations.

Based on the above discussion, the nonlinear identification procedure for the parametric resonance is performed using the following steps. First, we obtain the linear parameters μ_ϕ and ω_ϕ, as described in Chapter 4. Second, we conduct LAMP runs that exploit the parametric roll resonance, where the wave distribution is selected such that one of the input frequencies is near $2\omega_\phi$. Each run includes the roll and heave motions or the roll and pitch motions. Third, we determine the quantities a_ϕ, g_{zr}, $g_{\theta r}$, $\gamma_{zr\phi}$, and $\gamma_{\theta r\phi}$ from the spectral analysis. Fourth, we repeat the above procedure for several amplitude excitations. Fifth, we generate plots of $\frac{3}{4}\omega_\phi^2 a_\phi^2$, $\frac{3}{4\omega_\phi}$, $\frac{3}{4}\omega_\phi^2 a_\phi^2$, and $\frac{3}{4\omega_\phi}a_\phi^2$ versus $g_{zr}\sin(\gamma_{zr\phi})$, $g_{zr}\cos(\gamma_{zr\phi})$, $g_{\theta r}\sin(\gamma_{\theta r\phi})$, and $g_{\theta r}\cos(\gamma_{\theta r\phi})$, respectively, perform linear data fits, and determine the slopes and y-intercepts from which we determine the unknown coefficients. Finally, we validate the identified coefficients by integrating the governing equations and comparing them with the LAMP outputs.

6.5 Results of Nonlinear System Identification

In this section, we apply the methodology outlined above to identify the parameters, which cause parametric resonance in the roll motion. LAMP-2 is used to generate the ship-motion data in head sea state 3. We utilize LAMP to generate a Brettschneider two-parameter wave spectrum. The spectrum is discretized into nine input frequencies with random phases. One of the input frequency components is altered such that the encounter frequency at that component is near twice the roll natural frequency, which is around 0.263 (dimensionless). The record length used in the spectral analysis consists of $80,000$ samples to ensure steady-state conditions.

Figure 6.7 shows the heave, pitch, and roll motions for $U = 0.2$. Although the roll motion is not directly excited by the sea waves, it is parametrically excited by the heave and pitch motions. Figure 6.8 shows the spectra of the heave, pitch, and roll motions. It can be seen that the heave and pitch motions respond at several frequency components. On the other hand, the roll motion has one major frequency component. The response frequencies of the heave and pitch correspond to the frequencies of the input waves. This is expected since a linear system responds at the excitation frequencies. Although the excitation contains nine input waves, the response amplitudes of the heave and pitch are magnified at four of the nine input frequencies. These four frequencies are near the resonant frequencies of the heave and pitch motions. The spectra of the heave and pitch motions show that one of the response frequencies of the heave and pitch motions is approximately equal to 0.5276 (nondimensional). This frequency is near twice the roll natural frequency, which is equal to 0.263 (nondimensional). The spectrum of the the roll motion shows that it responds at a single frequency, which is approximately equal to 0.2627 (nondimensional). This frequency is near the roll natural frequency and is very close to half one of the excitation frequencies. The spectra described above are typical for parametric roll resonance, where the heave and pitch respond linearly to an input frequency which is equal approximately to twice the natural frequency of the roll. The heave and pitch, in turn, parametrically excite the roll motion.

We apply the nonlinear identification procedure described in the previous section to find the parameters μ_3, α_3, $K_{\phi z}$, and $K_{\phi\theta}$ that appear in the roll equation. For the identification purpose, we used $U = 0.05$ and the amplitude of the resonant frequency was varied between 0.00625 and 0.01125. As mentioned before, two sets of runs were performed. The first included the roll and heave motions. The second included the roll and pitch motions.

Figures 6.9a through 6.9d show plots of $\frac{3}{4}\omega_\phi^2 a_\phi^2$, $\frac{3}{4\omega_\phi}$, $\frac{3}{4}\omega_\phi^2 a_\phi^2$, and $\frac{3}{4\omega_\phi}a_\phi^2$ versus $g_{zr}\sin(\gamma_{zr\phi})$, $g_{zr}\cos(\gamma_{zr\phi})$, $g_{\theta r}\sin(\gamma_{\theta r\phi})$, and $g_{\theta r}\cos(\gamma_{\theta r\phi})$, respectively, We note that the linear variations presented by the plots validate the theory described above. Using the slopes and y-intercepts, we identify the unknown coefficients as

$$\mu_3 = -0.0361$$

$$\alpha_3 = -0.162$$

$$K_{\phi z} = 10.988$$

$$K_{\phi\theta} = -2.107$$

Using these coefficients, we integrated Eq. (6.126) to obtain the roll motion at different input amplitudes. The time-domain predictions of the roll motion for the heave-roll and pitch-roll parametric resonances are shown in Figs. 6.10 and 6.11, respectively. The resonant input amplitude is 0.00625. The results show that the time prediction can be determined with an accuracy level of $96 - 99\%$. The input level was varied between 0.00625 and 0.0125 and the roll amplitude was predicted for each input level. Figures 6.12 and 6.13 compare the predicted roll amplitudes for the heave-roll and pitch-roll parametric resonances, respectively, using the governing equations with the roll amplitudes obtained using LAMP. The accuracy of the prediction at each input amplitude is shown at the lower part of each figure. It is clear that the accuracy of the roll-amplitude predictions is above 96%.

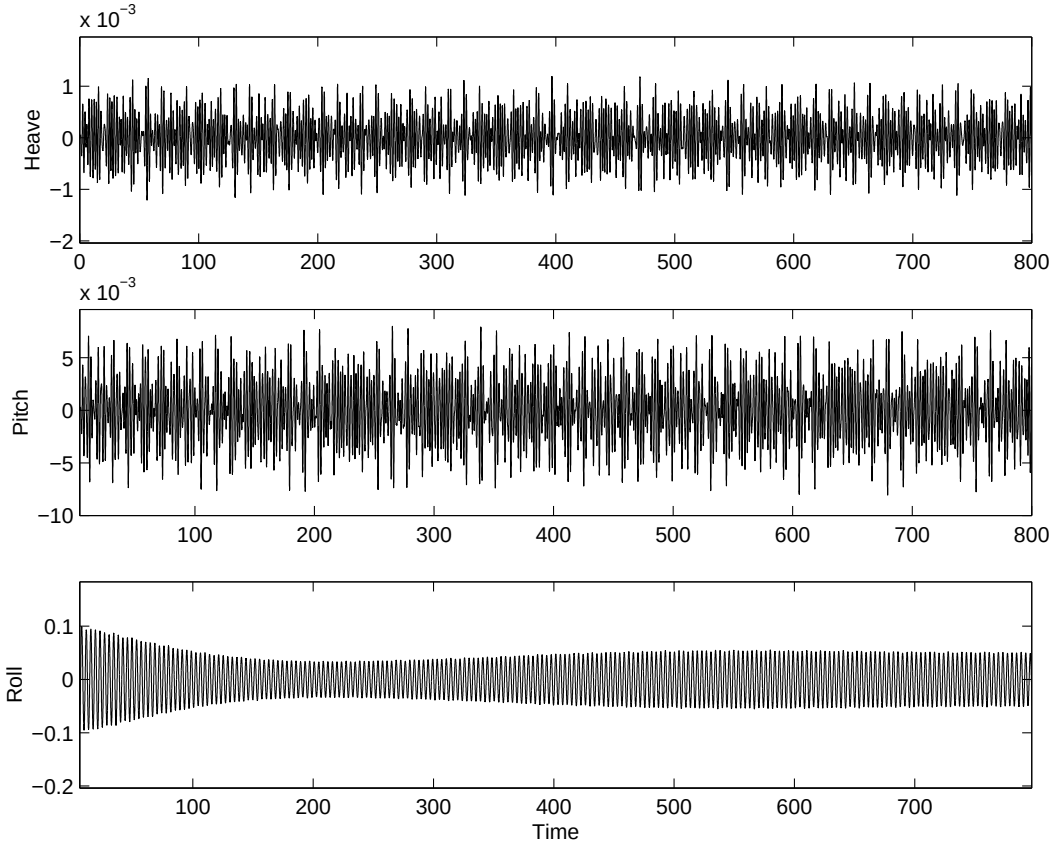

Figure 6.7: Time-domain data for nonlinear parametric roll resonance.

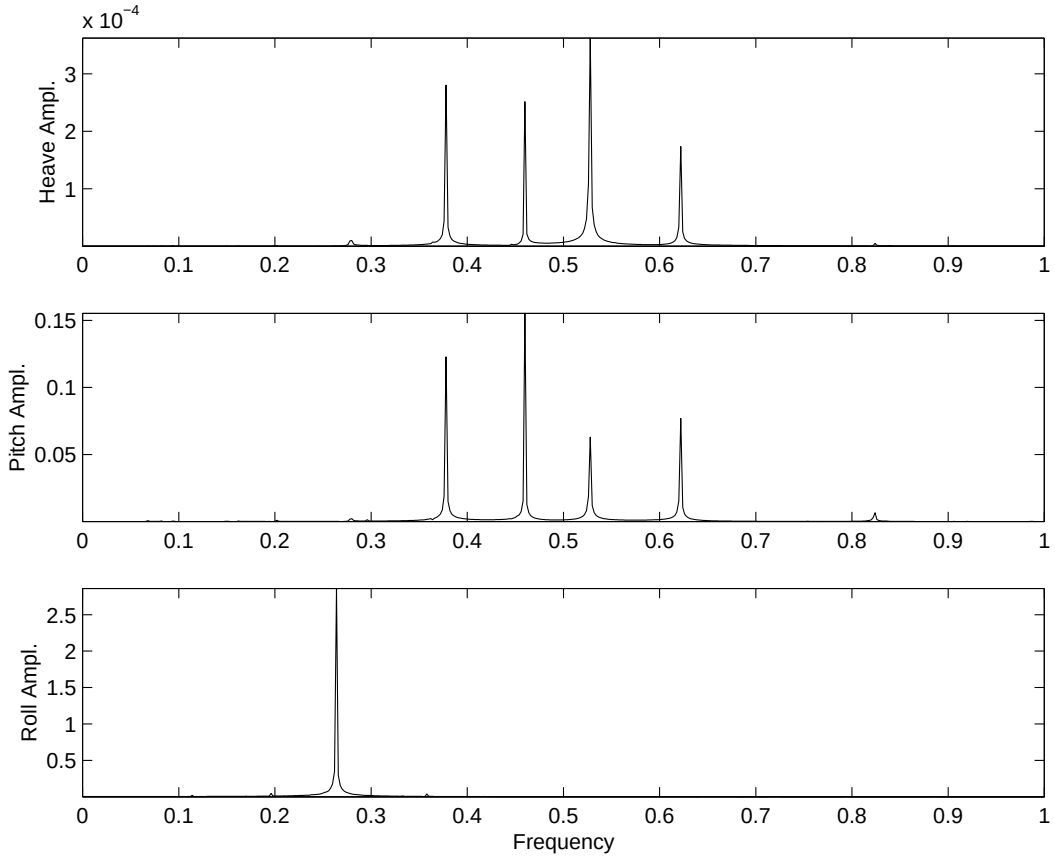

Figure 6.8: Frequency-domain data for nonlinear parametric roll resonance.

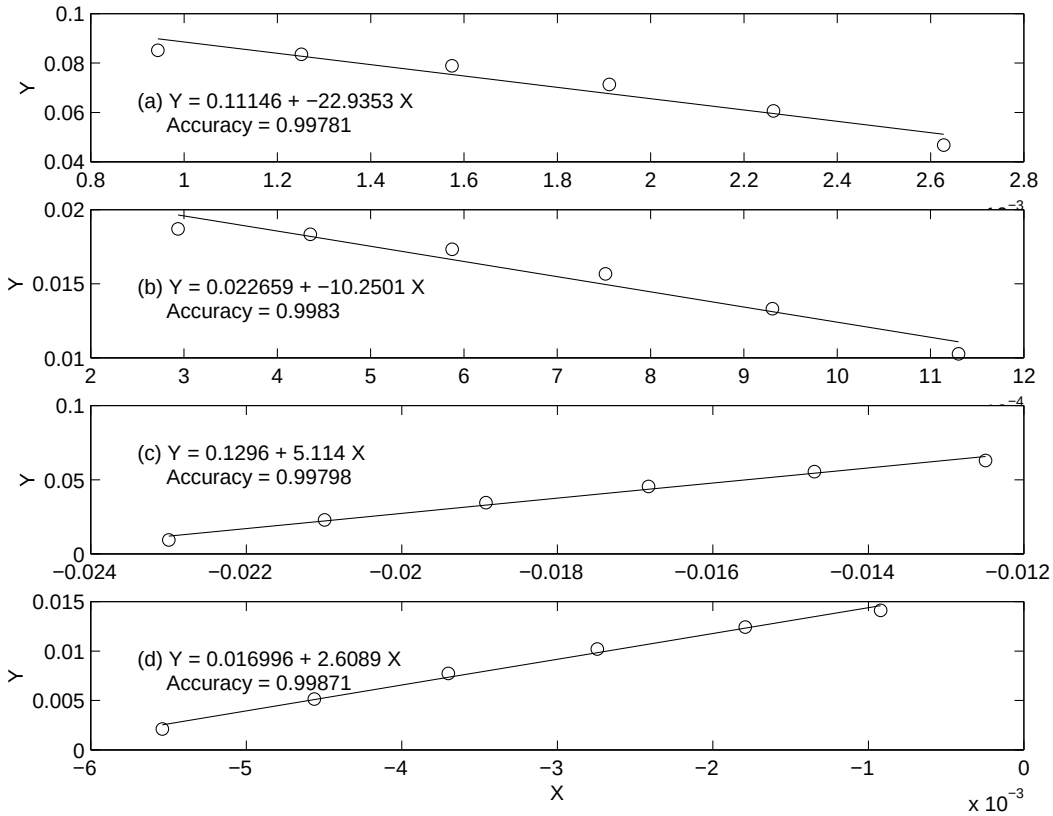

Figure 6.9: Variation of the roll amplitude with the bi-spectral quantities.

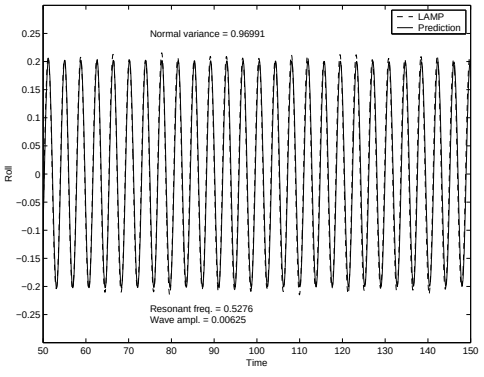

Figure 6.10: Prediction of the roll motion for the case of heave-roll parametric resonance.

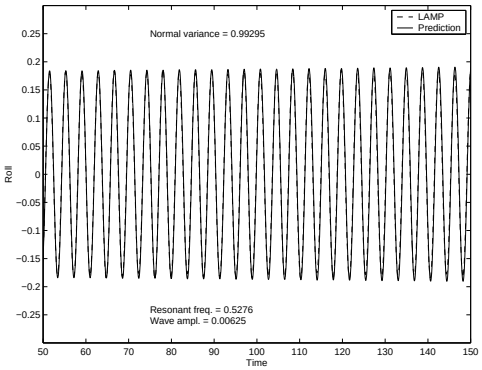

Figure 6.11: Prediction of the roll motion for the case of pitch-roll parametric resonance.

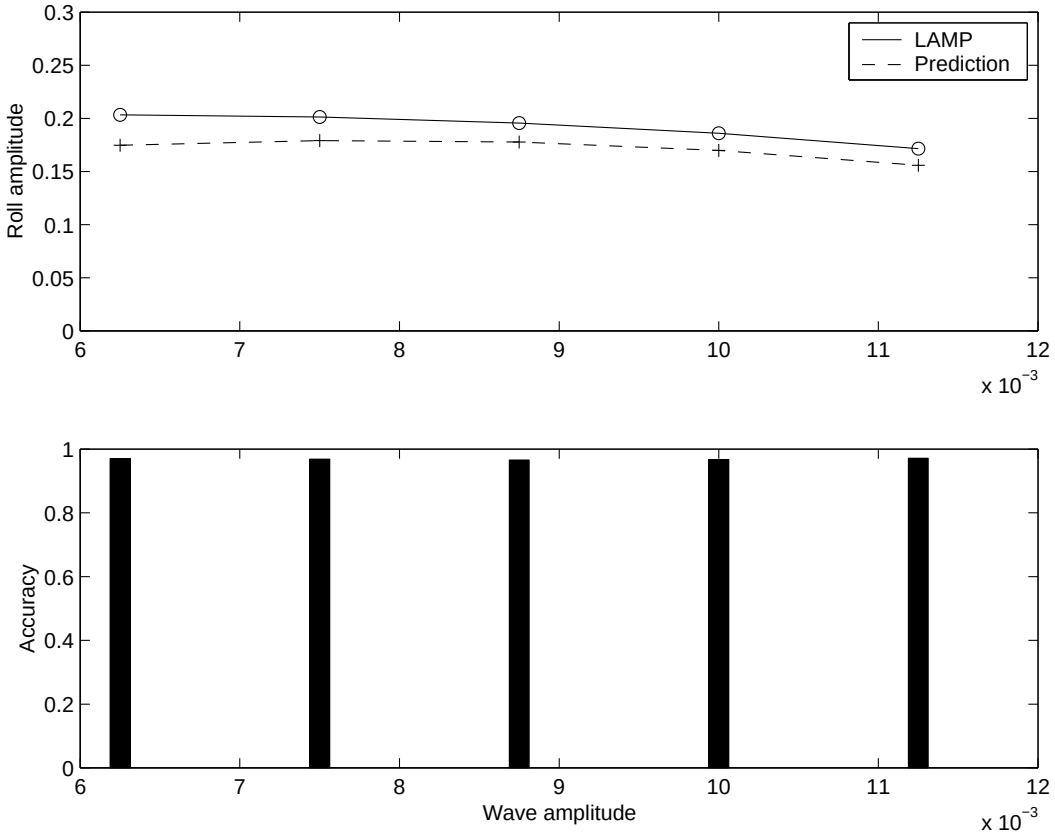

Figure 6.12: Prediction of the roll amplitudes for the case of heave-roll parametric resonance.

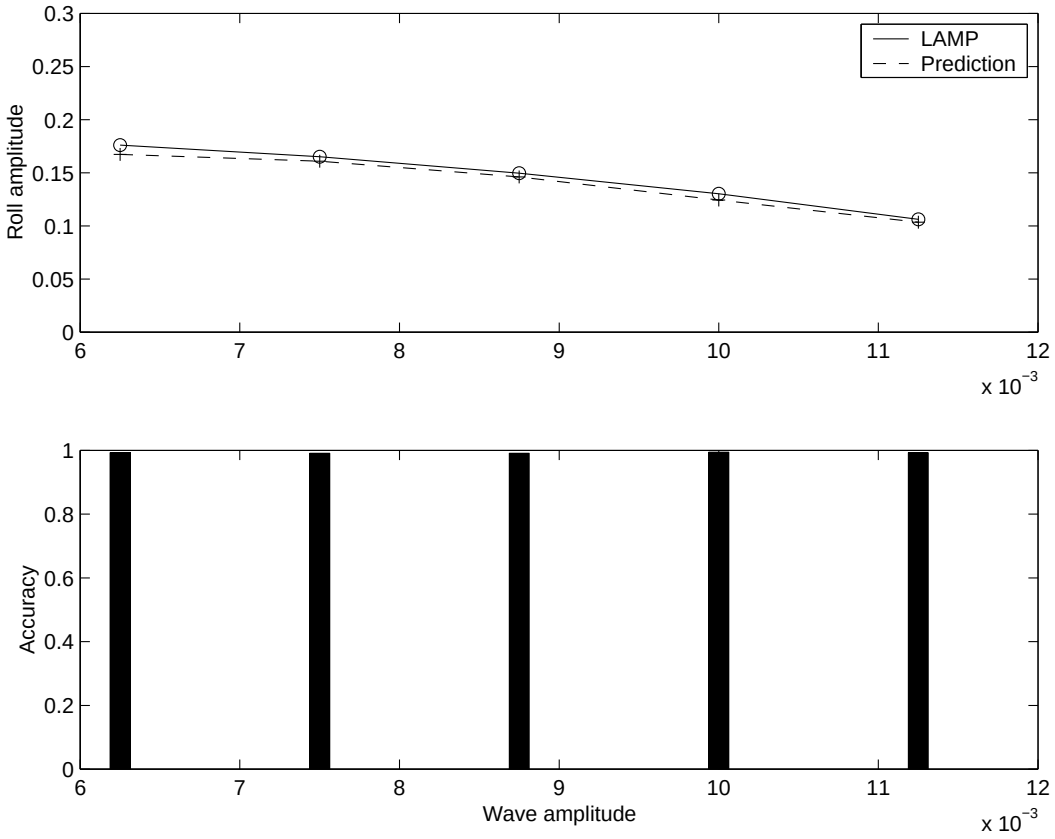

Figure 6.13: Prediction of the roll amplitudes for the case of pitch-roll parametric resonance.

Chapter 7

Summary and Conclusions

7.1 Summary and Conclusions of the Current Work

In this work, we establish a system-identification methodology for general finite-degree-of-freedom (FDOF) linear and nonlinear models of ship motions. As a first step, we use the energy-formulation approach to derive full nonlinear six-degree-of-freedom ship-motion models. These models contain all of the coupling terms between the different motions and explicitly specify the dependence of the linear and nonlinear parameters on the forward speed. As special cases, the linear, second-order, and third-order equations were extracted. The linear equations were found to be consistent with those derived in previous work. The models show that the added mass coefficients are always independent of the forward speed. On the other hand, the restoring coefficients are always dependent on the forward speed. This applies for the linear, second-order, and third-order terms in the equations of motion. The dependence of the restoring forces on the forward speed is linear, quadratic, and cubic, while the dependence of the damping forces on the forward speed is linear and quadratic. Furthermore, the dependence of the zeroth-order term (forward speed force) on the forward speed is a cubic polynomial with zero y-intercept.

To identify the linear parameters of the coupled ship-motion equations and determine the correct form of their dependence on the forward speed, we use the Large Amplitude Motions Program (LAMP) to generate data for the heave and pitch motions in different sea states and with different forward speeds. Then, we apply the eigensystem realization algorithm (ERA) to the LAMP data to identify the linearly coupled coefficients. The identified linear coefficients are fitted against the forward speed using three different forms; the first fit is based on strip theory, the second fit is based on the energy approach, and the third is a polynomial equation with terms up to ninth order. The coefficients obtained with the different fits are used to predict ship motions in different sea states with different forward speeds. By comparing these coefficients to the LAMP data, we determine the most suitable form of the dependence of the linear coefficients on the forward speed. The procedure outlined above is repeated to obtain exact fits for the coupled sway, roll, and yaw motions. Exact fits for the full 5 DOF ship motions are also obtained, and regimes of motions where linear modeling fails are discussed.

By examining the results, we conclude that the ERA is capable of extracting the linear system coefficients for a variety of sea conditions and forward speeds. We conclude that the dependence on the forward speed derived with the energy-formulation approach produces more accurate predictions than those derived with the strip-theory approach. The accuracy of the heave and pitch predictions is excellent for all sea states. On the other hand, the accuracy of the sway, roll, and yaw predictions is good up to sea state 4. Beyond this sea state, the accuracy deteriorates. It can be concluded that the linear model of the heave and pitch motions is applicable for all sea states, where the nonlinear effects are negligible. On the other hand, the linear model of the sway, roll, and yaw motions fails above sea state 4 because the nonlinear effects are strong. The worst accuracy occurs at sea state 5 because at this sea state and forward speed of 0.2, the roll motion is excited by a nonlinear parametric resonance. This happens because one of the discretized encounter input frequencies is near twice the roll's natural frequency. We note here that a parametric roll resonance can be excited at any sea state, as long as one of the discretized encounter input frequencies is near

twice the roll's natural frequency.

We also present a new analysis technique, which is closely related to Prony's method, namely, the circular-hyperbolic decomposition (CHD). This decomposition technique provides a means to estimate the frequency components of a signal that avoids the leakage problem encountered in the discrete Fourier transform (DFT). We apply the CHD to determine the transfer functions and RAOs of the coupled heave and pitch motions of a Series 60 ship. The data is generated using the linear version of the LAMP code. We defin the RAO and the steps used to obtain the response spectra and compare the RAOs obtained with the DFT with those obtained with the CHD. The CHD is found to be superior to the DFT in uncovering system characteristics in situations where the system frequencies are not known in advance.

The nonlinear effects in ship motions based on the different LAMP versions are discussed. In LAMP-1 and LAMP-2, linearized free-surface and body boundary conditions are implemented. Both linearized and nonlinear forms of the Bernoulli equation are used to calculate the pressure distribution. By using linearized boundary conditions with the nonlinear Bernoulli equation, the LAMP code can account for some of the nonlinearities that exist in the system, but not all of them. In this work, we restrict ourselves to identifying the nonlinearities that exist in the LAMP code. Although these nonlinearities do not include all of the physical ones, the identification methodology can be applied for any motion data, whether it was generated with a numerical code, model tests, or full-scale experiments. We also present some LAMP data that show the effect of nonlinearity on the different ship motions.

Once the linear parameters are accurately found, the nonlinear parameters can be identified. Using traditional "brute-force" techniques requires solving for a large number of unknown parameters simultaneously. This approach reduces the accuracy of the identified parameters. In this work, we eliminate these problems by adopting a technique that is based on exploiting nonlinear resonances in ship motions. The technique combines the method of multiple scales and higher-order spectral moments. The reason for adopting this technique is that a few

parameters are identified from each nonlinear resonance.

As a special case, we study the nonlinear parametric roll resonance, which occurs due to nonlinear interactions between the heave and/or pitch motions and the roll motion. In this resonance, the heave and pitch motions are coupled linearly and uncoupled linearly from the roll motion. However, they occur nonlinearly in the roll equation. The nonlinear parameters responsible for this resonance are found and predictions are performed based on these parameters. The results are validated through comparisons with results from the LAMP code.

7.2 Recommendations for Future Work

When identifying the linear parameters, we used LAMP-1, which is the most linear version of LAMP. Nevertheless, LAMP-1 includes nonlinear rigid-body dynamics. The use of LAMP-1 is justified since the identification is performed for small-amplitude motions, where the effect of these nonlinearities is small. However, for better identification of the linear parameters, it is recommended that a completely linearized LAMP code be developed with linear rigid-body dynamics. Also, a completely linear LAMP will allow for separating the effect of the rigid-body dynamics from other types of nonlinearity.

The surge motion was not included in the identification work because small frequency components were found in the surge motion. These components are artifacts of the method of solution in LAMP. Inclusion of the surge motion leads to bad linear predictions of the surge, heave, and pitch motions. It is recommended that either the LAMP formulation be modified to get rid of these frequency components or efforts be made to provide suitable motion filters to remove the effects of these components from the LAMP data without affecting the accuracy of the linear identification.

Once a better nonlinear version of LAMP is developed, it is to recommended to apply the methodology used here to identify all of the nonlinear parameters in the ship-motion

equations, exploiting other types of nonlinear resonances, like the two-to-one resonance. This will also help to separate the effects of the different nonlinearities in the nonlinear parameters that cause the roll parametric resonance. It is also recommended to extend the CHD to determine nonlinear transfer functions.

Bibliography

[1] D. Burton, deKat, J., R. Sheinberg, and R. Minnik. Extreme motion analysis and simulation for ship design and operations. *Naval Engineers Journal*, 110:73–90, March 1998.

[2] D. X. Zhu and M. Katory. 3-d time domain numerical model for the prediction of ship motions in random seas. *International Journal of Offshore and Polar Engineering*, 5(2):120–126, June 1995.

[3] Science Applications International Corporation, Annapolis, MD. *User's Guide to the LAMP System, version 2.9.2*, 1998.

[4] J. F. Wellicome, P. A. Wilson, and X. Cheng. prediction of sway force and yaw moment on slender ships. *International Shipbuilding Progress*, 42(431):259–275, September 1995.

[5] B. V. Korvin-Korvosky and W. R. Jacobs. Pitching and heaving motions of a ship in regular waves. *SNAME Transactions*, 65:590–632, 1957.

[6] N. Salvesen, E. O. Tuck, and O. Faltinsen. Ship motions and sea loads. *SNAME Transactions*, 78:250–287, 1970.

[7] T. F. Ogilvie and E. O. Tuck. A rational strip theory of ship motions: part I. Technical report, Department of Naval Architecture and Marine Engineering, University of Michigan, March 1969.

[8] J. R. Spouge and N. Ireland. An experimental investigation of large amplitude motion. In *International Conference on the Safeship Project: Ship Stability & Safety*, London, June 9-10 1986. Paper no. 8.

[9] J. R. Spouge and J. P. Collins. Seakeeping trials on the fisheries protection vessel "sulisker". In *International Conference on the Safeship Project: Ship Stability & Safety*, London, June 9-10 1986.

[10] M. A. Abkowitz. Measurement of hydrodynamic characteristics from ship maneuvering trials by system identification. *SNAME Transactions*, 88:283–318, 1980.

[11] A. H. Nayfeh, D. T. Mook, and L. R. Marshall. Perturbation-energy approach for the development of the nonlinear equations of ship motion. *Journal of Hydronautics*, 8(4):130–136, 1974.

[12] L. R. Marshall, A. H. Nayfeh, and D. T. Mook. Forward speed effects in the equations of ship motion. *Journal of Sound and Vibration*, 85(3):303–313, 1982.

[13] J. F. O'Dea and D. A. Walden. The effect of bow shape and nonlinearities on the prediction of large amplitude motions and deck wetness. In *15th Symposium - Naval Hydrodynamics: Seakeeping Problems, Hull-Propeller Interactions, Nonlinear Free-Surface Problems, Frontier Problems in Hydrodynamics. Hamburg, W Germany*, pages 163–176, 1985.

[14] T. Ohyama and M. Tsuchida. Development of a partially three-dimensional model for ship motion in a harbor with arbitrary bathymetry. In *24th International Conference on Coastal Engineering, Part 1*, pages 871–885, October 23-28 1994.

[15] G. Van Oortmerssen, J. A. Pinkster, and H. J. J. Van Den Boom. Computer simulation of moored ship behavior. *Journal of Watreway, Port, Coastal and Ocean Engineering*, 112(2):296–308, March 1986.

[16] G. X. Wu and R. E. Taylor. The hydrodynamic force on an oscillating ship with low forward speed. *Journal of Fluid Mechanics*, 211:333–353, 1990.

[17] H. L. Wong and S. M. Calisal. Numerical algorithms for slender bodies with vortex shedding and density stratification. *Joural of Ship Research*, 40(1):11–21, March 1996.

[18] W.-M. Lin, S. Zhang, K. Weems, and D. K. P. Yue. A mixed source formulation for nonlinear ship-motion and wave-load simulations. In *Proceedings of the 7th International Conference on Numerical Ship Hydrodynamics, Nantes, France*, July 19-22 1999.

[19] B. V. Korvin-Korvosky. Investigation of ship motions in regular waves. *SNAME Transactions*, 63:386–435, 1955.

[20] R. Timman and J. N. Newman. The coupled damping coefficients of a symmetric ship. *Journal of Ship Research*, 5(2):1–7, March 1962.

[21] S. Wang. Dynamical theory of potential flows with a free surface: a classical approach to strip theory of ship motions. *Journal of Ship Research*, 20(3):137–144, September 1976.

[22] A. W. Troesch. Sway, roll and yaw motion coeficients based on a forward-speed slender-body theory-part 1. *Journal of Ship Research*, 25(1):8–15, March 1981.

[23] A. W. Troesch. Sway, roll and yaw motion coeficients based on a forward-speed slender-body theory-part 2. *Journal of Ship Research*, 25(1):16–20, March 1981.

[24] Y. Z. Liu, Y. L. Li, and G. P. Miao. An engineering prediction method for large amplitude motions of ships in waves. In *6th International Offshore and Polar Engineering Conference*, volume III, pages 438–444, May 26-31 1996.

[25] P. Crossland, P. A. Wilson, and J. C. Bradburn. The free decay of coupled heave and pitch motions of a model frigates. *Transactions of the Royal Institution of Naval Architects*, 135:121–131, 1993.

[26] Z. Tao and A. Incecik. Time domain simulation of vertical ship motions and loads in regular head seas. In *17th International Conference on Offshore Mechanics and Arctic Engineering*, volume 2. ASME, 1998. OMAE98-0591.

[27] L. A. Zadeh. From circuit theory to system theory. In *IRE*, volume 50, pages 856–865, 1962.

[28] P. Eykhoff. *System Identification; Parameter and State Estimation*. John Wiley & Sons, 1974.

[29] J.-N. Juang. *Applied System Identification*. PTR Prentice Hall, New Jersey, 1994.

[30] J. S. Bendat. *Nonlinear System Analysis and Identification from Random Data*. John Wiley & Sons, Inc., 1990.

[31] H. Unbehauen and G. P. Rao. *Identification of Continuous Systems*. North-Holland, 1987.

[32] G. C. Goodwin and L. P. Robert. *Dynamic System Identification: Experiment Design and Data Analysis*. Academic Press, Inc., 1977.

[33] J. P. Norton. *An Introduction to Identification*. Academic Press, Inc., 1986.

[34] K. J. Astrom and P. Eykhoff. System identification-a syrvey. *Automatica*, 7:123–162, 1971.

[35] S. A. Billings. Identification of nonlinear systems-a survey. *IEEE Proceedings*, 127 Pt. D(6):272–285, 1980.

[36] R. K. Mehra. Nonlinear system identification: selected survey and recent trends. *5th IFAC Symposium, Darmstadt, Federal Republic of Germany, Ed. Isermann, R.*, 1:77–83, September 24-28 1979.

[37] A. Niederliski and A. Hajdasinski. Multivariable system identification-a survey. *5th IFAC Symposium, Darmstadt, Federal Republic of Germany, Ed. Isermann, R.*, 1:43–76, September 24-28 1979.

[38] V. Strejc. Trends in identification. *5th IFAC Symposium, Darmstadt, Federal Republic of Germany, Ed. Isermann, R.*, 1:1–16, September 24-28 1979.

[39] P. Young. Parameter estimation for continuous-time models-a survey. *5th IFAC Symposium, Darmstadt, Federal Republic of Germany, Ed. Isermann, R.*, 1:17–41, September 24-28 1979.

[40] H. Unbehauen. A review of identification in continuous-time systems. *Annual reviews in control*, 22:145–171, 1998.

[41] S. K. Pandit and Wu, S.-M. *Time Series and System Analysis with Applications*. Krieger Publishing Company, 1993.

[42] D. G. Lainiotis and S. K. Kaisikas. Linear and nonlinear lainiotis filters: survey and comparative evaluation. In *IFAC Workshop on Expert Systems and Signal Processing in Marine Automation, Denmark*, 1989.

[43] D. G. Lainiotis, C. Charalampous, P. Giannakapoulos, and S. Katsikas. Real time ship motion estimation. In *Oceans '92*, volume 1. IEEE, 1992.

[44] J.-N. Juang and R. S. Pappa. An eigensystem realization algorithm for modal parameter identification and model reduction. *Journal of Guidance, Control, and Dynamics*, 8(5):620–627, 1985.

[45] R. L. Ho and R. E. Kalman. Effective construction of linear state-variable models form input/output data. In *Proceedings of the 3rd Annual Allerton Conference on Circuit and System Theory*, pages 449–459, 1965.

[46] S. R. Ibrahim and E. C. Mikulcik. A method for the direct identification of vibration parameters from the free response. *The Shock and Vibration Bulletin*, 47(4):183–198, 1977.

[47] S. R. Ibrahim and R. S. Pappa. Large modal survey testing using the Ibrahim Time Domain (ITD) identification technique. 1981. AIAA Paper 81-0528.

[48] R. S. Pappa and S. R. Ibrahim. A parametric study of the Ibrahim time domain modal identification algorithm. *The Shock and Vibration Bulletin*, 61 Pt. 3:96–111, May 1981.

[49] R. Prony. Essai expérimental et analytique: Sur les lois de la dilatabilité des fluides élastiques et sur celles de la force expansive de la vapeur de l'eau et de la vapeur de l'alkool, à différentes températures. *Journal de l'École Polytechnique, Paris*, 1:24–76, 1795.

[50] F. R. Spitznogle and A. H. Quazi. Representation and analysis of time-limited signals using a complex exponential algorithm. *Journal of the Acoustical Society of America*, 47:1150–1155, 1970.

[51] D. L. Brown, R. J. Allemang, R. Zimmerman, and M. Mergeay. Parameter estimation techniques for modal analysis. *SAE Paper no. 790221*, 1979.

[52] S. O'F. Fahey, B. M. Suleiman, A. H. Nayfeh, and M. R. Hajj. A Prony-based circular-hyperbolic decomposition. In *IMAC XVIII*, San Antonio, TX, February 2000. Society for Experimental Mechanics.

[53] B. M. Suleiman, S. O'F. Fahey, A. H. Nayfeh, and M. R. Hajj. Estimation of response amplitude operators for ships via the circular-hyperbolic decomposition. In *41st AIAA/ASME/ASCE/AHS/ASC Structure, Structural Dynamics, and Materials Conference & Exhibit, Atlanta, Georgia*, April 3-6, 2000. AIAA Paper 2000-1344.

[54] S. O'F. Fahey and J. Pratt. Time domain modal estimation techniques. *Experimental Techniques, Society for Experimental Mechanics*, 22(6):45–49, 1998.

[55] S. O'F. Fahey and J. Pratt. Frequency domain modal estimation techniques. *Experimental Techniques, Society for Experimental Mechanics*, 22(5):33–37, 1998.

[56] T. K. Caughey and H. J. Stumpf. Transient response of a dynamioc system under excitation. *Journal of Applied Mechanics*, pages 563–566, December 1961.

[57] J. K. Vandiver, A. B. Dunwoody, R. B. Campbell, and M. F. Cook. A mathematical basis for the random decrement vibration signature analysis technique. *Journal of Mechanical Design*, 104:307–313, April 1982.

[58] S. R. Ibrahim. Random decrement technique for modal identification of structures. *Journal of Spacecraft*, 14(11):696–700, 1977.

[59] M. R. Haddara. On the random decrement for nonlinear rolling motion. In *OMAE 1992, 11th International Conference on Offshore Mechanics and Arctic Engineering*, volume II, Safety and Reliability. ASME, 1992.

[60] S. F. Masri and T. K. Caughey. A nonparametric identification technique for nonlinear dynamic problems. *Journal of Applied Mechanics*, 46:433–447, June 1979.

[61] F. E. Udwadia and C.-P. Kuo. Non-parametric identification of a class of non-linear close-coupled dynamic systems. *Earthquake Engineering and Structural Dynamics*, 9:385–409, 1981.

[62] Y. Yang and S. R. Ibrahim. A nonparametric identification technique for a variety of discrete nonlinear vibrating systems. *Journal of Vibration, acoustics, Stress, and Reliability in Design*, 107:60–66, January 1985.

[63] M. R. Haddara. On the use of neural network techniques for the identification of ship stability parameters at sea. In *OMAE 1995, 15th International Conference on Offshore Mechanics and Arctic Engineering*, volume 2, pages 127–135. ASME, 1995.

[64] C.-B. Yun and M. Shinozuka. Identification of nonlinear structural dynamic systems. *Journal of Structural Mechanics*, 8(2):187–203, 1980.

[65] S. R. Ibrahim. Time-domain quasi-linear identification of nonlinear dynamic systems. In *24th Structures, Structural Dynamics, and materials Conference, Lake Tahoe, Nevada*, May 2-4, 1983. AIAA Paper 83-0811.

[66] L. G. Horta and B. R. Hanks. A study of the effect of a cubic nonlinearity on a modern modal identification technique. In *24th Structures, Structural Dynamics, abd Materials Conference, Lake Tahoe, Nevada*, May 2-4, 1983. AIAA Paper 83-0810.

[67] A. H. Nayfeh. *Perturbation Methods*. John Wiley & Sons, Inc., 1973.

[68] A. H. Nayfeh. *Introduction to Perturbation Techniques*. John Wiley & Sons, Inc., 1981.

[69] A. H. Nayfeh and D. T. Mook. *Nonlinear Oscillations*. John Wiley & Sons, Inc., 1979.

[70] S. V. Hanagud. Method of multiple scales and identification of nonlinear structural dynamic systems. *AIAA Journal*, 23(5):802–807, 1985.

[71] A. H. Nayfeh. Parametric identification of nonlinear dynamic systems. *Computers & structures*, 120(1-3):487–493, 1985.

[72] A. A. El-Badawi. *Nonlinear vibration testing and control of a twin-tail aircraft scale model*. PhD thesis, Virginia Polytechnic Institute and State University, Blacksburg, VA, USA, 2000.

[73] S. O'F. Fahey and A. H. Nayfeh. Experimental nonlinear identification of a single structural mode. In *16th IMAC, Santa Barbara, CA*, pages 737–745, February 2-5 1998.

[74] B. F. Feeny. Identification of nonlinear ship motion using perturbation techniques. Master's thesis, Virginia Polytechnic Institute and State University, Blacksburg, VA, USA, August 1986.

[75] M. R. Hajj, A. H. Nayfeh, and P. Popovic. Identification of nonlinear systems parameters using polyspectral measurement and analysis. In *15th Biennial Conference on*

Mechanical Vibration and Noise, volume 3, part A, pages 651–661, September 17-20 1995. DE-Vol. 84-1.

[76] A. H. Nayfeh, M. R. Hajj, J. Fung, and S. O'F. Fahey. Characterization and identification of damping with bispectral analysis. In *16th Biennial Conference on Mechanical Vibration and Noise*, September 14-17 1997. ASME DETC97/VIB-4407.

[77] A. H. Nayfeh and D. T. Mook. A saturation phenomena in the forced response of systems with quadratic nonlinearities. In *VIII th International Conference on Nonlinear Oscillations*, pages 511–516, 1978.

[78] I. G. Oh, A. H. Nayfeh, and D. T. Mook. Theoretical and experimental study of the nonlinearly coupled heave, pitch, and roll motions of a ship in longitudinal waves. In *14th Biennial Conference on Mechanical Vibration and Noise*, pages 105–124, September 19-22 1993. DE-Vol. 54.

[79] A. H. Nayfeh, D. T. mook, and L. R. Marshall. Nonlinear coupling of pitch and roll modes in ship motions. *Journal of Hydronautics*, 7(4):145–152, October 1973.

[80] D. T. Mook, L. R. Marshal, and A. H. Nayfeh. Subharmonic and superharmonic resonances in the pitch and roll modes of ship motions. *Journal of Hydronautics*, 8(1):32–40, January 1974.

[81] A. H. Nayfeh. On the undesirable roll characteristics of ships in regular seas. *Journal of Ship Research*, 32(2):92–100, June 1988.

[82] A. H. Nayfeh and I. G. Oh. Nonlinearly coupled pitch and roll motions in the presence of internal resonance: part I, theory. *International Shipbuilding Progress*, 42:295–324, 1995.

[83] A. H. Nayfeh. The response of two-degree-of-freedom systems with quadratic nonlinearities to parametric excitation. *Journal of Sound and Vibration*, 88(4):547–557, 1983.

[84] A. H. Nayfeh and A. E. S. Jebril. The response of two-degree-of-freedom systems with quadratic and cubic non-linearities to multifrequency parametric excitation. *Journal of Sound and Vibration*, 115(1):83–101, 1987.

[85] M. R. Hajj, J. Fung, A. H. Nayfeh, and S. O'F. Fahey. Damping identification using perturbation techniques and higher-order spectra. *Nonlinear Dynamics*, 23:189–203, 2000.

[86] M. R. Hajj, R. W. Miksad, and E. J. Powers. Fundamental-subharmonic interaction: effect of phase relation. *Journal of Fluid Mechanics*, 256:402–426, 1993.

[87] C. Duthoit and J. L. Armand. Nonlinear stochastic response of marine vehicles. In *OMAE 1988, 7th International Conference on Offshore Mechanics and Arctic Engineering, Houston*, volume 2, pages 339–344. ASME, 1988.

[88] P. J. Gawthrop, A. Kountzeris, and J. B. Roberts. Parametric identification of nonlinear ship roll motion from forced roll data. *Journal of Ship Research*, 32(2):101–111, June 1988.

[89] J. B. Roberts. Estimation of nonlinear ship roll damping from free-decay data. *Journal of Ship Research*, 29(2):127–138, June 1985.

[90] J. B. Roberts, J. F. Dunne, and A. Debonos. Stochastic estimation methods for nonlinear ship roll motion. *Probalistic Engineering Mechanics*, 9:83–93, September 1994.

[91] J. B. Roberts, J. F. Dunne, and A. Debonos. Estimation of ship roll parameters in random waves. *Journal of Offshore Mechanics and Arctic Engineering*, 114:114–121, May 1992.

[92] C. B. Smith and N. M. Werely. Nonlinear damping identification from transient data. *AIAA Journal*, 37:1625–1632, December 1999.

[93] Gawthrop. Parametric identification of transient signals. *IMA Journal of Mathematical Control & Information*, 1:117–128, January 1984.

[94] J. B. Mathisen and W. G. Price. Estimation of ship roll damping coefficients. *Transactions of the Royal Institution of Naval Architects*, 127:295–307, 1985.

[95] A. Kountzeris, J. B. Roberts, and P. J. Gawthrop. Estimation of ship roll parameters from motion in irregular seas. *Transactions of the Royal Institution of Naval Architects*, 132:253–266, 1991.

[96] M. A. Abkowitz and G. Liu. Measurement of ship resistance, powering and maneuverability coefficients from simple trials during a regular voyage. *SNAME Transactions*, 98:97–128, 1988.

[97] G. Liu. Application of EKF techniques to ship resistance measurement. *Automatica*, 29(2):275–283, 1993.

[98] J. O. Flower and W. A. K. S. Aljaff. Kryloff-Bogoliuboff solution to decaying nonlinear oscillations in marine systems. *International Shipbuilding Progress*, 27(313):225–230, September 1980.

[99] D. W. Bass and M. R. Haddara. Nonlinear models of ship roll damping. *International Shipbuilding Progress*, 35(401):5–24, 1988.

[100] M. R. Haddara and P. Bennet. A study of the angle dependence of roll damping moment. *Ocean Engineering*, 16(4):411–427, 1989.

[101] M. R. Haddara and D. Cumming. Experimental investigation into the physics of roll damping of a long slender hull form. *International Shipbuilding Progress*, 39(420):323–343, 1992.

[102] M. R. Haddara and X. Wu. Parameter identification of nonlinear rolling motion in random seas. *International Shipbuilding Progress*, 40(423):247–260, 1993.

[103] M. R. Haddara, M. Wishahy, and X. Wu. Assessment of ship's transverse stability at sea. *Ocean Engineering*, 21(8):781–800, 1994.

[104] M. R. Haddara and J. Xu. On the identification of ship coupled heave-pitch motions using neural networks. *Ocean Engineering*, 24:381–400, 1999.

[105] M. R. Haddara. Parametric identification of coupled sway and yaw motions. In *OMAE 1996, 16th International Conference on Offshore Mechanics and Arctic Engineering*, volume I, Part A, Offshore Technology, pages 267–273. ASME, 1996.

[106] A. Kountzeris. *Investigation of Ship Roll Motion by Parametric Identification Techniques*. PhD thesis, The University of Sussex, UK, April 1988.

[107] A. Debonos. *Estimation of Nonlinear Ship Roll Parametrs Using Stochastic Identification Techniques*. PhD thesis, The University of Sussex, UK, February 1993.

[108] A. Francescutto and G. Contento. Bifurcations in ship rolling: experimental results and parameter identification techniques. *Ocean Engineering*, 26:1095–1123, 1999.

[109] A. H. Nayfeh, J. Fung, M. R. Hajj, and D. T. Mook. Parametric identification for a roll instability in a series S60-70 ship. In *8th International Offshore and Polar Engineering Conference*, pages 499–503, May 24-29 1998.

[110] J. Fung. Parameter identification of nonlinear systems using perturbation methods and higher-order statistics. Master's thesis, Virginia Polytechnic Institute and State University, Blacksburg, VA, USA, August 1998.

[111] B. Bikdash, M. Balachandran and A. H. Nayfeh. Melnikov analysis for a ship with a general roll-damping model. *Nonlinear Dynamics*, 6:101–124, 1994.

[112] J. F. Dalzell. A note on short-time prediction of ship motions. *Journal of Ship Research*, 9:118–121, September 1965.

[113] H. A. Cole. On-the-line analysis of random vibrations. In *AIAA/ASME 9th Structure, Structural Dynamics, and Materials Conference, Palm Springs, CA*, April 1-3, 1968. AIAA Paper 68-288.

[114] P. Kaplan. A study of prediction techniques for aircraft carrier motions at sea. In *AIAA 6th Aerospace Science Meeting*, January 22-24, 1968. AIAA Paper 68-123.

[115] I. R. Yumori. Real time prediction of ship response to ocean waves using time series analysis. In *Oceans '81*, volume 2, pages 1082–1089. IEEE, 1981.

[116] M. S. Triantafyllou, M. Bodson, and M. Athans. Real time estimation of ship motions using kalman filtering techniques. *IEEE Journal of Oceanic Engineering*, OE-8(1):9–20, January 1983.

[117] N. K. Lin. Real time estimation of ship motion using ARMA filtering techniques. *OMAE 1987, 6th International Conference on Offshore Mechanics and Arctic Engineering*, 2:325–329, 1987.

[118] D. R. Broome and A. Pittaras. Ship motion prediction. *OMAE 1990, 9th International Conference on Offshore Mechanics and and Arctic Engineering*, 1, Part A:303–311, 1990.

[119] D. R. Broome and M. S. Hall. Application of ship motion prediction I. *Transactions of the Institute of Marine Engineers*, 110, Part 1:77–93, 1998.

[120] D. R. Broome. Application of ship motion prediction II. *Transactions of the Institute of Marine Engineers*, 110, Part 2:135–153, 1998.

[121] D. G. Lainiotis and K. N. Plataniotis. Neural network estimators: Application to ship estimation. In *1994 IEEE International Conference on Neural Networks*, volume 7, pages 4710–4717, 1994.

[122] D. G. Lainiotis, K. N. Plataniotis, D. Menon, and C. J. Charalampous. Adaptive heave compensation via dynamic neural networks. In *Oceans '93*, volume 1, pages 243–248. IEEE, 1993.

[123] J. C. Chung, Z. Bien, and Y. S. Kim. A note on ship-motion prediction based on wave-excitation input extimation. *IEEE Journal of Oceanic Engineering*, 15(3):244–250, July 1990.

[124] R. P. Dallinga, Th. Elzinga, and R. H. M. Huijsmans. Ship simulation models: an aid to harbor design. *Journal of waterway, port, coastal and ocean engineering*, 112(2):255–269, March 1986.

[125] E. O. Tuck. Shallow water flow past slender bodies. *Journal of Fluid Mechanics*, 26(2):81–95, March 1966.

[126] C.-L. Guo. Nonlinear theory of ship maneuvering. *Journal of Ship Research*, 25:21–43, 1981.

[127] T. I. Fossen. *Guidance and Control of Ocean Vehicles*. John Wiley & Sons, New York, 1994.

[128] J.-N. Juang, L. G. Hortai, and M. Phan. *System/Observer/Controller Identification Toolbox, User's Guide*. NASA, Langley Research Center, December 1991.

[129] B. V. Korvin-Kroukovsky. *Theory of Seakeeping*. The Society of Naval Architects and Marine Engineers, New York, 1961.

[130] N. E. Sanchez and Nayfeh. Nonlinear rolling motions of ships in longitudinal waves. *International Shipbuilding Progress*, 37(411):247–272, 1990.

[131] I. G. Oh, A. H. Nayfeh, and D. T. Mook. A theoretical and experimental investigation of indirectly excited roll motion in ships. *Philosophical Transactions of the Royal Society*, 358(1771):1853–1881, June 2000.

[132] F. J. Harris. On the use of windows for harmonic analysis with the discrete Fourier transform. *Proceedings of IEEE*, 66:51–84, 1978.

[133] Woei-Min Lin, S. Zhang, K. Weems, and D. K. P. Yue. A mixed source formulation for nonlinear ship-motion and wave-load simulations. In *Proceedings of the 7th International Conference on Numerical Ship Hydrodynamics, Nantes, France*, July 19-22 1999.

[134] R. Bhattacharyya. *Dynamics of Marine Vehicles*. John Wiley & Sons, New York, 1976.

[135] S. O'F. Fahey, B. M. Suleiman, A. H. Nayfeh, and M. R. Hajj. A new Prony-based circular-hyperbolic decomposition. *Journal of Sound and Vibration (accepted)*, 2000.

[136] M. R. Hajj, R. W. Miksad, and E. J. Powers. Perspective: measurements and analysis of nonlinear wave interactions with higher-order spectral moments. *Journal of Fluids Engineering*, 119:3–13, March 1997.

[137] Y. C. Kim and E. J. Powers. Digital bispectral analysis and its application to nonlinear wave inteactions. *IEEE Transactions on Plasma Science*, PS-7:120–131, 1979.

Vita

Baha M. Suleiman was born on November 10, 1966 in Kuwait City, Kuwait. He was raised in Kuwait City and received his General Education Certificate in June 1984. He joined Kuwait University in September, 1984. He received his Bachelor of Science degree in Mechanical Engineering in January, 1989. In June 1992, he moved to Amman, Jordan. He received his Master of Science degree in Mechanical Engineering from the University of Jordan in June 1994. He then traveled to the United States to join the School of Aerospace Engineering at Georgia Institute of Technology (Georgia Tech) in Atlanta, Georgia. He received his Master of Science degree in June 1996. In January 1998, he moved to Blacksburg, Virginia where he joined the Department of Engineering Science and Mechanics at Virginia Polytechnic Institute and State University (Virginia Tech). On December 11, 2000, he successfully defended his dissertation to receive a Doctor of Philosophy degree in Engineering Mechanics.